Facultad de Medicina

Departamento de Bioquímica

Programa de Doctorado en Biociencias Moleculares

Unraveling the dynamic oxidative processes after ischemia/reperfusion in the heart using new proteomics approaches

TESIS DOCTORAL

Celia Castañs García

Graduada en Bioquímica

Codirectores de tesis:

Prof. Jesús Vázquez Cobos

Dr. Inmaculada Jorge Cerrudo

Madrid, 2019

Jesús Mª Vázquez Cobos, DOCTOR en Ciencias Químicas por la Universidad Autónoma de Madrid y Profesor de Investigación del Consejo Superior de Investigaciones Científicas; actualmente Full Professor en el Centro Nacional de Investigaciones Cardiovasculares (CNIC) de Madrid; e **Inmaculada Jorge Cerrudo**, DOCTORA en Ciencias por la Universidad de Córdoba.

CERTIFICAN que,

Doña Celia Castañs García, Graduada en Bioquímica por la Universidad Complutense de Madrid, ha realizado bajo su dirección el trabajo de investigación titulado:

"***Unraveling the dynamic oxidative processes after ischemia/reperfusion in the heart using new proteomic approaches***"

y consideran que el trabajo realizado reúne todas las condiciones requeridas por la legislación vigente, así como la originalidad y calidad científicas necesarias, para poder ser presentado y defendido con el fin de optar al grado de Doctor, con Mención Internacional, por la Universidad Autónoma de Madrid.

Y para que así conste y surjan los efectos oportunos, firmo el presente certificado en

Madrid, a 27 de febrero de 2019	Madrid, a 27 de febrero de 2019
Director de la Tesis Doctoral	Co-director de la Tesis Doctoral
Dr. Jesús Mª Vázquez Cobos	Dra. Inmaculada Jorge Cerrudo

Esta tesis doctoral ha recibido financiación del Ministerio de Educación, Cultura y Deporte para la Formación de Profesorado Universitario

GOBIERNO DE ESPAÑA
MINISTERIO DE EDUCACIÓN, CULTURA Y DEPORTE

SEVENTH FRAMEWORK PROGRAMME

CARDIO NEXT

GOBIERNO DE ESPAÑA
MINISTERIO DE CIENCIA, INNOVACIÓN Y UNIVERSIDADES

Instituto de Salud Carlos III

Fundaciónprocnic

EXCELENCIA SEVERO OCHOA

cnic

“Y cuando la tormenta de arena haya pasado, tú no comprenderás cómo has logrado cruzarla con vida. ¡No! Ni siquiera estarás seguro de que la tormenta haya cesado de verdad. Pero una cosa sí quedará clara. Y es que la persona que surja de la tormenta no será la misma persona que penetró en ella. Y ahí estriba el significado de la tormenta de arena.”

Haruki Murakami

Agradecimientos

Me gustaría agradecer a Jesús Vázquez la oportunidad brindada para iniciar esta aventura, así como toda su ayuda, energía y disposición. Gracias también a mi codirectora, Inma, por toda la ayuda durante la elaboración de la tesis y a mi tutor de la UAM, Miguel, por su apoyo en cada trámite.

Tengo que agradecer a todos los trabajadores del CNIC por toda su ayuda durante estos casi 5 años, desde la cafetería a RRHH, y en especial a nuestros colaboradores del laboratorio de Borja Ibañez.

Muchas gracias a todos mis compañeros del Laboratorio de Proteómica y de la Unidad de Proteómica: los que están y los que se fueron, los de la cueva, el laboratorio, la primera sur, la zona postdoc, los establos y las oficinas. Todos los miembros de esta gran "familia" han dejado su marca en el desarrollo de esta experiencia. En especial me gustaría agradecer a Marco, Juan Antonio y Navratan por su generosidad y amistad.

Uno de los mejores resultados de esta tesis es un grupo de personas que aparecieron en este viaje en distintas estaciones para quedarse una vez concluido: Aleks, Ricardo, Ile, Fer, Jesús L, Rocío, Alessia, Diego e Irene. Con ellos he vivido las más surrealistas e inolvidables aventuras dentro y fuera del CNIC, en España y en el extranjero; y realmente no sé qué hubiera sido de mí sin su amistad, su ayuda, su buen humor y sus consejos. En especial no tengo palabras suficientes para agradecer a Aleksandra todo lo que ha hecho por mí en su papel de amiga, de compañera y de mentora.

Gracias a mi familia por su amor y apoyo incondicional, y a mis amigos por ser prácticamente mi familia.

Gracias, Jaime, por obligarme a construirme unas alas en la caída.

Summary

After an episode of coronary artery occlusion, myocardial response to reperfusion does not remain stable during time. Although there are many relevant proteomic changes taking place in the tissue, systematic studies are lacking on the protein modification changes occurring in the post-reperfused myocardium along the first week after I/R. In this Doctoral Thesis we present the application of global PTMs analysis combined with the mapping of redox-active thiols in myocardial tissue proteins to study the oxidative and molecular dynamic changes after I/R.

After ischemia, blood flow restoration generates an initial oxidative damage, generated in the mitochondria, that we detected at 20 minutes after reperfusion. This initial and intracellular oxidative wave consisted on irreversible monooxidations and affected intracellular proteins essential for cardiac function. Later, starting at 2h and peaking at 24h after reperfusion, immune cells, including neutrophils, are recruited to the lesion site as part of the cardiac inflammatory process. We detected an increase in neutrophil's granule peroxidases in the tissue, as well as a second oxidative wave consisting on irreversible dioxidations and trioxidations and also Cysteine reversible oxidation, in extracellular and membrane proteins. Towards the end of the first week and with the start of the repair and fibrotic phase, we detected an increase in collagen proline-hydroxilations as well as lipid peroxidation accumulation in the tissue. Additionally, these results were validated in other animal models.

This doctoral thesis provides the first systematic understanding of the timeline of the different oxidative processes during the first week after I/R. This study comprises the deep study of the posttranslationally modified peptidome, the redoxome and the proteome in a highly translational pig model, and might have implications on the definition of the disease progression and in the prediction and future approaches of the disease.

Resumen

Después de un episodio de oclusión de una arteria coronaria, la respuesta del miocardio a la reperfusión no permanece estable en el tiempo. En este sentido, aunque estudios previos han mostrado cambios importantes en el proteoma durante este periodo, faltan estudios sistemáticos sobre los cambios en modificaciones de proteínas que ocurren en el miocardio durante la primera semana después de la reperfusión. En esta Tesis Doctoral mostramos un análisis global de PTM combinado con el estudio del proteoma redox y la biología de sistemas para revelar los cambios moleculares que tienen lugar en la semana posterior a la I/R.

Después de la isquemia, la restauración del flujo sanguíneo genera un daño oxidativo inicial, originado en las mitocondrias, que detectamos 20 minutos tras la reperfusión. Esta onda oxidativa inicial se caracteriza por monooxidaciones irreversibles que afectan proteínas intracelulares esenciales para la función cardíaca. Más tarde, desde las 2 horas y, especialmente a las 24 horas tras la reperfusión, las células del sistema inmune se infiltran en la lesión como parte del proceso inflamatorio. De esta forma detectamos un aumento en las peroxidasas de los gránulos de neutrófilos en el tejido, así como una segunda onda oxidativa consistente en dioxidaciones y trioxidaciones irreversibles y oxidaciones reversibles en cisteínas, afectando proteínas extracelulares y de membrana. Hacia el final de la primera semana y dando lugar a la fase de fibrosis, detectamos un aumento en las hidroxilaciones de prolina de colágeno y una acumulación de lípidos peroxidados en el tejido.

Esta tesis doctoral proporciona la primera comprensión sistemática del transcurso de los diferentes procesos oxidativos durante la primera semana después de la I/R. Estos resultados fueron validados, además, en otro modelo animal y comprenden un estudio profundo del peptidoma modificado postraduccionalmente, el redoxoma y el proteoma en un modelo de cerdo altamente traslacional, pudiendo tener implicaciones en la definición del progreso de la enfermedad y en la predicción y enfoque futuro de la misma.

Table of contents

Abbreviations

TERM	***DESCRIPTION***
AMI	Acute myocardial infarction
Asn	Asparagine
Asp	Aspartic Acid
C	Cysteine
CM	Cardiomyocyte
CMR	Cardiac magnetic resonance
CNIC	Fundación Centro Nacional de Investigaciones Cardiovasculares Carlos III
CVD	Cardiovascular disease
Cys	Cysteine
D	Aspartic Acid
Da	Dalton
ECM	Extracellular Matrix
EGC	Electrocardiogram
ETC	Electron Transport Chain
F	Phenylalanine
FA	Fatty Acid
FC	Fold change
FDR	False discovery rate

GO	Gene Ontology
HCA	Hierarchical Clustering Analysis
HNE	Hydroxynonenal
HPLC	High performance liquid chromatography
i.v.	Intravenous
I/R	Ischemia/reperfusion
ICAT	Isotope-coded affinity tag
IgG	Immunoglobulin G
K	Lysine
LAD	Left anterior descending
LF	Label Free
Ly6G	Lymphocyte antigen 6 complex locus G6D
Lys	Lysine
Mat&Met	Materials and Methods
MDA	Malondialdehyde
MI	Myocardial infarction
MPO	Myeloperoxidase
MPTP	Mitochondrial permeability transition pore
MS	Mass spectrometry
MS/MS	Tandem mass spectrometry
N	Asparagine

nanoLC-MS/MS	Nano-liquid chromatography-tandem mass spectrometry
NOR	Non-reperfusion
NSTEMI	non-ST-elevation myocardial infarction
P	Proline
PANTHER	Protein ANalysis THrough Evolutionary Relationships
PC	Pre-conditioning
PCA	Principal Components Analysis
PCI	Percutaneous coronary intervention
Phe	Phenylalanine
ppm	parts-per-million
Pro	Proline
PSM	Peptide-Spectrum Match
PTM	Postranslational modifications
ROS	Reactive oxygen species
rpm	revolutions per minute
SBT	Systems biology triangle
SD	Standard Deviation
SIL	Stable isotope labeling
STEMI	ST-elevation myocardial infarction
TCA	Tricarboxylic acid cycle
TMT	Tandem Mass Tag

Trp	Tryptophan
Tyr	Tyrosine
W	Tryptophan
WB	Western Blot
WSPP	Weighted spectrum, peptide and protein model [Statistical Model]
Y	Tyrosine

Introduction

Acute myocardial infarction: relevance

Acute myocardial infarction (AMI) is an event of myocardial necrosis caused by an unstable ischemic syndrome [1]. In the clinic, patients with AMI usually present with chest pain and it is eventually diagnosed in the basis of electrocardiogram (ECG), biochemical tests, imaging, pathological and clinical evaluation [2, 3].

In most developed countries, AMI is a significant clinical burden. Heart attacks and strokes are responsible of the 80% of cardiovascular disease (CVD) deaths. Individuals at risk of CVD may demonstrate raised blood pressure, glucose, and lipids as well as overweight and obesity. Although its high incidence, there has been a significant decrease in cardiovascular mortality since the 1970s due to advances in the diagnosis and management of AMI [2, 4]. Today, with percutaneous coronary intervention (PCI) and stenting, antithrombotic therapy and the routine use of complementary medical treatment, in-hospital mortality from AMI has significantly decreased [2, 5].

AMI can be classified into two categories based on the ECG manifestation of ST-elevation: non-ST-elevation myocardial infarction (NSTEMI) and ST-elevation myocardial infarction (STEMI)[4]. The major cause of STEMI is coronary atherosclerosis with luminal thrombus, which accounts for more than 80% of all infarcts[6]. STEMI most frequently arises with a rupture of an atherosclerotic plaque, which exposes the blood to thrombogenic lipids and leads to activation of platelet and clotting factors, generating a thrombotic formation that completely occludes a major epicardial coronary vessel [2-4]. Artery occlusion produces a life-threatening ischemic damage that requires urgent intervention. Extending the period of acute myocardial ischemia for more than 20 minutes causes massive necrotic cell death within the infarcted tissue [7, 8]. Thus, the most effective therapeutic intervention is myocardial blood reperfusion using thrombolytic therapy or primary percutaneous coronary intervention to rescue the ischemic myocardium [7].

I/R injury and Edema

The degree of necrosis in the heart tissue produced by myocardial infarction has been shown to be critical to determine subsequent chronic complications that infarct survivors suffer from [9]. Hence, there is an urgent need to develop novel therapies to minimize infarct size, which would result in better long term heart performance with fewer adverse clinical events, reduced mortality, and a significant relief of the huge socioeconomic burden [10, 11]. Blood flow restoration always accompanies the treatment for myocardial infarction, in a process known as reperfusion, which is the only available treatment to stop the progression of ischemic damage during an AMI[6]. Although early reperfusion is the best strategy to stop the damage progression, it paradoxically produces an additional stress to the myocardium (reperfusion injury), which may account for up to 40% of infarct size [12, 13]. These two processes together constitute what is known as I/R injury.

Myocardial infarction and infarct size is revealed by a manifestation of different forms of cardiomyocyte (CM) cell death: necrosis, apoptosis, autophagy, and necroptosis. During ischemia, the anaerobic glycolysis increases the influx of sodium ions (Na^+) through the Na^+/hydrogen ion (H^+) exchanger due to developing acidosis. Moreover, intracellular Na^+ accumulation is increased by the inhibition of Na^+/ potassium ion (K^+) ATPase due to the lack of available ATP molecules [14]. The subsequent exchange of Na^+ for Ca^{2+} by reverse mode operation of the sarcolemmal Na^+/Ca^{2+} exchanger induces intracellular Ca^{2+} overload. After reperfusion, the rapid normalization of pH in the context of elevated cytosolic Ca^{2+} induces subsequent release and reuptake of Ca^{2+} into the sarcoplasmic reticulum, causing uncontrolled hypercontracture [15, 16]. The high cytosolic concentrations of Na^+ and Ca^{2+} also results in intracellular edema when extracellular osmolarity is abruptly normalized by reperfusion. Furthermore, the opening of the mitochondrial permeability transition pore (MPTP) appears to be decisive for necrosis, apoptosis, and necroptosis, and mitochondria are also decisive in mitophagy/autophagy.

While the contribution of reperfusion injury to final infarct size has been disputed in the past, today it is accepted that reperfusion alters post-myocardial infarction (MI) repair and appears to produce dynamic molecular changes that evolve within the first week after the ischemia/reperfusion (I/R) onset [17-22]. The typical microscopic features of reperfused myocardial infarction include: contraction band necrosis, nuclear dissolution, mitochondrial swelling and disruption, CM membrane disruption, microvascular destruction, interstitial hemorrhage, and inflammation [11].

Under basal conditions, water is the main component of healthy heart tissue, since the water content in the myocardium is stable and, mostly, intracellular, with a very small part as interstitial component in the extracellular matrix. During myocardial infarction, edema initially occurs as swelling of CM during the early stages of ischemia [23]. Then, myocardial edema is significantly increased after restoring blood flow to the ischemic region due to reperfusion. This increase associated with reperfusion appears to be due to an increase in cellular swelling [24] and, more importantly, interstitial edema [25] due to reactive hyperemia and leakage of damaged capillaries when hydrostatic pressure is restored after reperfusion [26, 27].

It has been believed for many years that the intense edematous reaction that is occurred early after MI in the post-ischemic region remained stable for at least a week. [28, 29]. Only recently, post-I/R myocardial edema has been shown to follow a consistent bimodal pattern in animal model and in MI patients [17, 19]. In these studies, serial cardiac magnetic resonance (CMR) imaging shows that tissue composition changes dynamically during the first week after infarction as initial edema was detected within the first 3h after the onset of reperfusion, dissipated at 24h, and was followed by a delayed wave that reappeared 4-7 days after infarction [17, 19].

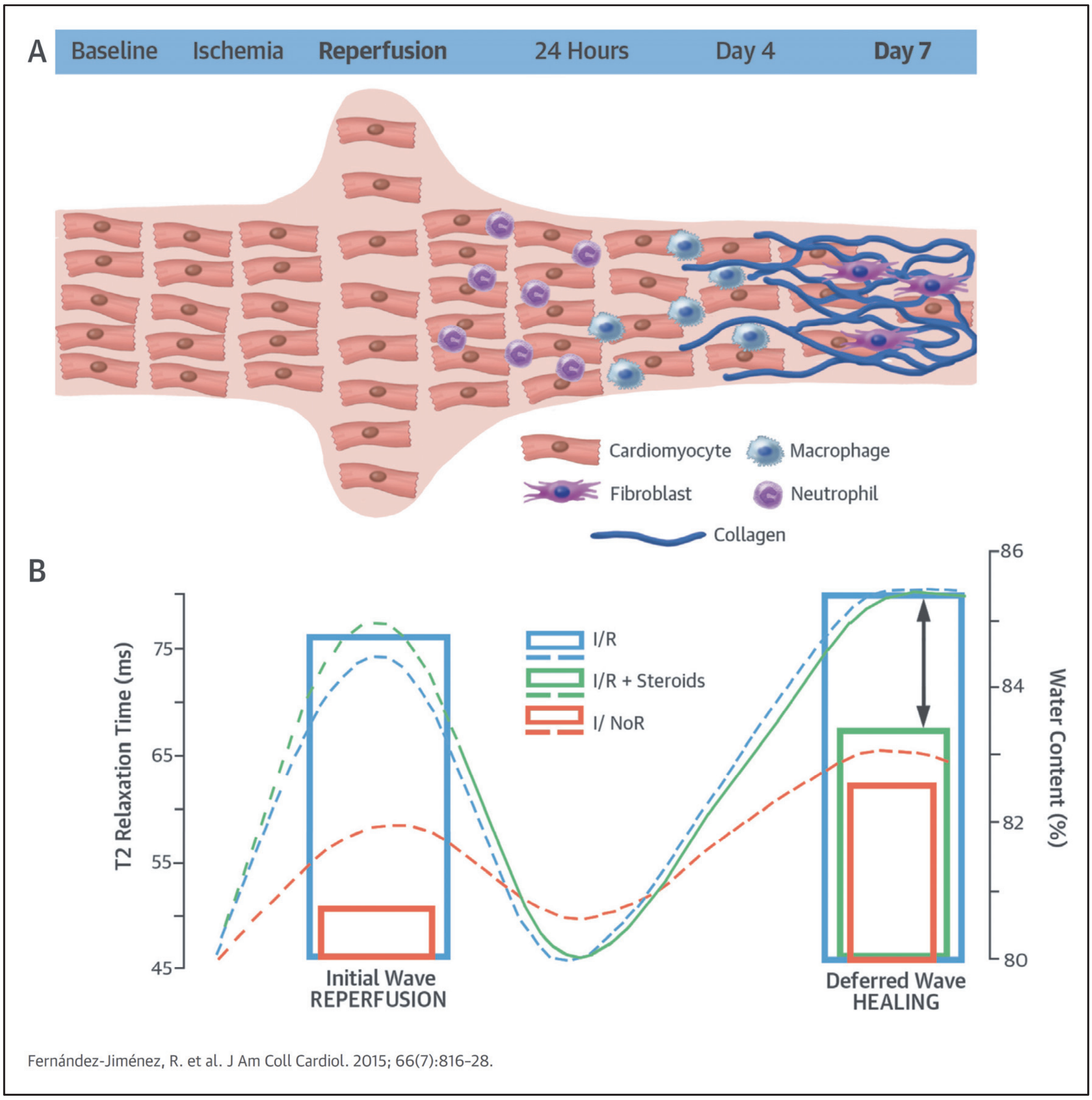

Figure 1. Mechanisms Underlying the Bimodal Edema Phenomenon After Myocardial Ischemia/Reperfusion. Two distinct waves of edema emerge within the first week after ischemia/reperfusion (I/R) because of different pathophysiological processes. The initial wave, appearing abruptly on reperfusion, is a direct consequence of the reperfusion process itself, whereas the deferred wave, appearing progressively days after I/R, is mainly caused by tissue healing processes. (A) Reperfusion is associated with a very abrupt edematous reaction that separates myocardial fibers from each other, resolving by day 1. (B) Boxes represent water content measurements in pigs; blue ¼ regular I/R protocol; salmon ¼ permanent coronary occlusion (nonreperfused myocardial infarction; initial edema wave abrogated, deferred wave significantly attenuated); green ¼ I/R plus steroid therapy (deferred wave significantly attenuated). The lines show cardiac magnetic resonance T2 relaxation time course in the ischemic myocardium; blue ¼ first week after infarction (2 peaks closely track the water content changes); salmon ¼ nonreperfused myocardial infarction (both waves of cardiac magnetic resonance–evaluated edema significantly attenuated); and green ¼ I/R plus steroid therapy (continuous line after initiation of therapy). **(Source Fernández-Jiménez, R. et al. 2015 [18]).**

Moreover, our group recently described detailed protein expression changes that take place in both the ischemic and remote myocardium during the first week after infarction in a pig model [20]. This study revealed a highly coordinated, multimodal pattern of functional protein alterations in both myocardium regions in the early stages post I/R. First, early reperfusion can be characterized by an abrupt edematous response [17, 18] and a rapid and profound acute inflammatory reaction [13, 30]. Intracellular, mitochondrial and sarcolemmal Ca^{2+} levels increase strongly upon reperfusion, resulting in hypercontraction of the CM and opening of the MPTP, the hallmark of reperfusion-induced CM death [31]. The previous proteomic characterization performed by our group [20] has showed the temporal dynamics of hundreds of protein changes involved in inflammation, wound healing, and reactive oxygen species as early as 120 minutes after the reperfusion procedure. This comprehensive study identified a rich repository of early-response proteins directly related to reperfusion injury that indicates an early event after reperfusion.

Later, at 4 and 7 days after reperfusion, coordinated protein changes in the ischemic myocardium revealed the activation of protein biosynthesis, the synthesis of collagen and interstitial proteins, and the formation of new vessels, along with the depletion of muscle and mitochondrial proteins. These processes reflected a phenotypic change in infarcted myocardial tissue characterized by the replacement of necrotic myocytes, rich in mitochondria, by collagen, extracellular matrix proteins, and fibroblasts with low mitochondrial content, suggesting a later event of repair and remodeling. This study also demonstrated that I/R significantly impacts the remote myocardium, inducing transient molecular alterations of sarcomere components, coinciding with CMR-detected transient stunned myocardium [19, 32], which reverts to control levels by 7 days after reperfusion.

The exact molecular and cellular events that occur during this very dynamic early post-I/R phases are still largely unknown. Experimental procedures for the study of I/R response using reperfused and non-reperfused MI models and preconditioning strategies can accurately reflect healing processes. Thus, experimental models on animals are of crucial importance in I/R research, as there are only a limited number of in vitro models [32, 33]. Much of the prevailing knowledge about I/R and the molecular modifications involved comes from studies performed with animal models, mainly rodents [34-37] or pigs [38]. The similarity in size, physiology, and in heart development and disease progression make the swine an ideal model for I/R research and its direct translation of results into humans [39].

Cardioprotective interventions to decrease I/R injury

Although the mortality of STEMI in Western countries has declined in the past decades, the still high incidence encourages the seek for new therapies focused on reducing the I/R injury.

First, it was reported [40] that brief cycles of ischemia and reperfusion performed before a prolonged coronary artery occlusion with reperfusion could substantially reduce final infarct size in dogs to 25%, what was referred as “ischemic pre-conditioning”. Unfortunately, the unpredictability of coronary artery occlusion event in STEMI patients means that ischemic pre-conditioning cannot be applied in this clinical setting, but it could have an important role in planned procedures like cardiac surgery [41] or in diabetic and non-diabetic patients with stable coronary artery disease [42].

Later, “ischemic post-conditioning” was described in 2003 [43], showing that brief episodes of ischemia and reperfusion performed immediately after reperfusion following ischemia could reduce final infarct size in dogs by 30% to 40%. This intervention is applied after flow restoration; consequently, it has no connection to the duration of ischemia and must be related to the prevention of events occurring after reperfusion. In other study in 2005 [44], it was also demonstrated that ischemic post-conditioning could reduce infarct size in STEMI patients. Another form of myocardial conditioning well described in animal models is remote ischemic conditioning: conditioning performed in a distant organ [45]. These promising results in were followed by clinical studies, and this might potentially translate into clinical setup [46].

Oxidative PTMs and I/R injury

While reperfusion of ischemic tissue is essential for survival, it also initiates oxidative damage through generation of reactive oxygen species (ROS). This event has been consistently demonstrated by measuring free radical generation in perfused rabbit hearts by electron paramagnetic resonance spectroscopy [47], in reperfused rat hearts by electron spin resonance spectroscopy [48], in Langendorff guinea pig hearts through fluorescent indicators [49] and measurement of superoxide-derived free radicals [50], showing a burst of ROS generation on the start of reperfusion, peaking from 4 to 10 minutes. Mitochondria are considered to be a major source of ROS as well as a major target for ROS damage due to the role of mitochondrial electron transport chain (ETC) as one of the primary sources of ROS in the cell [51, 52]. Additionally, accumulation of succinate and its re-oxidation after reperfusion has been pointed out as the main contributor to extensive ROS peaking at 10-15 min after reperfusion at mitochondrial complex I in *in vivo* and Langendorff mice hearts [53].

Postranslational modifications (PTMs) are well known to have a pivotal role in the control of signaling cascades and protein structure and functionality. Some studies have tried to shed some light into the effect in proteins of mitochondrial disease or initial ROS production 5 minutes after reperfusion studying the thiol redox status in mitochondria using ICAT reagents [54, 55]. Other approaches have made it possible to measure protein oxidation and s-nitrosylation of Cys after I/R in Langendorff mice hearts using Resin-Assisted Capture and showing an increase in protein oxidation 5 minutes after reperfusion [56]. In this line, GELSILOX [57] has been presented as a technology that allows the simultaneous quantification of proteins and of reduced and oxidized Cys sites in the same experiment, allowing the identification of Cys-reversible oxidation ROS targets. This method revealed an increase in Cys-oxidation 5 minutes after reperfusion in Langendorff rat hearts and isolated mice mitochondria and made it able to identify the specific site of oxidation [58]. Moreover, it showed that ischemic preconditioning substantially reduces the extent of Cys-oxidation and that isolated mitochondrial preconditioning reduces mitochondrial ROS production [57, 58], suggesting that the mitochondria has all the machinery necessary for ROS production and preconditioning protection. All these studies consistently demonstrate that initial mitochondrial ROS production caused by reperfusion is having an effect in protein modification, while the global extent or the nature of this damage remains unknown.

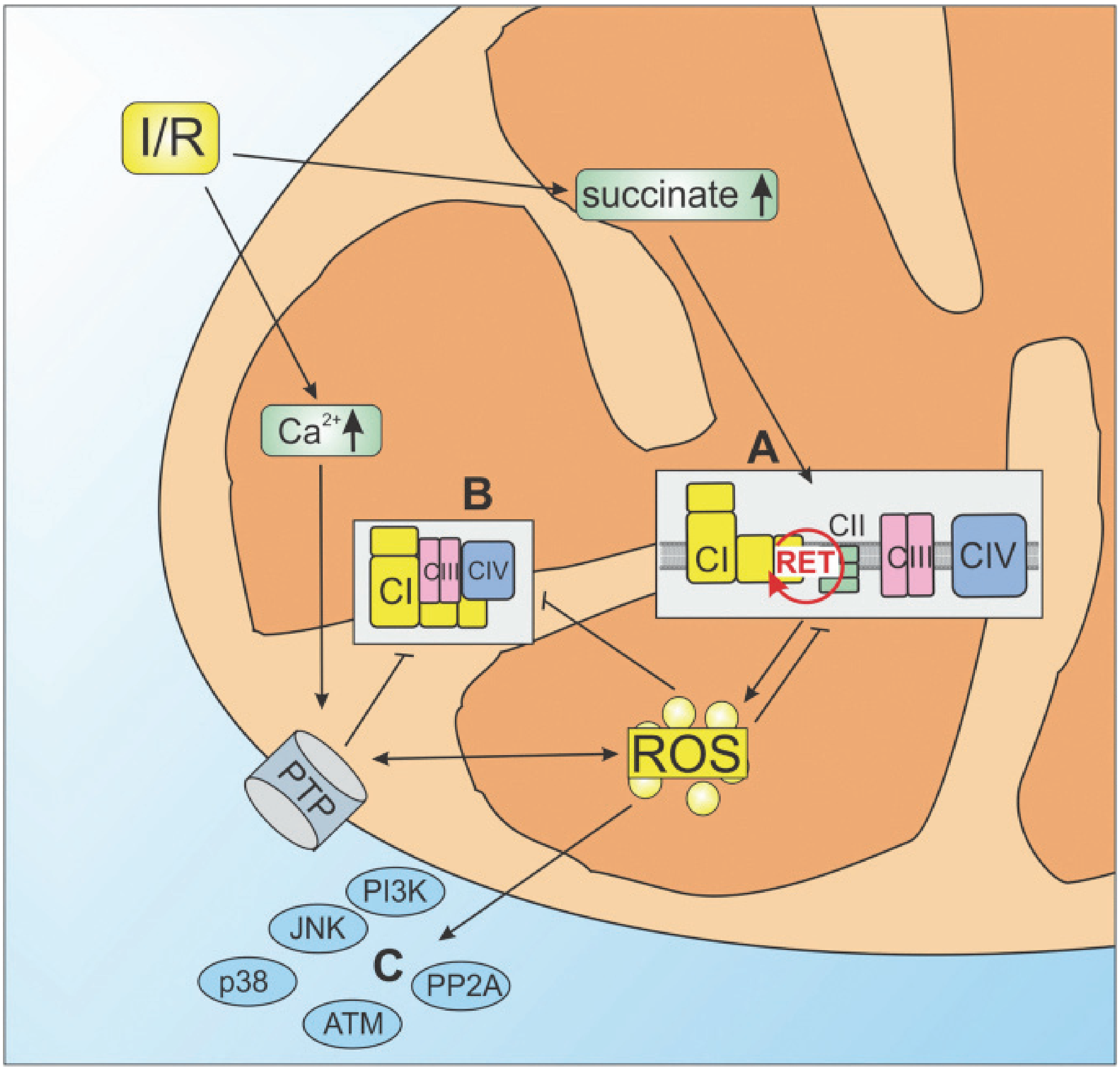

Figure 2. I/R induces mitochondrial ROS. During I/R, the activity of ETC complexes is reduced by an extraordinary increase in ROS, which is a result of succinate accumulation under ischemia. Upon reperfusion, succinate is rapidly oxidized resulting in a burst of ROS, probably mediated by a reverse electron transport from complex II to complex I. The increase of ROS together with an I/R-induced calcium influx into mitochondria opens the MPTP, further increasing ROS formation, decreasing ETC activity, and finally provoking cell death. **(Source Fuhrmann, D. C. et al, 2017 [59]).**

Mitochondrial ROS production after I/R has been considered as an initial damage burst that gradually recovers during the next few hours after reperfusion [47, 48, 50, 60, 61]. In contrast, the bimodal nature of edematous myocardial response [17-19], and the previous molecular characterization of the dynamic protein changes during the first week after reperfusion [20] suggests that there are more than one initial oxidative event. Supporting these assumptions, some authors have showed an increase in 4-HNE and MDA lipid-peroxidation markers peaking as late as 24h after reperfusion [62, 63]. Unlike mitochondrial ROS, these studies suggest the role of NADPH oxidases as major sources of later ROS production in the heart and mediating myocardial I/R injury. Additionally, authors described that this peak of 4-HNE and MDA can be markedly ameliorated at 4h after reperfusion in mice with the administration of interleukin-37 [63]. Interleukin-37 is a newly identified member of the IL-1 family, and functions as a fundamental inhibitor of innate immunity and inflammation. It has been thoroughly reviewed that early after reperfusion, tissue injury and necrosis initiate an inflammatory phase [8, 64]. It consists of an intense inflammation and the dynamic recruitment of neutrophils, monocyte/macrophages, dendritic cells, and lymphocytes. Furthermore, it has been suggested that part of the myocardial ROS could be generated by infiltrated leucocytes, especially activated neutrophils in the injured myocardium [65], but the relation between myocardial injury and neutrophil infiltration remains unknown. These results suggests that the innate immune and inflammatory responses are playing a major role in later I/R injury, which might be part of a different oxidative event in the myocardium.

Very recently, Aleksandra Binek, from our group, described in her PhD thesis [66] an analysis of the Cys redox status in ischemic and remote tissue in a pig model at 2h, 24h, 4 days and 7 days after I/R. In this study, the authors showed that, while no apparent increase in thiol-redox levels was detected in the remote tissue, data from pooled (n=5) protein extracts revealed a very clear transient increase in reversible oxidation of Cys sites in the infarcted area, peaking at 24h post-reperfusion (Figure 3) but starting at 2h after reperfusion. The previous results from our group [20] described that early after reperfusion, the ischemic myocardium showed a coordinated increase in the expression of proteins involved in acute-phase response signaling, response to wounding, wound healing, blood cell adhesion, and production of nitric oxide and reactive oxygen species. These processes find its peak at 24h and remain activated during the first week of I/R in agreement with the presented Cys-oxidation increase. These results also confirmed that there are relevant oxidative processes going on in the ischemic tissue before 120 minutes after reperfusion.

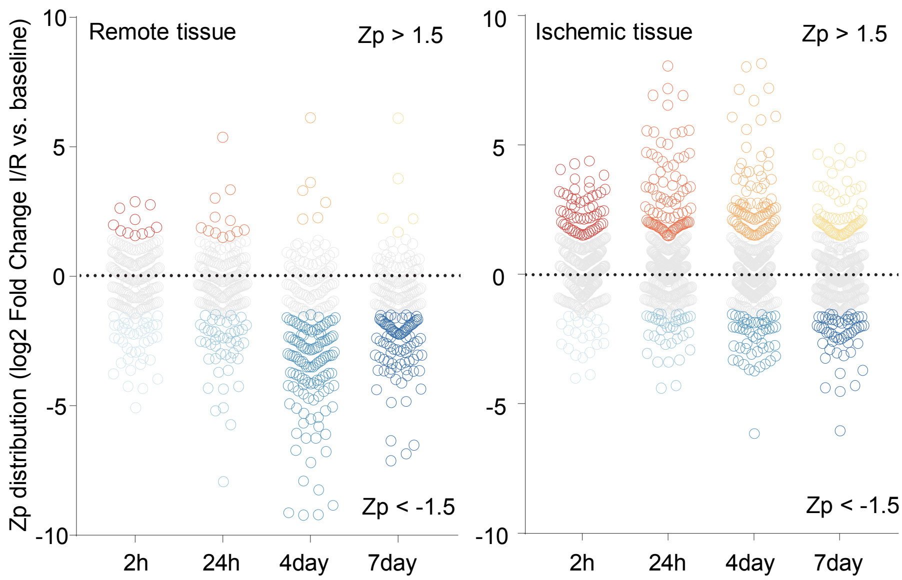

Figure 3 Cysteine reversible oxidation in the infarcted and remote tissues during the first week after MI. Oxidized Cys-peptides changes along time course (2h-7 days) in the remote and ischemic tissue. Total population of oxidized cysteines Zp values are reported as the log2-fold changes expressed in units of standard deviation around the averages with respect to controls. Data from Aleksandra Binek PhD Thesis [66].

Despite all these advances, to date there have been no systematic studies on the protein modification changes occurring in the post-reperfused myocardium along time after I/R. Considering that it has been showed that myocardial response to reperfusion does not remain stable during the first week after I/R [17-19] and, additionally, there are many relevant proteomic and redox changes taking place in the tissue [20], local and time-restricted studies remain insufficient. Ample temporal information about the extent of I/R-induced proteome-wide modifications, their nature and pathophysiological source is needed to establish timely and properly addressed administration of antioxidant therapies, which would in turn more effectively minimize the infarct size.

MS based proteomics and PTM analysis

Enormous efforts are made to get a complete glimpse of PTMs in biological systems, but we are still far away from understanding and unravelling the combinatorial complexity of PTMs. In spite that MS is without any doubt the most powerful technique for PTMs identification and quantitation, and that a large number of relevant PTMs can be directly characterized in biological samples without prior enrichment, PTMs analysis in high throughput proteomics experiments is rarely performed in the routine. This is because database search engines used in proteomics need the exact change in mass and knowledge about the modifiable sites, and only a few PTMs (typically less than four) can be identified at the same time, due to the exponential increase in searching space. Hence, PTMs have to be searched consecutively, and analyzing only the most common modifications in just one high throughput experiment becomes so time-consuming that it is poorly affordable in the practice. A related recently reported problem is that accurate PTMs identification makes it necessary to compute the local FDR (False Discovery Rate; i.e. in the population of peptides with the modification), which may be considerably different from the global FDR (calculated with all the peptides) [67]. Thus, another currently unresolved challenge in the field is the identification of large number of PTMs without losing the identification accuracy provided by the local FDR.

Recently, a novel mass-tolerant database searching method has been proposed capable of identifying a considerable proportion of PTMs in high throughput experiments [68], revealing that many of the unassignable spectra in proteomics data represent peptides with post-translational modifications. Later report showed that mass-tolerant database search can be performed at faster speeds using fragmentation-ion indexing algorithms [69]. Although these methods are not able to identify the modified sites and misses many modifications, they opened the possibility of real hypothesis-free high-throughput systematic study of PTMs by MS.

On the other hand, quantification of PTMs is also very challenging. First, PTM-containing peptides are often low abundant. Second, the very high dynamic range of protein concentrations in a cell presents serious difficulties for the quantification of PTMs. Third, PTM quantification not only has to cover the proteins change in abundance but also the determination of the modification site. Many algorithms [70, 71] have provided a promising way for quantification of proteins and can be directly extrapolated to PTMs. However, these methods lack a generic quantification model for PTMs and a general statistical model for the analysis of data of this nature.

Our group recently reported Comet-PTM [72], an improved mass-tolerant database search engine for comprehensive identification of PTMs, which enhances the coverage attained by other existing algorithms, assigns the modified residues with an estimated accuracy of 85%, and enables their quantitative analysis through an integrated statistical model. Comet-PTM takes into account the mass shift produced by the modification in the fragmentation series, producing the same score as a narrow-tolerance database search using the same mass increment as a variable modification. This method also introduces a conservative three-layered approach to control the FDR of peptide identification: local, peak and global FDR.

Many of the quantitation limitations can be dealt with in a single statistical framework previously developed in our laboratory called weighted spectrum, peptide, and protein model (WSPP) [73]. WSPP model allows a systematic comparison and establishes a validity of null hypothesis at each one of the levels (spectrum, peptide and protein), which allows a more accurate modelling of the heterogeneous variance at all levels. Therefore, the statistical approach applied by this method enables quantitative analysis of the modified peptidome within the same framework used to analyze the unmodified proteome; this approach thus allows coherent interpretation of all the results and opens the way to integrated systems-biology analysis. Along with WSPP model, another model developed by our group called systems biology triangle (SBT) allows the study of protein coordination by pairwise quantitative proteomics [74].

Thus, this revolutionary PTM approach could be coupled with the dynamic thiol redox status analysis using differential alkylation technology [57] to study labile Cys modifications and irreversible protein modifications at different time-points after I/R in pig models, as well as the proteome global changes.

Objectives

The extent of ischemic injury produced by acute myocardial infarction (AMI) is critical to determine the subsequent treatment for the chronic complications that infarct survivors suffer. Despite the efforts devoted to study molecular mechanisms that regulate cardiac remodeling after AMI, it is mandatory to understand the crucial molecular events in order to improve the prediction of disease evolution after ischemia/reperfusion (I/R). Previous thiol oxidation, proteomics and physiopathological studies, as well as the vast knowledge of this area of research, have suggested the presence of more than one systemic molecular event in the ischemic myocardium during the first week after I/R.

Therefore, in this Doctoral Thesis we have pursued the following objectives:

1) Study the global thiol redox proteome events in early time points after AMI, from minutes to days after reperfusion, in the ischemic area of heart using a large pig model of I/R.

2) Identify proteome-wide, irreversible post-translational modifications and quantify their changes after AMI and study their relation to protein changes and chemical alterations.

3) Analyze the effects of cardioprotective treatments in protein modifications in the infarcted tissue.

4) Study the molecular impact of AMI on the remote myocardium in the early time points after I/R.

Materials and Methods

Study Design of the time-course after I/R

Pig I/R experiments were performed on a total of 40 castrated male Large-White pigs weighing 30 to 40 kg and were approved by the Institutional Animal Research Committee. The study design is summarized in Figure 5 in the *Results* section. In 36 pigs reperfused acute myocardial infarction (AMI) was induced experimentally by closed-chest 40-minute mid left anterior descending coronary artery occlusion. These pigs were sacrificed at 20 minutes (n=4), 40 minutes (n=4), 80 minutes (n=4), 2 hours (n=4), 6 hours (n=4), 12 hours (n=4) and 24 hours (n=4) after reperfusion. Four animals were sacrificed at 120 minutes after artery occlusion without reperfusion (120min NOR); and four animals were subjected to ischemic preconditioning prior to I/R and sacrificed at 24h (24h PreC). The other four pigs were sacrificed with no intervention other than baseline CMR, and served as controls. CMR scans were performed at every follow-up stage until sacrifice by Borja Ibañez's Laboratory at CNIC. Animals were immediately euthanized after the last follow-up CMR scan, and transmural myocardial tissue samples from ischemic and remote areas were rapidly collected for proteomics evaluation. Based on anatomical correlates and standard left ventricle segmentation, those areas from mid-apical ventricular short axis slices matching regional contractility analysis were selected for sampling collection. For mice I/R experiments, we used wild-type 8–13-week-old C57BL/6 mice. The study design is summarized in Figure 32 in the *Results* section. Three mice were sacrificed with no intervention and served as controls. In the other mice, surgically-induced MI was performed as previously described [75] and sacrificed at 10 minutes (n=3), 20 minutes (n=3), 40 minutes (n=3), 80 minutes (n=3), 2 hours (n=3), 6 hours (n=3), 12 hours (n=3), 24 hours (n=3) and 48 hours (n=3) after reperfusion.

Animal Experimentation

Animal experimental procedures related to the myocardial infarction pig and mouse models were carried out and kindly provided by the members of the Translational Laboratory for Cardiovascular Imaging and Therapy under the supervision of the principal investigator Borja Ibañez at CNIC.

Myocardial infarction procedure in pig

The I/R protocol has been detailed elsewhere [17]. Anesthesia was induced by intramuscular injection of ketamine (20 mg/kg), xylazine (2 mg/kg), and midazolam (0.5 mg/kg) and maintained by continuous intravenous infusion of ketamine (2 mg/kg/h), xylazine (0.2 mg/kg/h), and midazolam (0.2 mg/kg/h). Animals were intubated and mechanically ventilated with oxygen (fraction of inspired O_2: 28%). Central venous and arterial lines were inserted, and a single bolus of unfractioned heparin (300 IU/kg) was administered at the onset of instrumentation. The left anterior descending coronary artery, immediately distal to the origin of the first diagonal branch, was occluded for 40 minutes with an angioplasty balloon introduced via the percutaneous femoral route using the Seldinger technique. Balloon location and maintenance of inflation were monitored angiographically. After balloon deflation, a coronary angiogram was recorded to confirm patency of the coronary artery. A continuous infusion of amiodarone (300 mg/h) was maintained during the procedure in all pigs to prevent malignant ventricular arrhythmias. In cases of ventricular fibrillation, a biphasic defibrillator was used to deliver non-synchronized shocks.

Methods for I/R in mice

Male 8–12-week-old mice were subjected to 40 min occlusion of the LAD coronary artery followed by 10 min, 20 min, 40 min, 80 min, 2 hours, 6 hours, 12 hours, 24 hours or 48 hours of reperfusion. The I/R procedure was performed as previously described [75]. For the LAD procedure, mice were intra-peritoneal anesthetized with ketamine (60 mg/kg), xylacine (20 mg/kg), and atropine (9 mg/kg). Fully asleep animals were intubated and temperature controlled throughout the experiment at 36.5 °C to prevent hypothermic cardioprotection. Thoracotomy was then performed and the LAD was ligated with a nylon 8/0 monofilament suture for 40 min. The electrocardiogram was monitored to confirm total coronary artery occlusion (ST-segment elevation) throughout the 40 min ischaemia.

Neutrophil depletion procedure

Neutrophil depletion was performed as described before [76]. Briefly, Neutrophils were depleted in C57BL/6 male by i.v. injection of 50 μg anti-mouse Ly6G at 24h and 48h prior to I/R and sacrificed 24h after reperfusion (n=3). The study design is summarized in Figure 36 in the *Results* section. A second group consisting on three mice were injected with IgG Antibody as vehicle and subjected to I/R and 24h of reperfusion. A third group of three mice with no injection were also sacrificed 24h after reperfusion (n=3). Nine additional mice from the three previous groups were sacrificed without I/R intervention: control without injection (n=3), IgG injection (n=3) and Ly6G injection (n=3).

Proteomics analysis

Proteomics protocol is schematized in Figure 4.

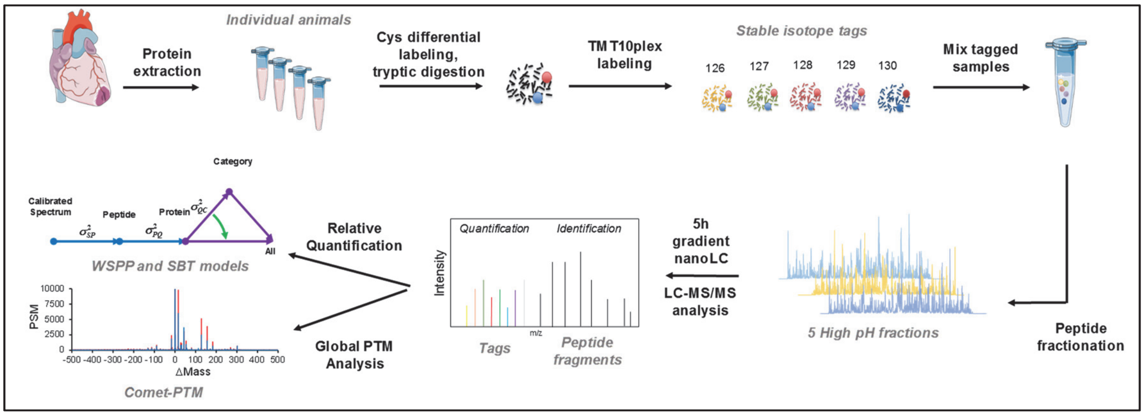

Figure 4 Proteomics protocol scheme. For proteomic analysis, remote and ischemic tissue samples from pig and whole hearts from mice were processed for protein extraction, tryptic digestion, differential Cys labelling, multiplexed stable isotope labelling (TMT 10-plex), and high pH fractionation followed by nano-liquid chromatography-tandem mass spectrometry (nanoLC-MS/MS), redox, PTMs analysis and systems biology analysis.

Tissue sample preparation for mass spectrometry analysis

To compare the pattern of protein alterations produced by I/R, myocardial tissue samples (from the ischemic and remote regions) were collected from the control group (no intervention) and at 20 min, 40 min, 80 min, 2 hours, 6 hours, 12 hours and 24 hours time-points after reperfusion. Samples from the ischemic and remote myocardium of all animals were collected within minutes of euthanasia and processed for proteomics analysis. Protein extracts from the homogenized tissue were obtained using the ceramic beads (MagNa Lyser Green Beads apparatus, Roche, Germany) in extraction buffer 50mM Tris-HCl, 1mM EDTA, 1.5% SDS, 50mM iodoacetamide (IAM), pH 8.5. Protein extracts were quantified and pooled accordingly to their concentration for each time-point. We applied a filter-based modification of the GELSILOX technology [77], which allows a simultaneous quantitative analysis of the alterations in the redox state of the Cys sites and of protein abundance [73, 74]. Briefly, proteins were extracted in the presence of an alkylating agent (IAM) that blocks free (reduced) thiol groups. Then, proteins were loaded on a FASP filter (Expedeon, San Diego, CA), which was used as a reaction chamber to 1) wash-away detergents and other contaminants that would hinder tryptic digestion; 2) reduce Cys with dithiothreitol (DTT); 3) alkylate previously oxidized Cys with 50mM methyl methanethiosulfonate (MMTS) and 4) trypsin-digest proteins. Thus, the original redox state of the Cys-containing peptides is determined by the specific mass shift introduced by each alkylating agent in the precursor ion and the fragments. Equal amounts of the resulting peptides were labelled with TMT 10-plex reagents (Thermo Scientific, San Jose, CA, USA).

Peptide fractionation

Labeled peptides were separated into 5 fractions using high pH reversed-phase peptide fractionation (Thermo Scientific) and graded concentrations of acetonitrile (ACN) in triethylamine (0.1%). Desalted and dried peptides were taken up in 300µl of 0.1% trifluoroacetic acid (TFA) solution. The spin column was equilibrated by passing 300µL of ACN twice, followed by 2x300µL of 0.1% TFA solution. Samples were applied and columns were centrifuged at 3000 x g for 2 minutes. Columns were then washed with 300µL of water. Bound peptides were eluted into 5 fractions with 300 µL of freshly prepared elution solutions: (1) 12.5% ACN, 87.5% triethylamine; (2) 15% ACN, 85% triethylamine; (3) 17.5% ACN, 82.5% triethylamine; (4) 20% ACN, 80% triethylamine and (5) 50% ACN, 50% triethylamine. Obtained fractions were dried and stored at −20°C until MS analysis.

Liquid chromatography tandem mass spectrometry (nanoLC-MS/MS)

For shotgun proteomics analysis, the tryptic peptide mixtures were subjected to nanoLC-MS/MS. High-resolution analysis was performed on a nano-HPLC Easy nLC 1000 liquid chromatograph (Thermo Scientific, San Jose, CA, USA) coupled to a QExactive HF Hybrid Quadrupole-Orbitrap mass spectrometer (Thermo Scientific). Peptides were suspended in 0.1% FA, loaded onto a C18 RP nano-precolumn (Acclaim PepMap100, 75-µm internal diameter, 3-µm particle size and 2-cm length, Thermo Scientific), and separated on an analytical C18 nano-column (EASY-Spray column PepMap RSLC C18, 75-um internal diameter, 3-um particle size and 50-cm length, Thermo Scientific) in a continuous gradient (8–31%B for 240 min, 31–90%B for 2 min, 90%B for 7 min, 90-5%B for 3 min and 2%B for 30 min, where A is 0.1% formic acid in HPLC H_2O and B is 90% ACN, 0.1% formic acid in HPLC grade H_2O). Spectra were acquired using full ion-scan mode over the mass-to-charge (m/z) range 390–1500 and 70,000 FT-resolution. MS/MS was performed on the top twenty ions in each full MS scan in data-dependent acquisition mode with 45s dynamic exclusion enabled. In label-free experiments, MS data were acquired with a Top10 data-dependent MS/MS scan method (topN method) with 30,000 FT-resolution.

Protein identification and quantification

Proteins were identified in the raw files using the SEQUEST HT algorithm integrated in Proteome Discoverer 2.1 (Thermo Finnigan). MS/MS scans were matched against a combined pig and human database (UniProtKB/Swiss-Prot 2017_06 Release). For database searching, parameters were selected as follows: trypsin digestion with 2 maximum missed cleavage allowed, precursor mass tolerance of 800 ppm, and a fragment mass tolerance of 0.02 ppm. The N-terminal and Lys TMT modifications were chosen as fixed modifications, whereas Met oxidation, Cys carbamidomethylation, and Cys methylthiolation were chosen as variable modifications. The same MS/MS spectra collections were searched against inverted databases constructed from the same target databases. SEQUEST results were analyzed by the probability ratio method [78]. False discovery rate (FDR) was calculated for peptides identified in the inverted database search results using the refined method [79, 80].

Dynamic protein expression profiles after myocardial I/R were characterized using the relative quantification approach by TMT 10-plex stable isotope labeling (SIL) with tandem mass spectrometry (MS/MS). Quantitative information was extracted from MS/MS spectra of TMT-labeled samples using an in-house MSQL library-based R script. The quantitative information from TMT reporter intensities was integrated from the spectrum level to the peptide level and then to the protein level on the basis of the WSPP model [57, 73] using the Generic Integration Algorithm (GIA) [74] . Briefly, for each sample i the values $x_{qps} = \log_2 S_i/C$ were calculated, where S_i is the intensity of the TMT reporter corresponding to sample i in the MS/MS spectrum s coming from peptide p and protein q, and C is the average intensity of all the TMT reporters from the control samples, which is used as a common reference. The $\log_2$-ratio of each peptide (x_{qp}) was calculated as the weighted average of its spectra, the protein values (x_q) were the weighted average of its peptides, and the grand mean ($\bar{x}$) was calculated as the weighted average of all the protein values [73] . The statistical weights of spectra, peptides and proteins (w_{qps}, w_{qp} and w_q, respectively) and the variances at each one of the three levels ($\sigma_{\mathbf{S}}^2$, $\sigma_{\mathbf{P}}^2$, and $\sigma_{\mathbf{Q}}^2$, respectively), were calculated as described [73] .

The spectrum, peptide and protein variances and the protein values were firstly determined including only non-modified peptides. In a second step, the modified peptides were included in the analysis, which was performed using the variances and protein values calculated previously. For each modified peptide, the standardized variable (z_{pq}) was calculated as

$$z_{pq} = \left(x_{qp} - x_q\right) \sqrt{w_{pq}} \sqrt{\frac{n_p}{n_p - 1}}, \qquad n_p > 1$$

where n_p is the number of non-modified peptides with which the corresponding protein was quantified. z_{pq} expresses the deviation between the peptide $\log_2$-ratio and the corresponding protein value in units of standard deviation. In absence of changes, the distributions of z_{pq} follows very closely the normal distribution $N(0,1)$ validating the accuracy of the model.

As input, WSPP uses a list of quantifications in the form of log2-ratios (for example a condition versus control sample) with their statistical weights. From these, WSPP generates the standardized forms of the original variables by computing the quantitative values expressed in units of standard deviation around the means (Zq). For the protein functional analysis, we used the Systems Biology Triangle (SBT) model developed in our group, which estimates functional category averages (Zc) from protein values by performing the protein-to-category integration. To facilitate detection of similar categories (categories sharing many proteins), a clustering algorithm was applied, as described [74].

Label Free (LF) absolute quantification method implemented in MaxQuant proteomics identification and quantitation software [81] was used for the analysis of the label-free proteomics experiments. We express the protein abundances as percentage of the identified proteome, obtained by normalizing the LF intensities of proteins of interest to the sum of all protein intensities.

Protein functional annotation

Quantified proteins were functionally annotated using the Ingenuity Knowledge Database (IPA) [82, 83] and DAVID [84]. The DAVID repository (david.ncifcrf.gov) included 13 functional databases, including Gene Ontology (www.geneontology.org), KEGG (www.genome.jp/kegg), and Panther (www.pantherdb.org), among others.

PTM identification and annotation

For the global PTM analysis, all searches were performed with Comet-PTM as specified before [72] using trypsin digestion without missed cleavages and fixed TMT labeling at N-terminal and Lys (229.162932 Da). Precursor ion tolerance was set to 500 Da. Output files from Comet-PTM were further analyzed using SHIFTS (Systematic Hypothesis-free Identification of modifications with controlled FDR based on ultra-Tolerant database Search) [72]. Bin was set to 0.001 Da for DeltaMass recalibration, and peptide identification filters were set at 1% for peak and local FDR and 5% for Global FDR. A Python in-house script was used for semisupervised annotation of the nature of peptide modifications. The script searched DeltaMass values against Unimod database [85] (http://www.unimod.org), taking into account the modified amino acid according to Comet-PTM output and also the preceding and consecutive residues, comparing them with the list of amino acids that could be subjected to the modification according to Unimod. If no amino acid was matched, the modification was considered as unassigned and was not taken into account for the analysis. Unexplained DeltaMass values were termed as unknown and were not taken into account for the analysis.

Enrichment analysis

To account for the proteome background, enrichment analysis for PTMs was performed calculating a hypergeometric p-value [86] using the total population of PTMs as the reference population. Biological processes enrichment analysis was performed calculating the hypergeometric p-value [86] for the enrichment of functional categories from GO database [87], using total count of PSMs as frequency value. To account for the contribution of the background cardiac proteome, we used the identified non-modified proteome as reference population.

PCA and HCA analysis

We performed the Principal Components Analysis (PCA) using the 'stats' package as part of R [88] and ggplot2 [89] for data visualization. Hierarchical Clustering Analysis (HCA) was performed using R [88]. First, we computed the distance matrix for all modified peptides applying the 'factoextra' package [90] in R and using Pearson correlation coefficient as distance measure. Then, we ordered the correlation matrix using the hierarchical clustering algorithm in the 'corrplot' [91] R package.

Immunoblotting

Western blot was performed according to standard protocols. Briefly, 10µg of heart tissue extracts were loaded per lane separated on the 4-10%

polyacrylamide gel and transferred to polyvinylidene fluoride (PVDF) (Immobilon-FL, Milipore) membranes for fluorescence applications. Results were obtained using the 4-hydroxynonenal (4-HNE, Abcam, ab46545) antibodies. Secondary antibodies goat anti-mouse IgG DyLight 800 (Rockland, 610-145-121) and goat anti-rabbit IgG Alexa Fluor 680 (Thermo Fisher Scientific, A-21076) were used against the corresponding primary antibodies and the images were acquired with the ODYSSEY Infrared Imaging System (LI-COR).

Myeloperoxidase activity detection

MPO activity was measured as an indicator of neutrophil infiltration in the ischaemic myocardium using a Myeloperoxidase Colorimetric Activity Assay Kit (Abcam, ab105136) according to the manufacturer's instructions. One unit of MPO is defined as the amount of MPO that hydrolyzes the substrate and generates taurine chloramine to consume 1 mmol trinitrobenzene (TNB) per min at 25°C.

Assays for Oxidative Stress Measurement

Malondialdehyde (MDA)

Cardiac tissue homogenates were assessed for the presence of lipid peroxidation product (MDA presence) (Abcam; ab118970) according to the manufacturer's instructions. Briefly, ischemic tissue from pig at different times after I/R were collected in 303µL of MDA lysis solution using a TissueLyser LT (Qiagen, USA) homogenizer precooled on ice. Samples were then centrifuged at 13.000 x g for 10 min and total protein content was quantified using RCDC Assay (BIORAD). To generate MDA-TBA adduct, 600µL of TBA reagent was added into each vial containing the supernatant previously collected. Samples were then incubated at 95°C for 60 min and subsequently cooled in an ice bath for 10 min. Each 800µl of TBA/sample and standard mix (for the standard curve calculation) were added in a 96-wells plate (BD science). The absorbance of TBA-MDA adduct was measured at 532 nm. The MDA concentration in standard and samples was determined from their absorbance as per the manufacturer's instructions.

H_2O_2 Measurement

H_2O_2 production was measured with an Amplex Red H_2O_2 assay kit (Molecular Probes; Invitrogen) according to the manufacturer's instructions. In brief, left ventricular blocks (30–50mg) were incubated with Amplex Red (100μmol/L) and horseradish peroxidase (1 U/mL) for 30 min at 37°C in Krebs–HEPES buffer protected from light. The supernatant was then transferred to a 96-well plate, and absorbance was measured (560 nm). Background fluorescence, determined in a control reaction without sample, was subtracted from each value. H2O2 release was calculated using H2O2 standards and expressed as micromoles per milligram of tissue.

Statistical and Data Analysis

Western blot analysis to determine significant differences between groups after densitometry analysis and statistical analysis of label free proteomics, enzymatic and biochemical assays were performed using the Mann-Whitney test, using the GraphPad Prism 7.02 software. The statistical differences in the peptide and protein quantitative values (Zp and Zq, respectively) between all I/R groups as well as the results of all experiments for nonreperfused and preconditioned experimental groups were evaluated by Kruskal-Wallis test. For the assessment of changes in the individual oxidatively modified peptides in the neutrophil depletion experiments we employed multiple t tests (P value <0.05) with Benjamini and Hochberg's FDR method post hoc correction (q value <0.05). For the experiments in pig model the threshold was set to P value <0.01 and q value <0.01.

Results

Early reperfusion induces two temporally separated oxidative episodes in the ischemic tissue

Previous Cys-redox proteomics study in a pig model of I/R at 2h, 24h, 4d and 7d after reperfusion showed an increase in Cys reversible oxidation peaking at 24h and already increased as early as 2h after reperfusion [66]. This results as well as the evidence in growing body of research in the area of early reperfusion-induced oxidation [92-100] led us to design a detailed timeline from the earliest moments (20min) up to 24h after reperfusion time in a pig model of I/R (Figure 5).

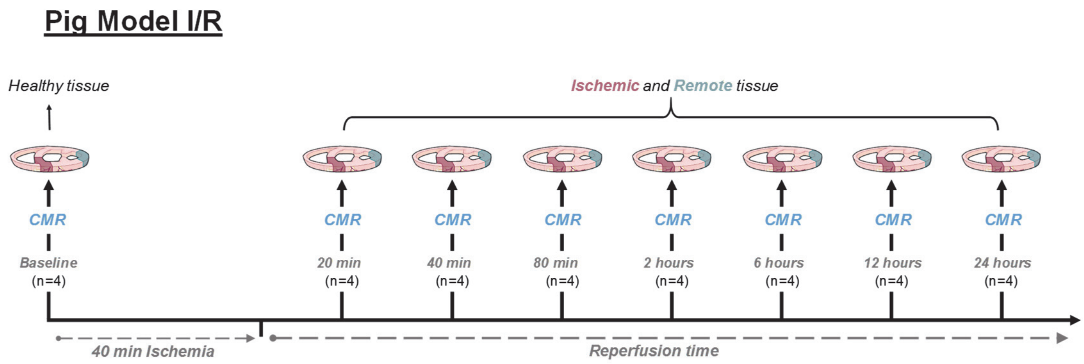

Figure 5 Study design. Pig model of ischemia reperfusion (I/R). The study population comprised 10 groups of pigs (n=4/group). Groups 1 to 8 were used for the analysis of redox, PTMs and protein expression changes during the first 24h after I/R in remote and ischemic tissue. Closed-chest 40min ischemia followed by reperfusion was performed and pigs sacrificed at 20min, 40min, 80min, 2h, 6h, 12h and 24h after reperfusion. Additional four sacrificed healthy pigs served as controls. CMR (cardiac magnetic resonance) scans were acquired by Borja Ibañez's group at CNIC (data not shown).

This new experimental setup allowed us to gain unique insights into the oxidative events taking place in the lesion area. The analysis of the dynamic thiol redox proteome allowed us to identify 491 oxidized and 1680 reduced Cys. Interestingly, this analysis revealed an increase in Cys-reversible oxidation (Figure 6).

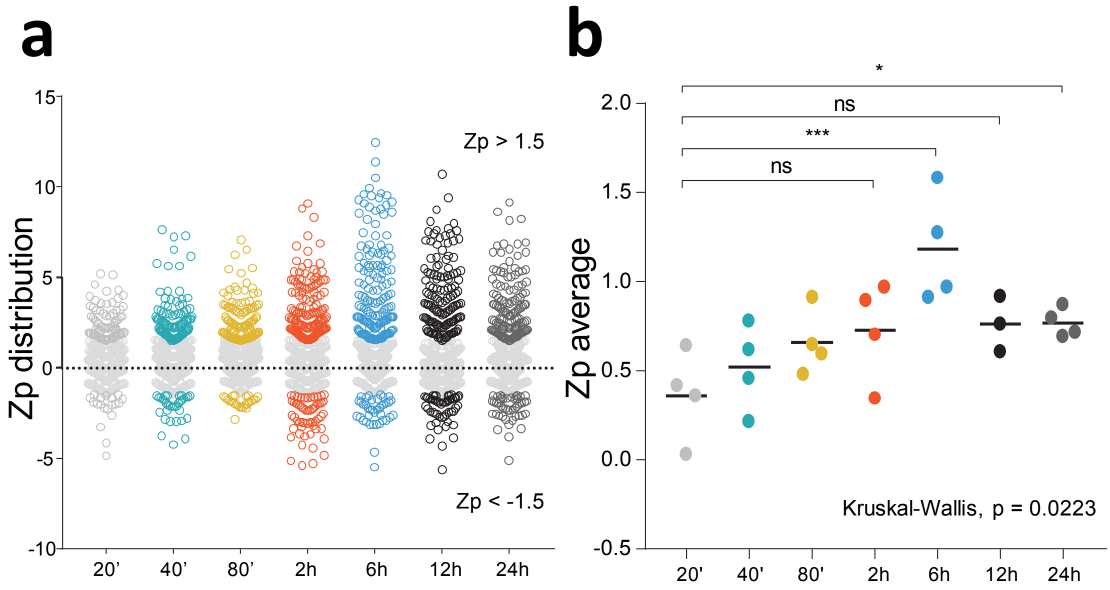

Figure 6 Reversible thiol redox alterations in the ischemic tissue during the first 24 hours after MI. Oxidized Cys-peptides changes along time course. (a) Total population of oxidized cysteines (491 peptides) Zp peptide values are reported as the log2-fold changes in each condition with respect to controls. (b) Zp averages are reported as the complete peptide population average value at each time point for each individual animal. ns indicates p value > 0.05, * Indicates p value < 0.05, *** indicates p value<0.001. P-values are calculated using Kruskal-Wallis test. Full list of oxidized and reduced Cys-containing peptides can be found in Supplementary Table S1.

The complete Cys population (Supplementary Table S1) of oxidized-Cys-containing peptides quantitative values (Zp; log_2 FC expressed in SD units) for each I/R time point with respect to the control group was subjected to hierarchical clustering analysis (HCA), revealing a subset of oxidized Cys population that significantly increase during 2h-24h after I/R (Figure 7, Supplementary Table S1, marked in red). This observation confirmed the previously mentioned maximal increase in Cys oxidation after 24h post-MI.

The high correlation of Zp values along the reperfusion time indicates that reversible oxidation affects the same peptide sequences (Figure 8). The experimental group of 6h reperfusion time had the highest correlation (R^2>0.7) with 3 other time points (2h, R^2=0.736; 12h, R^2=0.843; 24h, R^2=0.883), suggesting a focal time segment (2h to 24h) in the increase of reversible Cys oxidation (Figure 8).

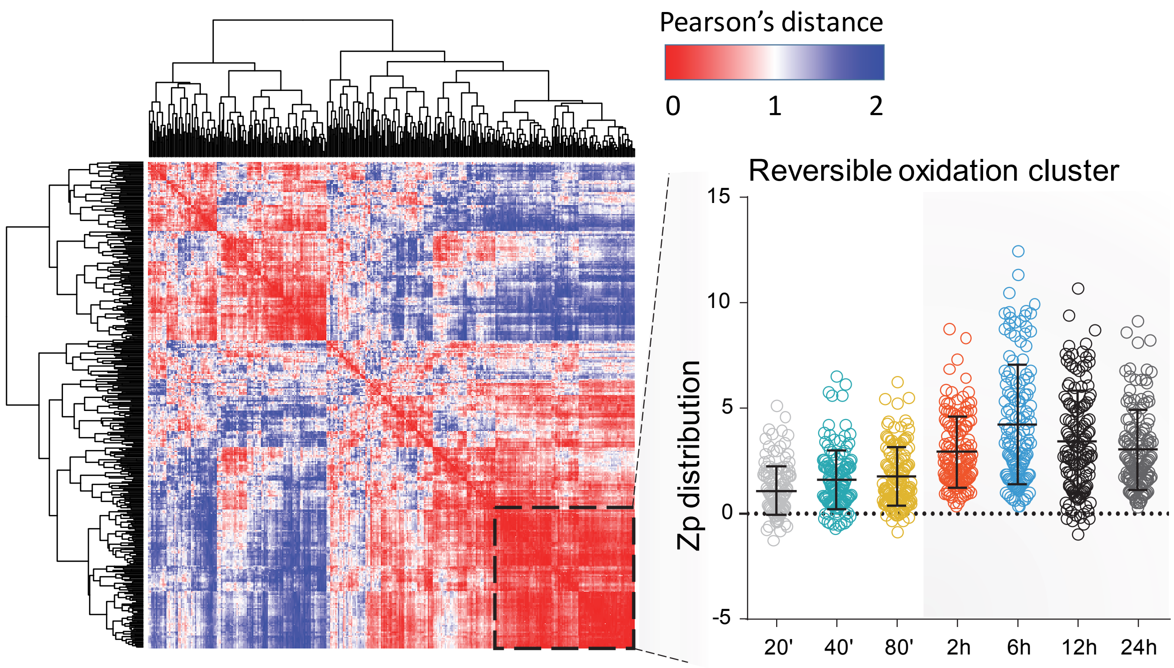

Figure 7 Hierarchical clustering Analysis (HCA) of Cys reversible oxidation. 491 Cys-oxidized peptides were subjected to HCA. First, the distance matrix was calculated between all peptides using Pearson correlation coefficient. Then, the obtained matrix was ordered using an hierarchical clustering algorithm described in Mat&Met section. A cluster of high similarity consisting on 128 oxidized peptides showed an increase in oxidation between 2h and 24h (Supplementary Table S1, marked in red). Zp values are reported as averages of 4 biological replicates for each peptide in each time point (log2-FC with respect to the controls).

To uncover the global PTMs status in the reperfused myocardial infarcted tissue we applied Comet-PTM [72], a suite of algorithms for comprehensive identification of detectable modifications with an accurate modified residue assignment, and quantification through an integrated statistical model.

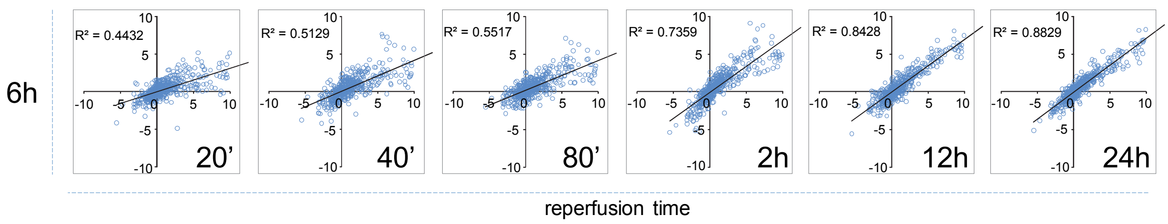

Figure 8 Correlation analysis of Cys-oxidized peptides Zp values at different time points. Correlation values were calculated as the coefficient of determination (R-Squared) between the peptides' averaged Zp values from each time point against Zp values from 6h.

This ultra-tolerant database search approach yielded more than 11500 peptide sequences with assigned mass differences (ΔM) that could potentially be PTM. To obtain a curated modified peptide list we considered modifications present in all biological replicates (n=4) and positioned in the expected amino acid according to Unimod database [85]. Moreover, we discarded combinations of various ΔM to ensure that measured peptide abundance changes were attributed to a single PTM. Chemical artefacts as well as modifications whose annotations were not recognized by Unimod were discarded from further analyses. With this approach, we were able to narrow down our curated dataset to 409 post-translationally modified peptides in approximately 150 proteins. Principal component analysis (PCA) of PTM changes showed a differential behaviour of two populations with distinguishing amino acid residues (Figure 9).

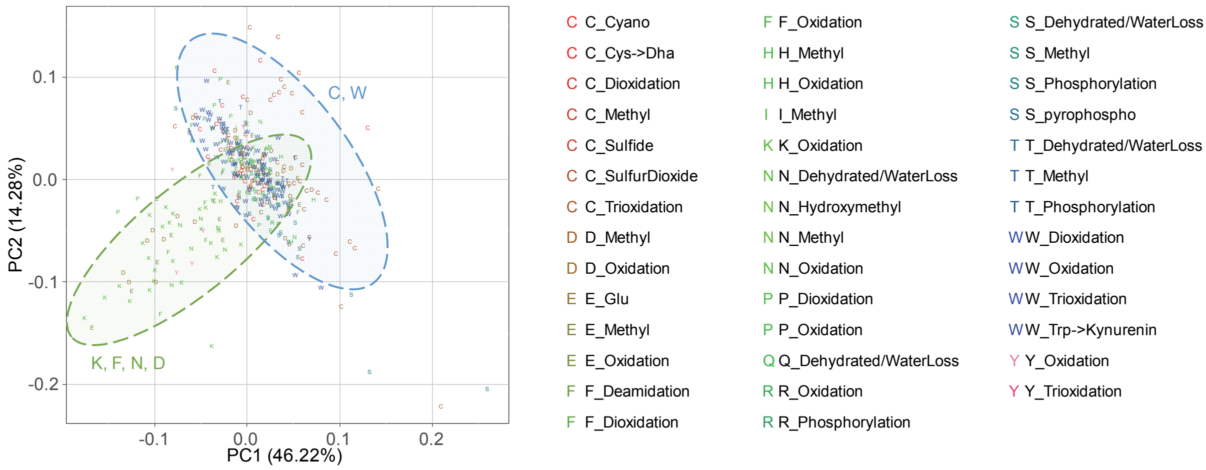

Figure 9 Principal Components Analysis (PCA) of PTMs. 409 peptides present in all biological replicates (n=4) and corresponding to known biologically relevant PTMs in the accurate modified residue were subjected to PCA analysis. The two shaded areas in green and blue show a distinctive behaviour of two groups of modified residues: monooxidations in Lys, Asp, Asn and Phe (K, D, N, F) and mono-, di- and trioxidations in Cys and Trp (C, W).

As this result suggested presence of distinct events (mainly oxidative), we carried out HCA to discern specific clusters of PTMs with similar behaviour along the reperfusion time-course. In agreement with PCA analysis, the clustering analysis revealed two different oxidative episodes within the first 24h after the onset of I/R (Figure 10).

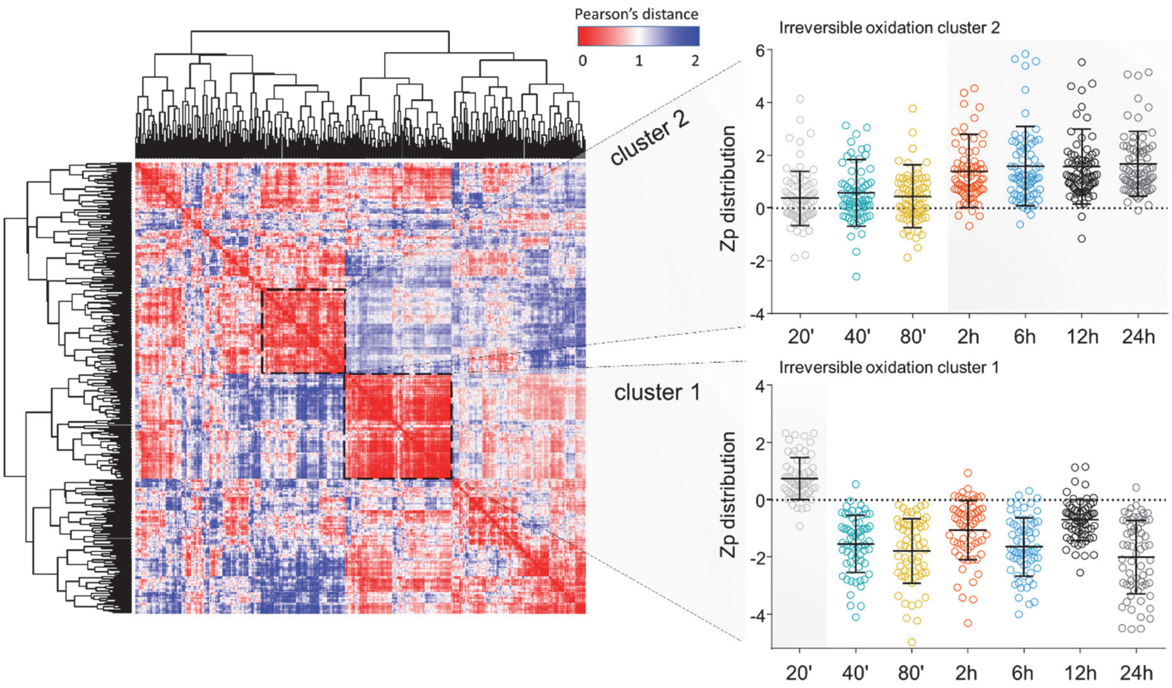

Figure 10 HCA of PTMs. 409 peptides present in all biological replicates (n=4) and corresponding to known biologically relevant PTMs in the accurately identified modified residue were subjected to HCA as in Figure 7. Two clusters of high similarity (cluster 1 and cluster 2) were selected and their peptides Zp values at different time points were reported as averages of four individuals with respect to the controls. In order to discard peptides that are not highly correlated (white fields) within the cluster 1, we only display peptides with a maximum Zp > 0 in at least one of the time points in the inset scatter plot. Only these peptides were considered for further functional enrichment analyses. Full list of modified peptides from cluster 1 and 2 can be found in Supplementary Tables S2 and S3).

One large cluster of irreversible oxidations (Figure 10, cluster 1, Supplementary Table S2) displayed an immediate increase (20min after reperfusion) of a specific peptide population. This subset was markedly represented by monooxidations that principally affect Lys, Trp, Phe, Asn and Asp (Figure 11a).

Absolute frequency (in PSMs) of different residues and modification together with the enrichment analysis also revealed that cluster 1 is significantly enriched (pvalue<0.0001) in PTMs such as Lys, Asn and Phe oxidation (Figure 11c-d).

a b

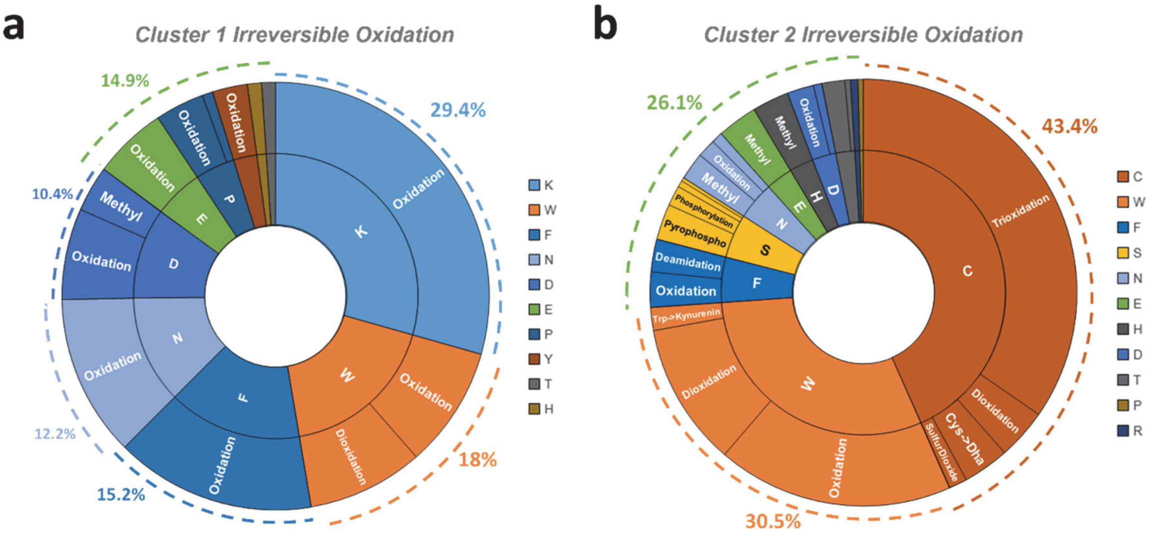

c

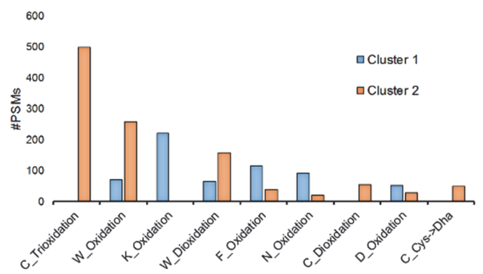

d

Residue and Modification	*p-values* Cluster 1	Cluster 2
K Oxidation	**<0.0001**	n.s.
F Oxidation	**<0.0001**	n.s.
N Oxidation	**<0.0001**	n.s.
D Oxidation	**0.0174**	n.s.
C Trioxidation	n.s.	**<0.0001**
W Oxidation	n.s.	**<0.0001**
W Dioxidation	n.s.	n.s.
C Dioxidation	n.s.	n.s.
C Cys->Dha	n.s.	n.s.

Figure 11 Characterization of the two irreversible oxidative events. (a) Protein modifications map of the first event of irreversible oxidation at 20 min after reperfusion (cluster 1, Supplementary Table S2). The circular inner bars and the outer bars show the modified amino acid residue and the modification type proportion (quantified in PSMs), respectively. Percentages are expressed in relation to the total number of PSMs in the cluster 1. (b) Protein modification map of the later event of irreversible oxidation at 2h-24h after reperfusion (cluster 2, Supplementary Table S3). (c) Total frequency (in PSMs) of each residue and modification in each cluster. Total PSMs count is calculated as the sum of all modified peptides of each individual (n=4). Only modifications with more than 50 PSMs are shown. (d) Hypergeometric p-values of each modification and amino acid site corresponding to each cluster. P-values were calculated as the probability of having more occurrences (PSMs) in each cluster in comparison to the total population of PTMs and modified sites analyzed by HCA. Only p-values from modifications with more than 50 PSMs are shown.

To study which processes were preferably modified in each cluster in respect with the background cardiac proteome, we performed an enrichment analysis of the biological processes using the total proteome as reference population (Table 1). This analysis demonstrated that immediate reperfusion-related increase in oxidations preferably affects ATP activity, cardiac contraction and stress and ROS response processes. Modified peptides affected early after reperfusion (20 min) and later (2h-24h) were grouped according to their affected processes (Table 2, Supplementary Table S4).

	Processes		Cluster 1	Cluster 2	Cys-Rev. Oxidation
ENRICHED IN CLUSTER 1	*ATP activity*				
		ATP binding [GO:0005524]	<0.0001	n.s.	n.s.
		ATPase activity [GO:0016887]	<0.0001	n.s.	n.s.
		ATP metabolic process [GO:0046034]	<0.0001	n.s.	n.s.
		Actin-dependent ATPase activity [GO:0030898]	<0.0001	n.s.	n.s.
	Cardiac Contraction				
		Muscle contraction [GO:0006936]	<0.0001	n.s.	n.s.
		Myosin filament [GO:0032982]	<0.0001	n.s.	n.s.
		Regulation of the force of heart contraction [GO:0002026]	<0.0001	n.s.	n.s.
		Striated muscle contraction [GO:0006941]	<0.0001	n.s.	n.s.
		Microfilament motor activity [GO:0000146]	<0.0001	n.s.	n.s.
		Myosin complex [GO:0016459]	<0.0001	n.s.	n.s.
	Stress and ROS response				
		Stress fiber [GO:0001725]	<0.0001	n.s.	n.s.
		Response to reactive oxygen species [GO:0000302]	<0.0001	n.s.	n.s.
ENRICHED IN CLUSTER 2 AND REV. OXIDATION	*Extracellular and Membrane*				
		Blood microparticle [GO:0072562]	n.s.	<0.0001	<0.0001
		Extracellular exosome [GO:0070062]	n.s.	<0.0001	0.0004
		Extracellular region [GO:0005576]	n.s.	<0.0001	<0.0001
		Extracellular space [GO:0005615]	n.s.	<0.0001	<0.0001
		Transmembrane transport [GO:0055085]	n.s.	<0.0001	<0.0001
		Cell adhesion [GO:0007155]	n.s.	<0.0001	<0.0001
	Other				
		Metal ion binding [GO:0046872]	n.s.	<0.0001	0.0032
		Gluconeogenesis [GO:0006094]	n.s.	<0.0001	<0.0001
		Protein complex [GO:0043234]	n.s.	<0.0001	<0.0001

Table 1 Functional enrichment of proteins impacted by the oxidative events after MI in the infarcted tissue of a pig model of I/R. Cluster 1 (early irreversible oxidation at 20 min), Cluster 2 (Irreversible oxidation at 2h-24h) and Cys reversible oxidation (2h-24h) P-values for enriched processes are shown. Enrichment analysis was performed by calculating the hypergeometric P-value for the enrichment of functional categories from GO database, using total count of PSMs as frequency value. To account for the contribution of the background cardiac proteome, we used the identified non-modified proteome as reference population.

We also detected a second pronounced cluster of irreversible oxidative modifications (Figure 10, cluster 2, Supplementary Table S3), which is constituted mainly by mono- and dioxidations in Trp and by di- and trioxidations in Cys (Figure 11b). This subset was found increased within 2h-24h, temporally coinciding with the increase of reversible Cys oxidation detected by dynamic thiol redox proteome analysis (Figure 6, Figure 7 and Figure 8) and reversible Cys oxidation detected before by our group [66]. Although we found mono- and dioxidations in Trp in both clusters (1 and 2), this residue is more frequently modified in the second cluster (p-value<0.0001, Figure 11c-d), similarly to the prevailing di- and trioxidations in Cys (p-value<0.0001, Figure 11c-d). What is more, this later irreversible oxidative event (cluster 2) and reversible Cys oxidation significantly affected extracellular and membrane proteins, as well as other metabolic and metal ion binding proteins (Table 1 and Table 2).

Table 2 Zp changes of modified peptides from enriched proteins in different clusters: Cluster 1 (early irreversible oxidation at 20 min), Cluster 2 (Irreversible oxidation at 2h-24h) and Cys reversible oxidation (2h-24h). Enrichment analysis was performed by calculating the hypergeometric P-value for the enrichment of functional categories from GO database, using total count of PSMs as frequency value and to account for the contribution of the background cardiac proteome, we used the identified non-modified proteome as reference population. Cys-reversible oxidation are shown as "@" in each peptide sequence. P-values for enrichment can be found in Table 1. Zp values are reported as the log2-fold changes expressed in units of standard deviation around the averages with respect to controls. Full list of enriched protein's modified peptides can be found in Supplementary Table S4.

Cluster	Enriched categories	Gene	Sequence	Modification
Cluster 1 Irreversible Oxidation — *ATP Activity, Cardiac Contraction, Stress and ROS response.*	ATP binding [GO0005524]	CKM	D[15.994843]IFDPIIQDR	D Oxidation
			ISVEAINSITGEF[15.994843]K	F Oxidation
			ISV[15.994843]EAINSITGEFK	E Oxidation
		CKMT2	EVENVAITAIEGI[15.994843]K	K Oxidation
		HEL-S-123m	TSIA[15.994843]IDTIINQK	D Oxidation
	muscle contraction [GO0006936]	CRYAB	VIGDVIEVHG[15.994843]K	K Oxidation
	myosin complex [GO0016459]	MYH16	IEE[15.994843]IEEEIEAER	E Oxidation
		MYL3	IEFTPEQIEEF[15.994843]K	F Oxidation
	actin-dependent ATPase activity [GO0030898] ATP binding [GO0005524] ATP metabolic process [GO0046034] ATPase activity [GO0016887] microfilament motor activity [GO0000146] muscle contraction [GO0006936] myosin complex [GO0016459] myosin filament [GO0032982] regulation of the force of heart contraction [GO0002026] response to reactive oxygen species [GO0000302] stress fiber [GO0001725] striated muscle contraction [GO0006941]	MYH6	I[15.994843]DEAEQIAIK	D Oxidation
		MYH	IIGSI[15.994843]DIDHNQYK	D Oxidation
			NITEEMAGIDEIIA[15.994843]K	K Oxidation
			IEIDDVTSNMEQII[15.994843]K	K Oxidation
			NI[15.994843]QEEISDITEQIGSSGK	N Oxidation
			N[15.994843]IQEEISDITEQIGSSGK	N Oxidation
			IEDEQAIGSQIQ[15.994843]K	K Oxidation
			IISNI[15.994843]FANYAGADTPVEK	F Oxidation
			NIQ[15.994843]EEISDITEQIGSSGK	E Oxidation
			DY[15.994843]HIFYQIISNK	Y Oxidation
			DYH[15.994843]IFYQIISNK	H Oxidation
			DYHIFYQIISN[15.994843]K	N Oxidation
			GQNVQQVMYATGAIA[15.994843]K	K Oxidation
			AQIEFNQI[15.994843]K	K Oxidation
			NN[15.994843]IIQAEIEEIR	N Oxidation
			IE[15.994843]IDDVTSNMEQIIK	E Oxidation
			IIN[15.994843]PAAIPEGQFIDSR	N Oxidation
			NIQEEISDITEQIGSSG[15.994843]K	K Oxidation
			N[15.994843]NIIQAEIEEIR	N Oxidation
			IE[15.994843]DEQAIGSQIQK	D Oxidation
Cluster 2 Irreversible Oxidation & Cluster Cys Rev. Oxidation — *Extracellular, membrane, metal ion binding proteins*	cell adhesion [GO0007155] extracellular exosome [GO0070062] extracellular region [GO0005576]	ACTN2	DGLGLC@ALIHR	C Rev. Oxidation
			ELPPDQAQYC@IK)	C Rev. Oxidation
			IASEIIEW[15.994843]IR	W Oxidation
			IASEIIEWI[15.994843]R	R Oxidation
			QFAAQANAIGPW[15.994843]IQNK	W Oxidation
			VGW[15.994843]EIIITTIAR	W Oxidation
			VGW[31.988578]EIIITTIAR	W Dioxidation
	blood microparticle [GO0072562] extracellular exosome [GO0070062] extracellular space [GO0005615]	AHSG	C@NLLVEK)	C Rev. Oxidation
			EPAC@DDVETEQAALAAVDYINK)	C Rev. Oxidation
			EPAC[31.988578]DDVETEQAAIAAVDYINK	C Dioxidation
			EPAC[47.984762]DDVETEQAAIAAVDYINK	C Trioxidation
		C3	DSC@VGTLVVK)	C Rev. Oxidation
			GIC@VADPYEVVVK)	C Rev. Oxidation
			VELLYNPAFC@SLATAK)	C Rev. Oxidation
		MSN	**EGIINDDIYC[47.984762]PPETAVIIASYAVQSK**	C Trioxidation
			EGILNDDIYC@PPETAVLLASYAVQSK)	C Rev. Oxidation
	extracellular exosome [GO0070062]	COMT	YLPDTLLLEEC@GLLR	C Rev. Oxidation
		VDAC1	YQIDPDAC@FSAK)	C Rev. Oxidation
		GPD1L	ITVVDDADTVELC@GALK)	C Rev. Oxidation
	extracellular exosome [GO0070062] extracellular region [GO0005576] extracellular space [GO0005615] transmembrane transport [GO0055085] blood microparticle [GO0072562]	CP	DLYSGLIGPLIVC@R	C Rev. Oxidation
			SGAGIDDSPC@IPWVYYSTVDQVK)	C Rev. Oxidation
		TF	DQYELLC@R	C Rev. Oxidation
			LLEAC@TFHSAK)	C Rev. Oxidation
			SSYIDC[-33.986144]IK	C Cys->Dha
			VTC@VAEELLK)	C Rev. Oxidation
	extracellular exosome [GO0070062] gluconeogenesis [GO0006094]	GAPDH	IVSNASC@TTNC@LAPLAK)	C Rev. Oxidation
			VPTPNVSVVDLTC@R	C Rev. Oxidation
		GOT2	**TC@GFDFTGALEDISK)**	C Rev. Oxidation
			TC[47.984762]GFDFTGAIEDISK	C Trioxidation
	metal ion binding [GO0046872]	OGDH	ELEQIFC@QFDSK)	C Rev. Oxidation
			FGLEGC@EVLIPALK)	C Rev. Oxidation
	transmembrane transport [GO0055085]	SLC8A1	GGGEDFEDTC@GELEFQNDEIVK)	C Rev. Oxidation

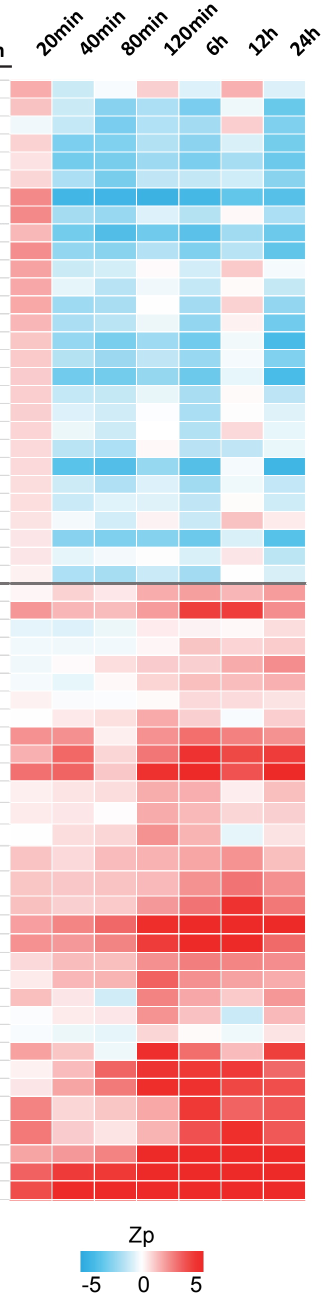

Interestingly, some residues from the same proteins were affected at the same time by different reversible and irreversible oxidations that are characteristic of this second wave and with the same pattern of changes (Table 2, sequences in bold, complete population in Supplementary Table S4), indicating that these residues are particularly sensitive to oxidation 24 h after I/R.

To summarize, two characteristic features of the first 24h of reperfusion were denominated by a short-term episode of irreversible monooxidations and a subsequent second episode comprised of reversible Cys thiol oxidations as well as di-and trioxidations found in Trp and Cys residues. Overall, these results indicate differences in nature of the two clusters of irreversible oxidation, suggesting different pathophysiological events associated with their occurrence.

Proteome changes mirror the oxidative alterations in the ischemic myocardium

We also analyzed the protein dynamic behavior in the ischemic proteome in the first 24 hours after I/R applying the systems biology triangle approach [74].

The study of protein coordinated behavior revealed an early (20-80 min after reperfusion) increase in processes responsible for cardiac muscle contraction (muscle myosin complex) and its regulation by calcium ion signaling, fatty acid beta-oxidation, acetyl-CoA transferase activity, carnitine shuttle sarcoplasmic reticulum (SR) membrane, RNA processing, ribosomal and DNA binding proteins (Figure 12, subset II) suggesting that within the first two hours after I/R several sarcomeric functional and energetic processes suffered alterations.

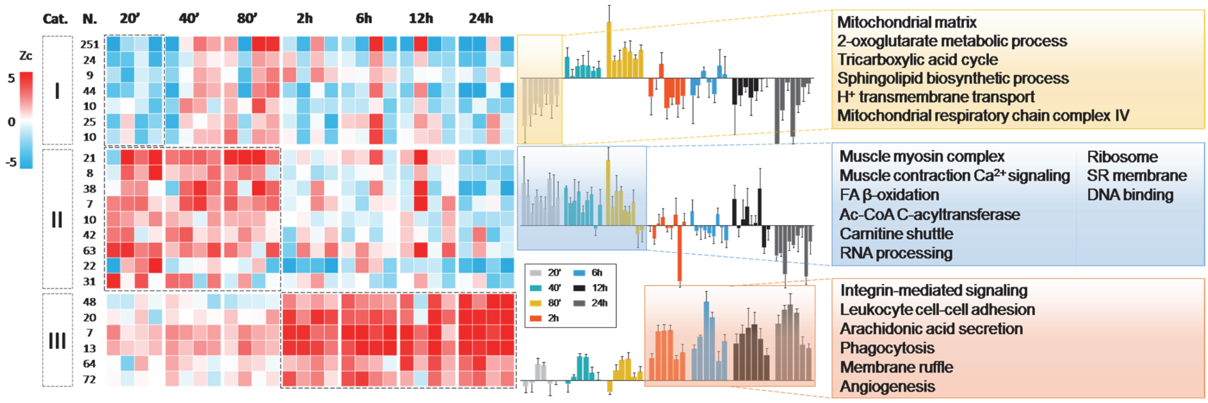

Figure 12 SBT analysis of early reperfusion after MI. Functional categories changes (Zc) over time (24h of reperfusion). Subset I include mitochondrial metabolism categories decreasing after 20min. Subset II contains biological processes increasing in early reperfusion (20min-80min) that mainly involve cardiac contraction and lipid metabolism proteins. Subset III represents leukocyte migration related protein categories that increase 2h-24h post-MI. Full list of protein's Zq changes for each category can be found in Supplementary Table S5.

We also observed an initial temporary decrease (20 min) in the mitochondrial matrix processes that principally involved proteins associated with tricarboxylic acid (TCA) cycle, 2-oxoglutarate and glutamate metabolism, sphingolipid biosynthesis, H^+ ion transmembrane transport and respiratory complex IV (Figure 12, subset I). These early disturbances timely correlate with the appearance of irreversible oxidation (Figure 10, cluster 1), which characteristically affected proteins implicated in ATPase activity, ATP metabolic process and muscle contraction (Table 1). After observing very early alterations in the mitochondrial matrix proteins (Figure 12), we examined the effect of early reperfusion on the components of the mitochondrial membrane. MS proteomics measurements detected temporary fluctuations in several proteins of respiratory complexes during the initial (20-80min) reperfusion (Supplementary Figure S1). These results indicate that the initial oxidation generated in cardiomyocyte mitochondria is modifying and quantitatively affecting the energetic machinery as well as the mitochondrial components.

SBT analysis also showed a significant coordinated increase in a subset of processes and pathways related to leukocyte infiltration (integrin-mediated signaling pathway, cell-cell adhesion, arachidonic acid secretion, phagocytosis, membrane ruffle and angiogenesis) within the time segment of 2h to 24h after I/R (Figure 12, subset III). Notably, this increase in immune responses within the span of 2h-24h of reperfusion coincides with the irreversible oxidation cluster 2 (Figure 10) as well as the increase in reversible oxidation of Cys residues (Figure 7).

As these results strongly suggested the presence of neutrophils in the ischemic lesion site as described before [18], we took a closer look at the protein most abundantly expressed by these cells. Myeloperoxidase (MPO) relative abundance values (standardized $\log_2$ FC of I/R with respect to control) were found increased at 2h-24h, correlating with irreversible and reversible oxidations (Figure 13a).

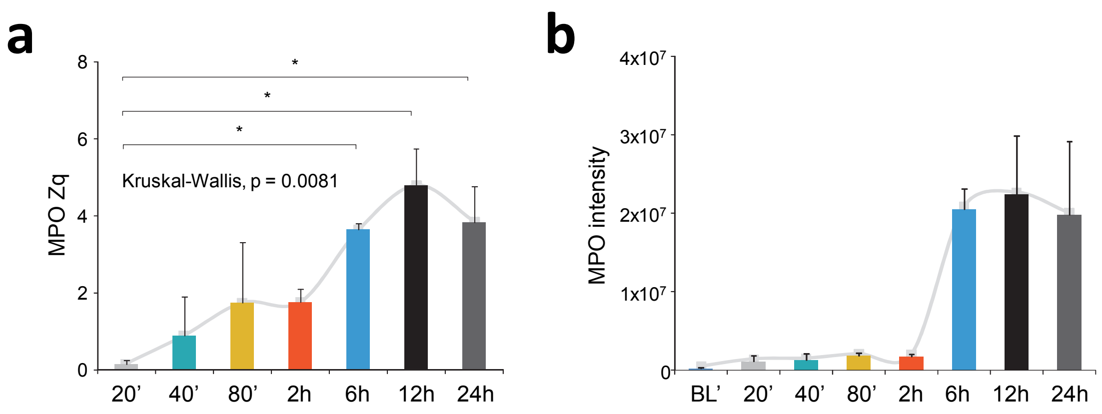

Figure 13 MPO protein expression changes along time course. (a) Protein relative abundance values (Zq) are reported as the log2-fold changes in each condition with respect to controls. (b) Label-free (LF) absolute quantification of MPO is expressed as the intensity of protein normalized by all proteins summed intensity. * Indicates p value < 0.05. P-values are calculated using Kruskal-Wallis test.

Additionally, label free proteomics experiments confirmed that MPO was absent in control samples and substantially increased between 6h-24h post I/R (Figure 13b). Moreover, MPO activity significantly increased between 6h-12h (Figure 14a), correlating with the above-mentioned increases in its abundance as well as reversible and irreversible protein oxidation. We could also appreciate a strong tendency towards an increase in MPO activity at 24h after I/R, however with prominent biological variability.

Hydrogen peroxide (H_2O_2) measurements in the ischemic region detected a maximum peak of significant increase 24h after reperfusion (Figure 14b). As H_2O_2 is a universal indicator of oxidative stress and ROS accumulation, its maximal concentration could be related to the aforementioned increase in MPO activity that showed a strong tendency to increase at 24h (Figure 14a), however, leukocytes presence in the lesion site might be not the only contributor to the overall high H_2O_2 concentrations at 24h post-I/R.

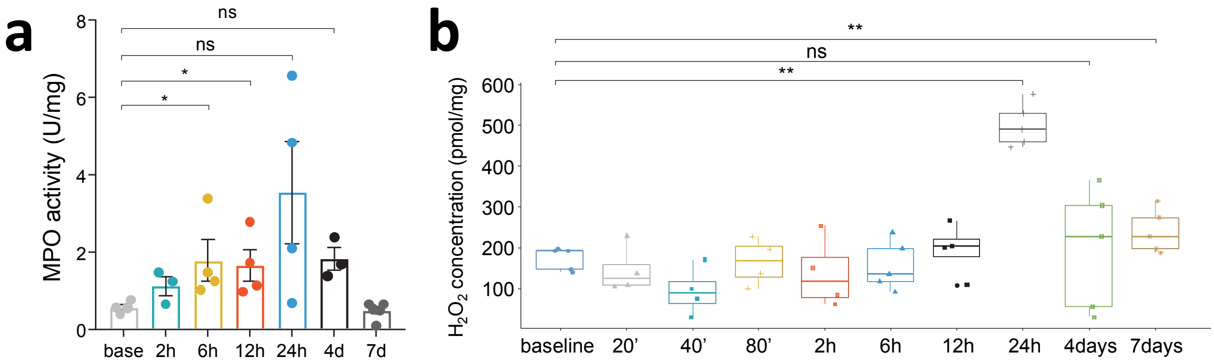

Figure 14 MPO activity and H2O2 concentration. (a) MPO activity measurement using Myeloperoxidase Colorimetric Activity Assay Kit. Enzymatic activity is expressed as units of MPO per mg of tissue. (b) Quantification of H2O2 concentration along the time course shows a maximum peaking at 24h after reperfusion. Concentration is expressed as pmol of H2O2 per mg of ischemic tissue. ns indicates p value > 0.05, * Indicates p value < 0.05, ** indicates p value <0.01. P-values were calculated by Mann-Whitney test.

Remote tissue shows extraordinary fluctuations within the first hours after MI

We also analysed the effect of early I/R in the remote myocardial region (posterior ventricular wall) in the pig model of I/R using the same experimental outline (Figure 5).

Analysis of Cys-reversible oxidation (Figure 15) showed no significant increase in the thiol redox status of the remote myocardium (Supplementary Table S6), confirming previous cys-oxidation studies in our laboratory [66] (Figure 3).

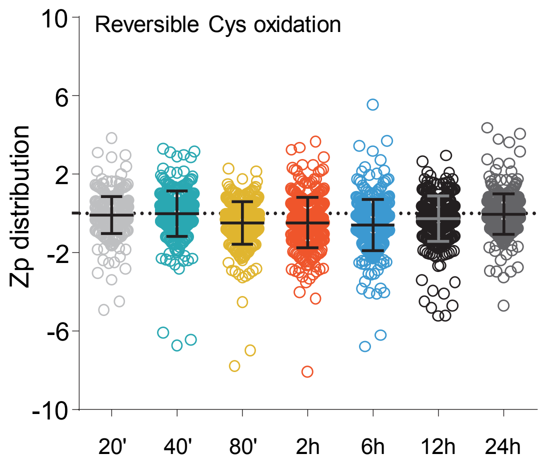

Figure 15 Oxidized Cys-peptides population shows no changes in the remote myocardium over time. Total population of oxidized Cys (355 peptides) peptide values (Zp) are reported as the log2-fold changes in each condition with respect to controls. Full list of oxidized Cys-containing peptides detected in the remote area can be found in Supplementary Table S6. P-values for the averages were calculated using Kruskal-Wallis test giving non-significant results.

The ultra-tolerant database search of PTM yielded more than 10800 peptide sequences with assigned mass differences (ΔM) in the remote tissue. Analysis of PTMs yielded a curated list of 309 modified peptides, which were subjected to PCA analysis showing a distinctive behaviour of trioxidated Cys (Supplementary Figure S2). Peptides were also subjected to HCA analysis. Although the previous oxidative events detected in the infarcted tissue were not present in the remote tissue, we were able to detect two different clusters of PTM changes.

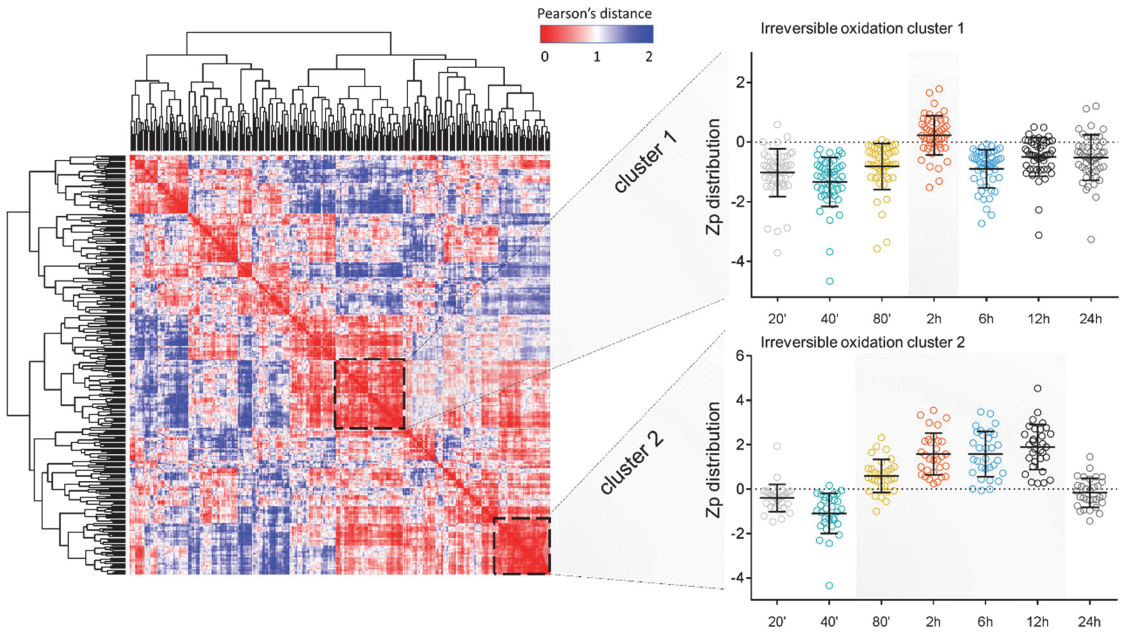

Figure 16 HCA of PTMs in the remote myocardium. 309 peptides present in all biological replicates (n=4) and corresponding to known biologically relevant PTMs in the accurately identified modified residue were subjected to HCA as described in Figure 10. Two clusters of high similarity (cluster 1 and cluster 2, inset) were selected and their peptides Zp values at different time points were reported as averages of four individuals in each condition with respect to the controls. Full list of modified peptides from cluster 1 and 2 can be found in Supplementary Tables S7 and S8.

The first cluster (Figure 16, cluster 1, Supplementary Table S7) showed a transitory increase in irreversible oxidation after 2h of reperfusion, which mainly affected Trp, Cys and Asp residues (Figure 17a-b, left), impacting a wide scope of cardiac proteins, including cardiac muscle, intracellular, plasmatic, mitochondrial and extracellular matrix proteins (Figure 17b, right).

This intriguing temporary increase in protein modifications was accompanied by differential changes in biological processes (Figure 18). Functional category (Zc) analysis revealed a coordinated transitory increase at 2h I/R in the expression of proteins involved in apoptosis regulation, proteasome complex (polyubiquitin binding proteins), heart contraction regulation, tropomyosin binding proteins (troponin complex) and response to H_2O_2 (antioxidant activity).

a

Residue and Modification	p-values Cluster 1	Cluster 2
W Dioxidation	<0.0001	n.s.
W Oxidation	<0.0001	n.s.
D Oxidation	<0.0001	n.s.
C Cys->Dha	<0.0001	n.s.
D Methyl	0.0001	n.s.
I Methyl	0.0002	n.s.
C Trioxidation	n.s.	<0.0001
C Dioxidation	n.s.	<0.0001
P Oxidation	n.s.	1

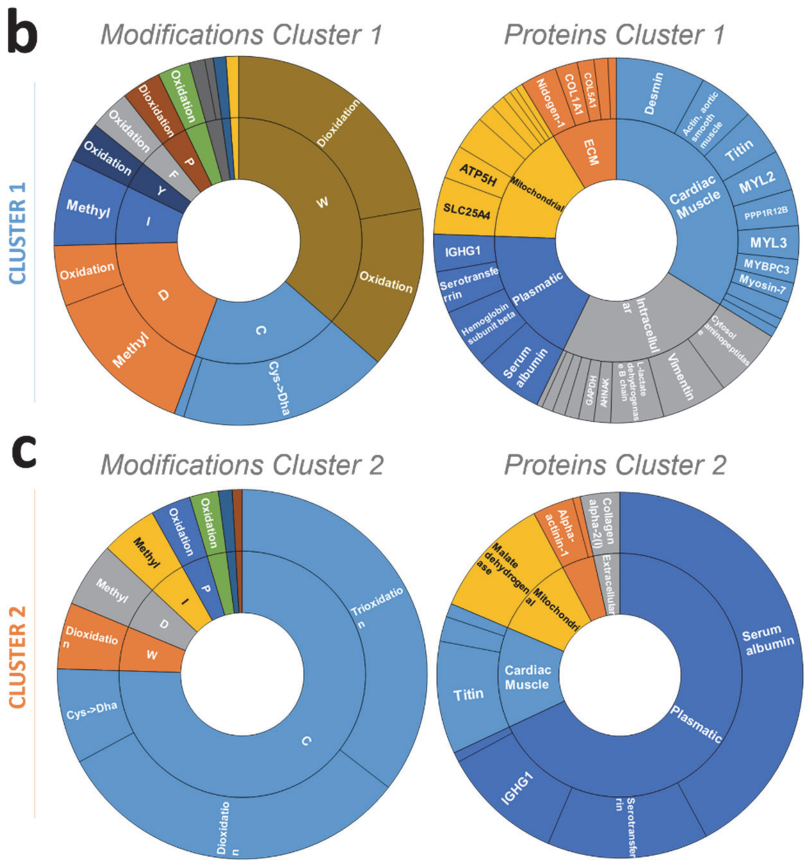

Figure 17 Characterization of oxidative events in the remote tissue. (a) Hypergeometric p-values of each modification and amino acid site corresponding to each cluster. P-values were calculated as the probability of having more occurrences (PSMs) in each cluster in comparison to the total population of PTMs and modified sites analyzed by HCA. Only p-values from modifications with more than 50 PSMs are shown. (b) Protein modifications map of the transitory increase in irreversible oxidation at 2h after reperfusion in the remote pig myocardium (cluster 1, Supplementary Table S7). The circular inner bars and the outer bars (on the left panel) show the modified amino acid residue and the modification type proportion (quantified in PSMs), respectively. On the right panel we report proteins affected by oxidative modifications in each cluster. Protein cellular localization is represented in the inner circular bars. (c) Protein modifications map of the transitory increase in irreversible oxidation within 80min-12h post-MI (cluster 2, Supplementary Table S8). The circular inner bars and the outer bars (on the left panel) show the modified amino acid residue and the modification type proportion (quantified in PSMs), respectively. On the right panel we report proteins affected by oxidative modifications in the cluster. Protein cellular localization is represented in the inner circular bars.

The last category is mainly represented by an increase in abundance of enzymes protecting the cell from superoxide toxicity, and includes thioredoxin (TXNRD), superoxide dismutase (SOD1) and peroxiredoxin (PRDX) among others (Supplementary Figure S3). This result suggests that this temporary increase (at 2h) in irreversible oxidative modifications in the remote region is addressed by an antioxidant proteins response.

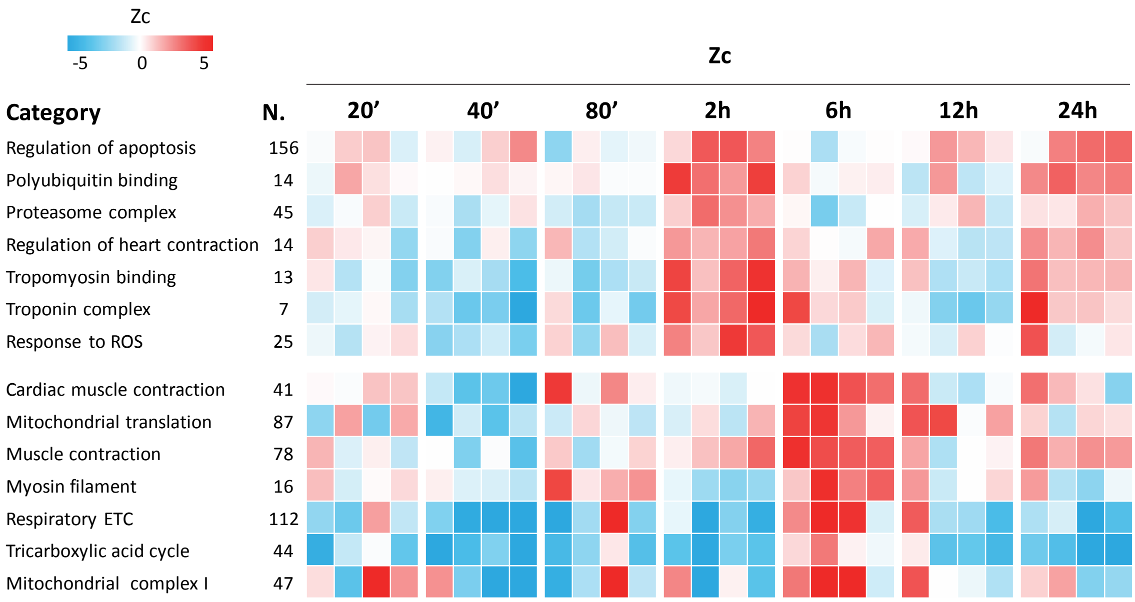

Figure 18 SBT analysis of remote tissue during early reperfusion after MI. Functional categories changes (Zc) over time. Subset I include categories involving regulation of apoptosis, proteasome and polyubiquitin binding proteins, regulation of heart contraction, especially troponin complex and tropomyosin binding proteins, and enzymes responding to ROS that temporally increase at 2h post-MI. Subset II contains biological processes showing a transitory increase 6h after reperfusion and mainly involve cardiac muscle contraction proteins, mitochondrial ribosome, mitochondrial respiratory complexes (especially complex I), and TCA cycle. Full list of protein's Zq changes for each category can be found in Supplementary Table S9.

HCA analysis also revealed a second cluster (Figure 16, cluster 2, Supplementary Table S8) showing an increase in Cys irreversible oxidative modifications during 80min-12h (Figure 17a-c), which principally affected plasmatic proteins such as albumin (ALB) and serotransferrin (TF) (Figure 17c, right). During this second episode of irreversible oxidative modifications in the remote region, another group of biological responses was found significantly increased 6h after I/R onset (Figure 18). These included cardiac muscle contractile machinery, mitochondrial ribosome, myosin filaments, respiratory electron transport chain (ETC), especially complex I, and TCA cycle (Figure 18). Interestingly these processes, whose spike of increase was detected at 6h of reperfusion, were found substantially decreased within the preceding and following hours. It should be noted that the appearance of the oxidative protein modifications in the remote region several hours after reperfusion might be related to the co-ocuring secondary oxidative episode taking place in the ischemic area.

A third oxidative event implies the accumulation of oxidative by-products

To evaluate how protein modifications alter at the end of the first week after I/R, we also applied the Comet-PTM suite [72] in a pig model dataset with later time points (2h to 7 days) after I/R [20]. A modified peptide population was detected that gradually increased towards day 7, and was mainly comprised of Proline (Pro) hydroxylations (Figure 19).

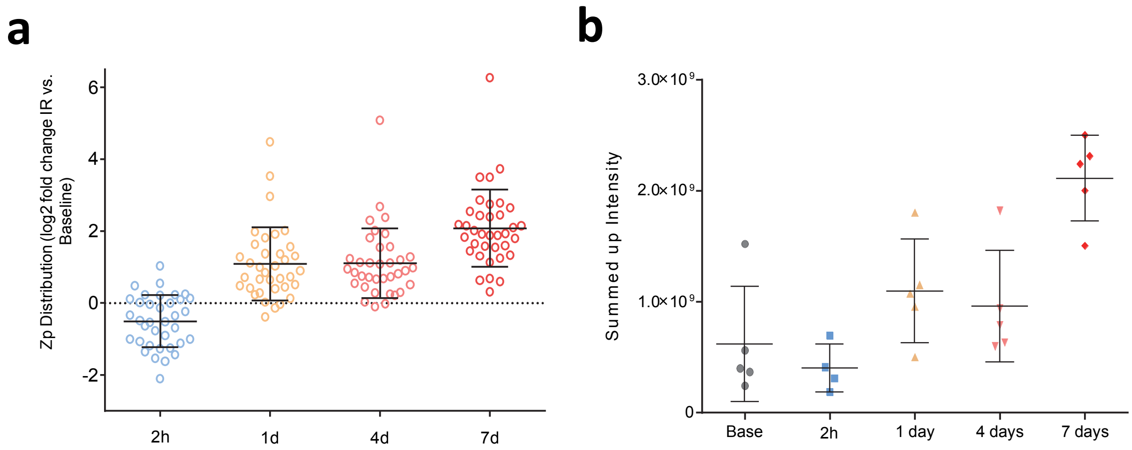

Figure 19 Changes of Pro-hydroxylized peptides. (a) Zp dristribution for Pro-hydroxylized peptides. Zp values of Pro hydroxylation are reported as the log2-fold changes expressed in units of standard deviation around the averages with respect to controls. Full list of hydroxyproline peptides can be found in Supplementary Table S10. (b) Label-free (LF) absolute quantification of Pro hydoxylized peptides. LF quantification is expressed as the intensity of modified peptide normalized by all peptides summed intensity.

Interestingly, hydroxilated-Pro was located on different collagen isoforms (Supplementary Table S10). This increase of irreversible oxidations also correlated with an increase in fibrillar collagen and collagen hydroxylases (Figure 20). We further validated these peptide changes by label free quantification of individual samples (Figure 19b).

These specific hydroxylations in Pro residues, essential for the stabilization of the fibrillar collagen structure concurs with previously reported increase in protein biosynthesis, angiogenesis-associated proteins, proteolysis and extracellular matrix proteins (principally collagens) found by our group, which reflect the late phase of repair and fibrosis evolving towards day 7 [20].

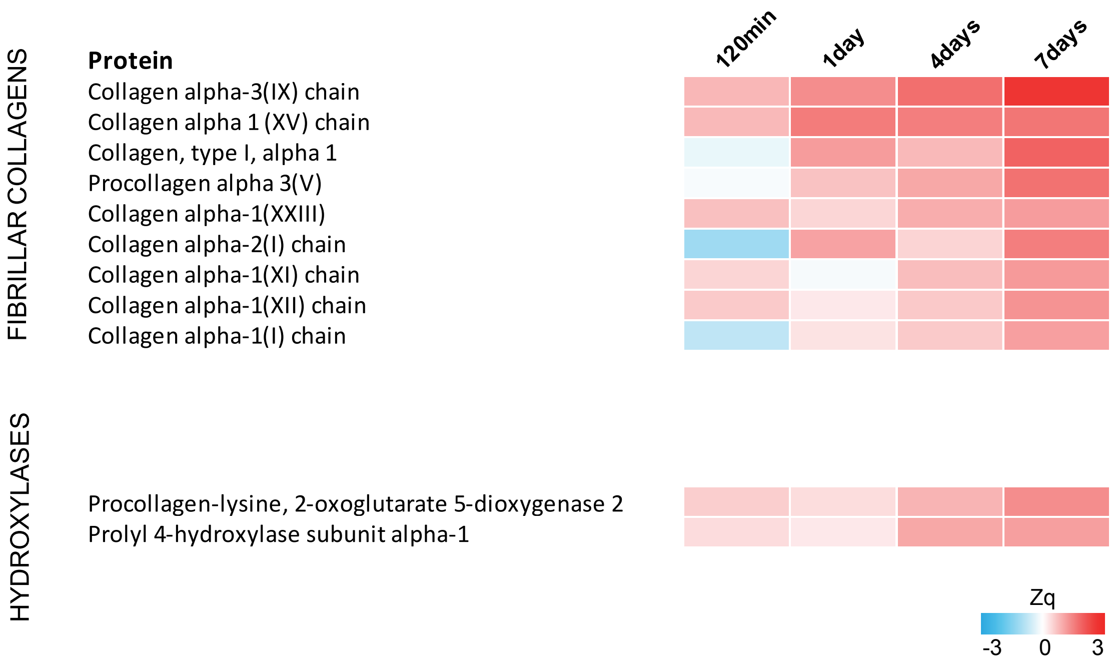

Figure 20 Changes in fibrillar collagen and collagen hydroxylases. Heatmap for protein expression changes along time course. Zq values for fibrillary collagens Pro- and Lys-hydroxylases are reported as the log2-fold changes expressed in units of standard deviation around the averages with respect to controls.

Moreover, we performed lipid peroxidation measurements quantifying MDA concentrations and 4-HNE protein adducts in the infarcted tissue. MDA concentration assay showed a cumulative increasing trend towards the end of the week, starting to show significant changes from 24h throughout day 4 and 7 after reperfusion (Figure 21).

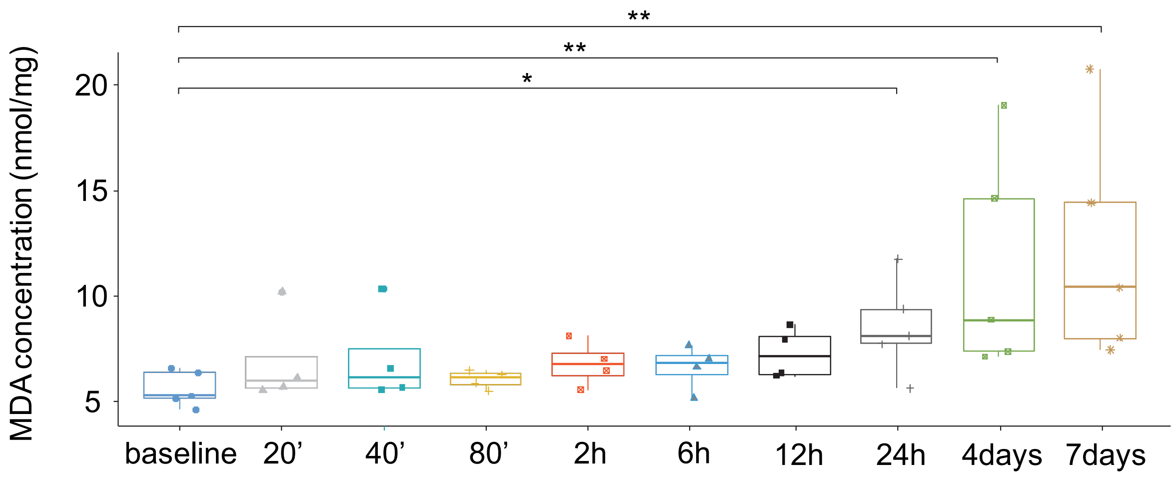

Figure 21 Lipid peroxidation measurements evaluated by MDA concentration in the ischemic tissue along time course. Concentration is expressed as nmol of MDA per mg of ischemic tissue. * Indicates p value < 0.05, ** indicates p value <0.01. P-values were calculated using Mann Whitney test.

Similarly, the data from immunoblotting analysis of peroxidised lipid-protein adducts presented a gradual and cumulative increase over time, with significant change after 2h and throughout the rest of the week of reperfusion (Figure 22 and Figure 23). These results confirmed the presence of an oxidative episode at the end of the week after I/R, which can be attributed to repair processes gradually building up in the ischemic region of the infarcted myocardium.

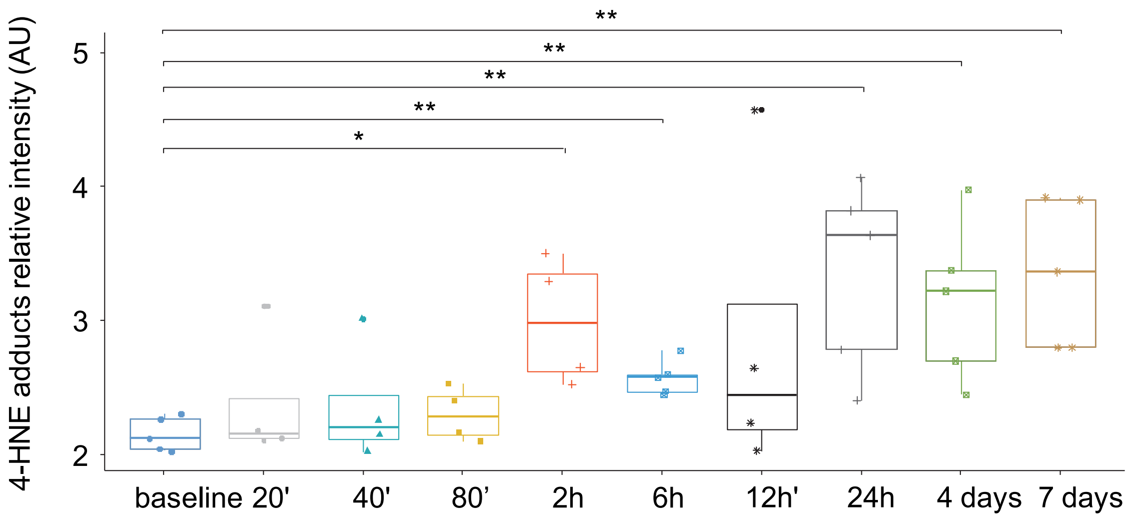

Figure 22 WB analysis of 4-HNE lipid peroxidation protein adducts. Total protein blot (right panel) was used for loading control. Values with superscripts are significantly different (*p < 0.05, **p<0.01, n=4, n=5 Mann-Whitney test).

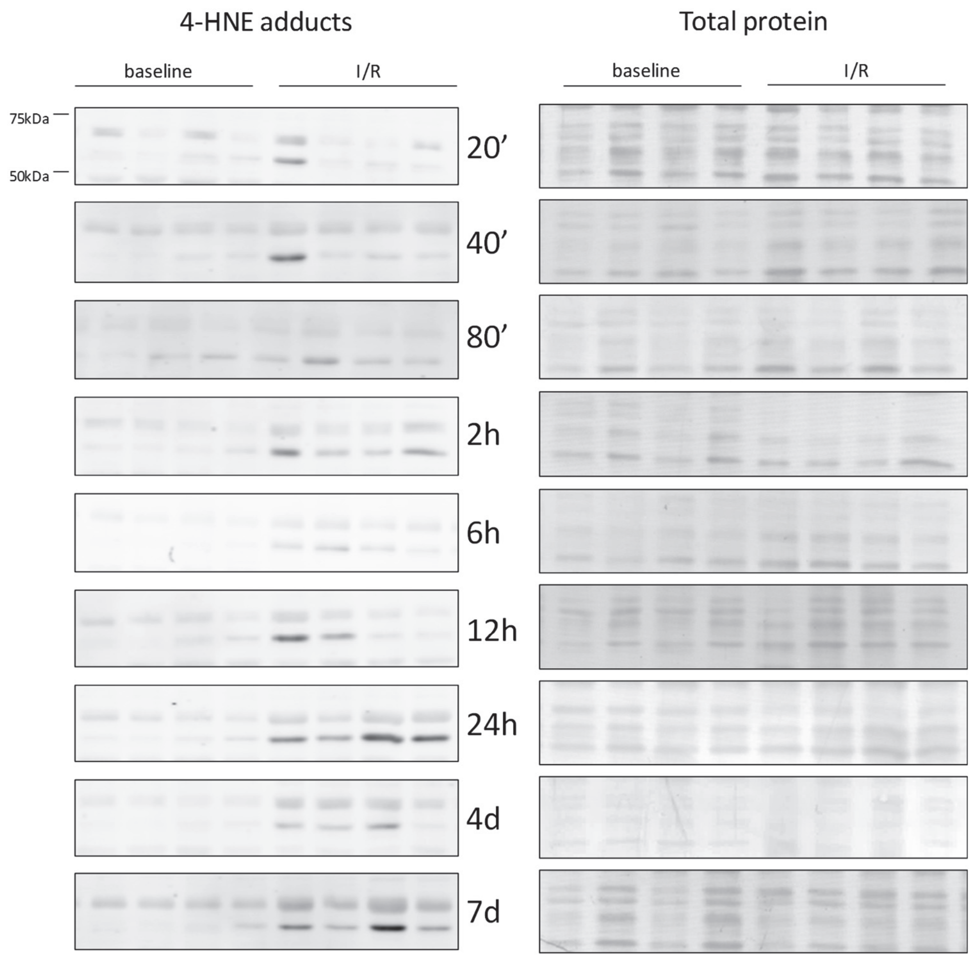

Figure 23 WB quantification of 4-HNE protein adducts. 4-HNE-adducts densitometry quantifications were expressed in relative values referred to total protein content in arbitrary units (AU).

Reperfusion induces oxidation in both ischemic and remote cardiac tissues

To study the potential association between the second wave of protein oxidative modifications and reperfusion, a group of 4 pigs were subjected to ischemia (angioplasty balloon LAD coronary occlusion) without reperfusion (Figure 24). To avoid prolonged and excessive ischemic effect, we selected the earliest time point where we detected the appearance of later oxidative events and sacrificed the animals after 2h of ischemia without posterior reperfusion (2h NOR).

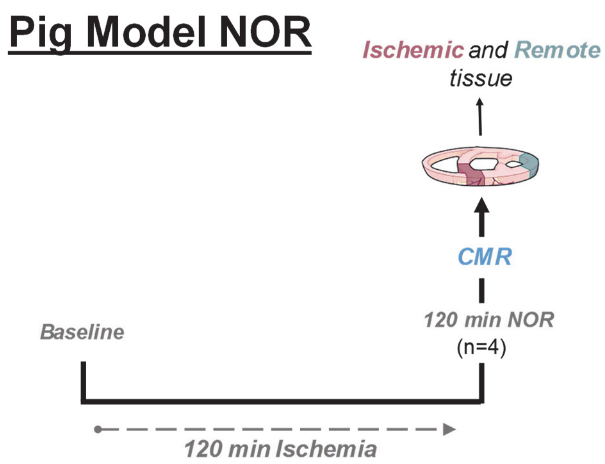

Figure 24 Study Design. A group of 4 pigs was used for the study of 2h of ischemia (angioplasty balloon LAD coronary occlusion) without reperfusion.

When compared to animals undergoing 40-min coronary occlusion followed by reperfusion (2h), protein oxidative (reversible and irreversible) impact in the ischemic region of the nonreperfused pigs was significantly lower than in reperfused animals (Figure 25a-b), settling the 2h NOR oxidation values closely to the baseline group. These results suggest that this oxidative impact is a direct consequence of reperfusion.

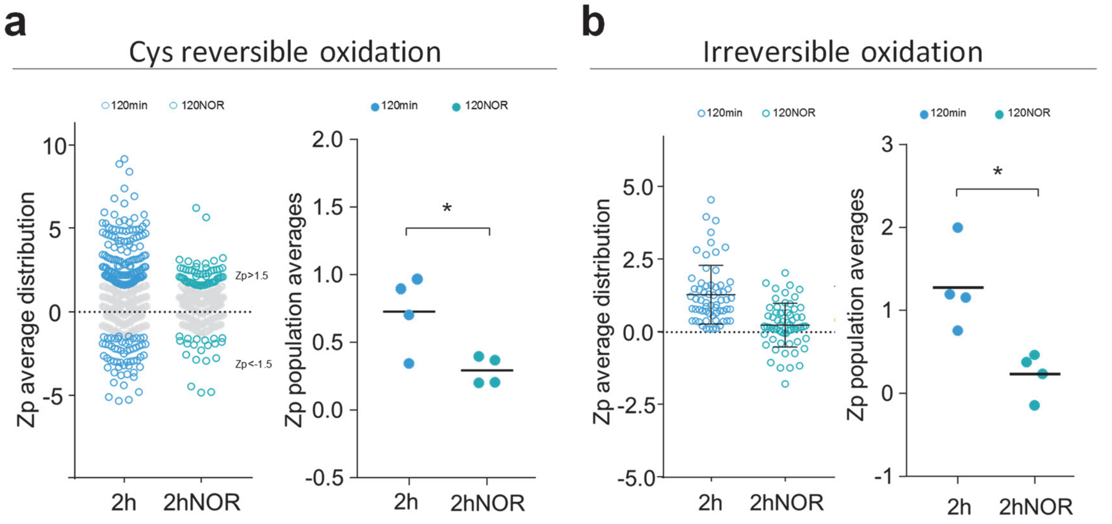

Figure 25 Effect of non-reperfusion (NOR) on reversible (left panel) and irreversible oxidation (right panel). (a) Effect of non-reperfusion on the total Cys-reversible oxidation population in the infarcted tissue (Figure 6). (b) Effect of non-reperfusion on the irreversible oxidations from the second oxidative event in the infarcted tissue (cluster 2, Figure 10). Oxidized peptides values log2-fold changes (Zp average distribution, a and b left panels) are reported as the averages of 4 biological replicates in each condition with respect to controls. Zp population averages (a and b right panels) are reported as the complete peptide population average value at each time point for each individual. * Indicates p value < 0.05. P-values are calculated using Kruskal-Wallis test.

Moreover, this new analysis (Figure 25a)confirmed the previous results by our group [66] that indicate that non-reperfusion reduces the impact in cys reversible oxidation. We identified 53 oxidized Cys residues (from 35 proteins) significantly attenuated (*P* value<0.01, FDR<0.01) by nonreperfusion when compared to regular I/R protocol group (2h I/R) (Supplementary Figure S4). Within this subset we found proteins with multiple (n≥2) oxidation sites, including TCA cycle enzymes (MDH2, OGDH), mitochondrial membrane carrier (VDAC2), mitochondrial matrix metabolism enzymes (ACADSB, ACSL1), sarcomere contractility modulator (MYBPC3), sarcoplasmic Ca2+ transporter (ATP2A2), cytoskeleton and cytoplasm components (TUBA1B, GAPDH), blood plasma (IGKC, PLG) and metal binding proteins (HPX, CP, TF), (Supplementary Figure S4). Additionally, in some of these significantly affected proteins Cys oxidation levels were at least 6-fold higher with reperfusion, including: 2 contractile proteins (TPM2 and MYBPC3), 3 mitochondrial membrane proteins (NDUFAB1, VDAC1, VDAC2 and SLC25A4), mitochondrial matrix enzymes (OGDH and MDH2), membrane Ca^{2+} channel (SLC8A1) as well as cytoskeletal protein (TUBA1B).

While 2h reperfusion clearly induces a significant upregulation of leukocyte migration-associated processes (integrin-mediated signaling pathway, leukocyte cell-cell adhesion, arachidonic acid secretion, phagocytosis, membrane ruffle and angiogenesis), these were found markedly less increased in nonreperfused group (Figure 26).

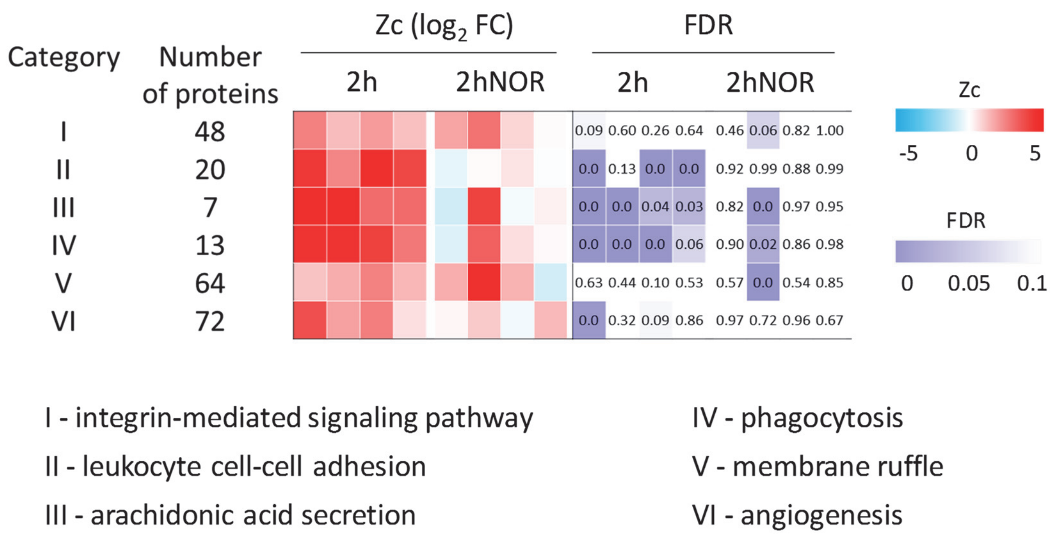

Figure 26 Effect of non-reperfusion (NOR) on inflammation-related processes. Functional category values (Zc) are reported as the log2-fold changes in each condition with respect to controls. FDR was calculated using the SBT method. Full list of protein's Zq changes for each category can be found in Supplementary Table S11.

Moreover, non-reperfusion not only affected the ischemic area of the heart but also significantly reduced the extent of irreversible oxidation of plasmatic proteins in the remote region (Figure 27).

Overall, impaired blood flow restoration most probably defers the migration of recruiting leukocytes with the following occurrence of reperfusion-induced inflammatory processes and its associated oxidative events.

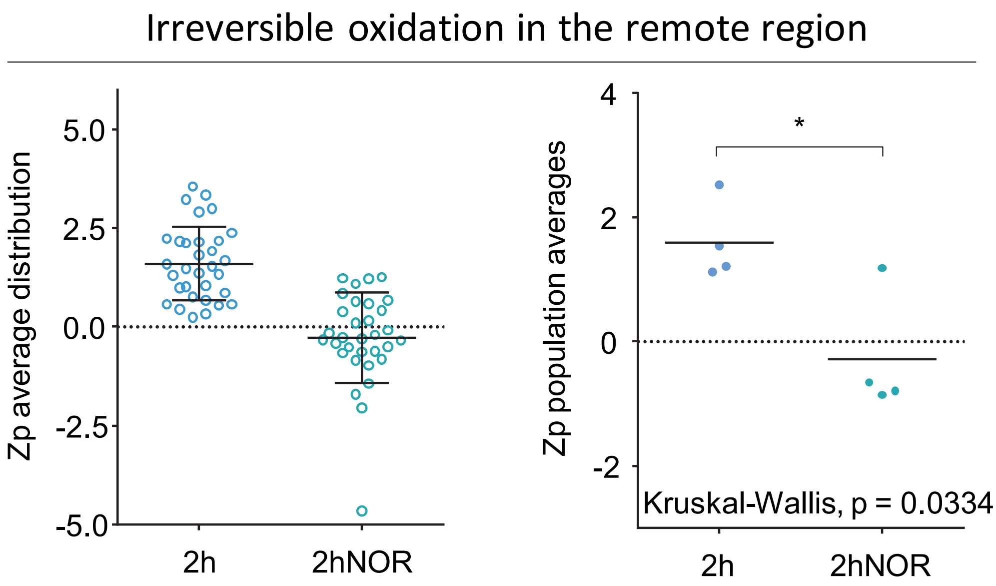

Figure 27 Effect of non-reperfusion (NOR) on irreversible oxidations in plasmatic proteins from the remote region tissue (cluster 2, Figure 16). Oxidized peptides values log2-fold changes (Zp average distribution, left panel) are reported as the averages of 4 biological replicates in each condition with respect to controls. Zp population averages (right panel) are reported as the complete peptide population average value at each time point for each individual. * Indicates p value < 0.05. P-values are calculated using Kruskal-Wallis test.

Cardioprotective intervention alters ischemic tissue oxidation levels and substantially reduces inflammatory reaction after MI

To study the effect of cardioprotective interventions on the second oxidative event (2h-24h) we performed an experiment of ischemic preconditioning (PC) followed by 24h reperfusion (Figure 28).

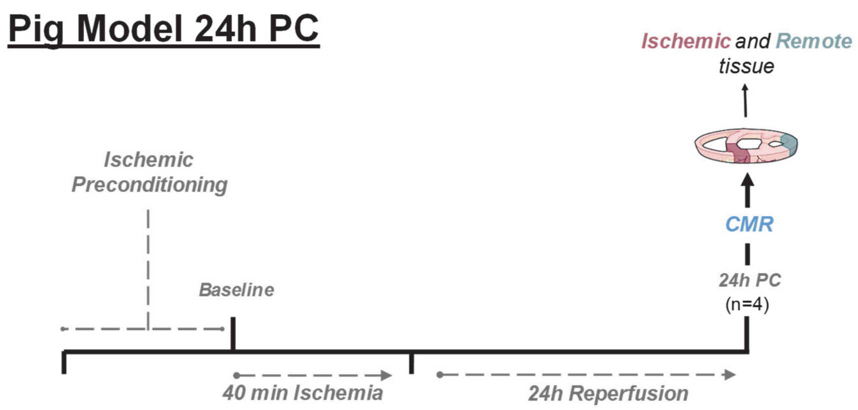

Figure 28 Study Design. A group of 4 pigs was used to study 24h of I/R with ischemic preconditioning (24h PC). Individuals were subjected to ischemic preconditioning prior to 40 min ischemia and 24 h reperfusion.

Confirming the previous results for Cys-reversible oxidation [66], preconditioning attenuated reversible Cys oxidation (Figure 29a) and also irreversible protein oxidation processes (Figure 29b) when compared to standard I/R protocol with 24h of reperfusion in the ischemic tissue. These results indicate that the second oxidative event (2-24h) can be mitigated with ischemic preconditioning.

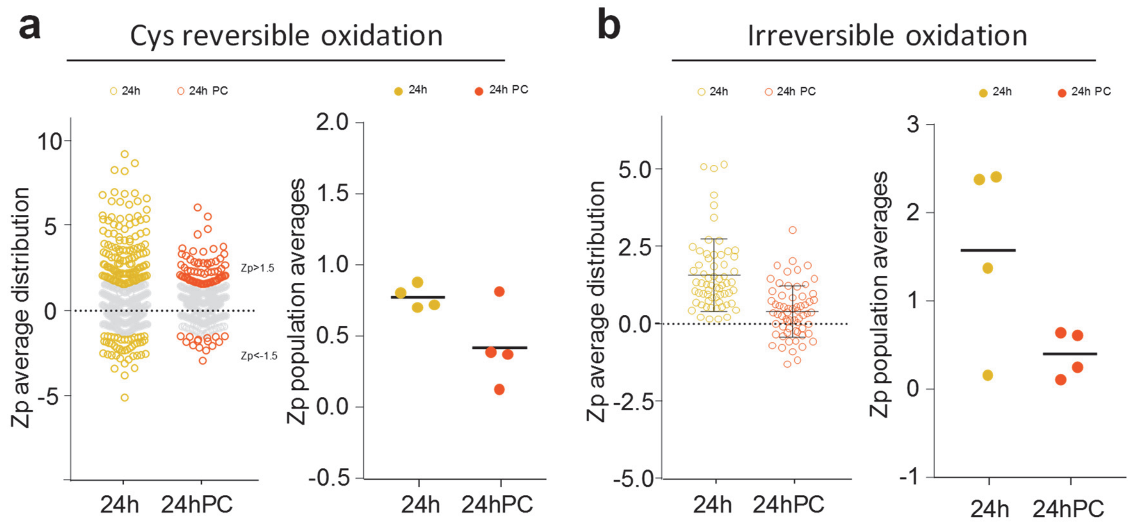

Figure 29 Effect of Preconditioning (PC) on reversible (left panel) and irreversible oxidation (right panel). (a) Effect of preconditioning on the total Cys-reversible oxidation population in the infarcted tissue (Figure 6). (b) Effect of preconditioning on the irreversible oxidations from the second oxidative event in the infarcted tissue (cluster 2, Figure 10). Oxidized peptides values log2-fold changes (Zp average distribution, a and b left panels) are reported as the averages of 4 biological replicates in each condition with respect to controls. Zp population averages (a and b right panels) are reported as the complete peptide population average value at each time point for each individual.

We inspected some of the proteins whose Cys residues turned out to be most responsive to the cardioprotective treatment (at least 4-fold difference when compared to regular 24h I/R) and these involved crucial myocardial contractile machinery components (MYH1, MYH6, MYBPC3, TMP1, TPM2), sarcoplasmic Ca2+ transporter (ATP2A2), mitochondrial respiratory complex I (NDUFA10), as well as two plausible components of the mitochondrial permeability transition (MPT) pore structure (SLC25A4, VDAC1) and mitochondrial outer membrane protein (NIPSNAP2 also known as GBAS), which was proposed as MPTP interactor [101] (Supplementary Figure S5). We also observed notably decreased inflammatory processes in proteomics analysis (Figure 30), which indicated that cardioprotective intervention alleviated the activation of inflammatory pathways and leukocyte migration.

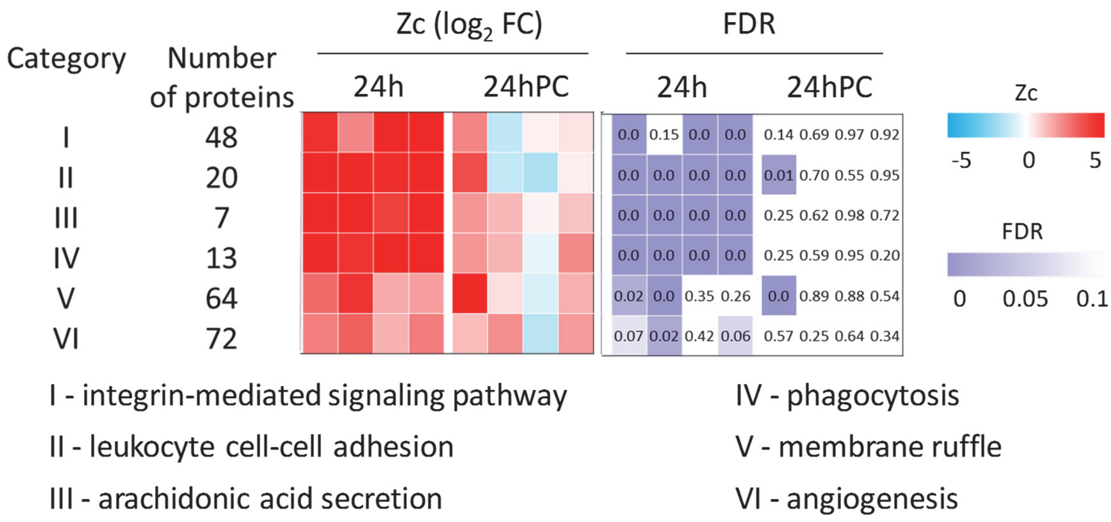

Figure 30 Effect of Preconditioning (PC) on inflammation-related processes. Functional category values (Zc) are reported as the log2-fold changes in each condition with respect to controls. FDR values were calculated using the SBT method. Full list of protein's Zq changes for each category can be found in Supplementary Table S11.

To further assess the impact and the potential source of the observed protein oxidation, we measured MPO abundance and activity in the ischemic tissue of preconditioned animals (24hPC) and regular I/R (24h) as an indicator of neutrophil-induced inflammation. As displayed in Figure 31a, we can appreciate a significant decrease in MPO protein abundance due to preconditioning. Enzymatic activity assay also showed a substantial decrease in MPO's activity in preconditioned animals (Figure 31b). Low enzymatic activity levels in the preconditioned group could suggest that the preconditioning effectively diminished the activation of inflammatory cells and possibly their recruitment to the lesion site.

Finally, the measurments of H_2O_2 levels were found significantly reduced in the presence of preconditioning (24hPC) when compared to standard I/R protocol (24h), which suggests that cardioprotective intervention decreased overall ischemic tissue oxidation levels (Figure 31c).

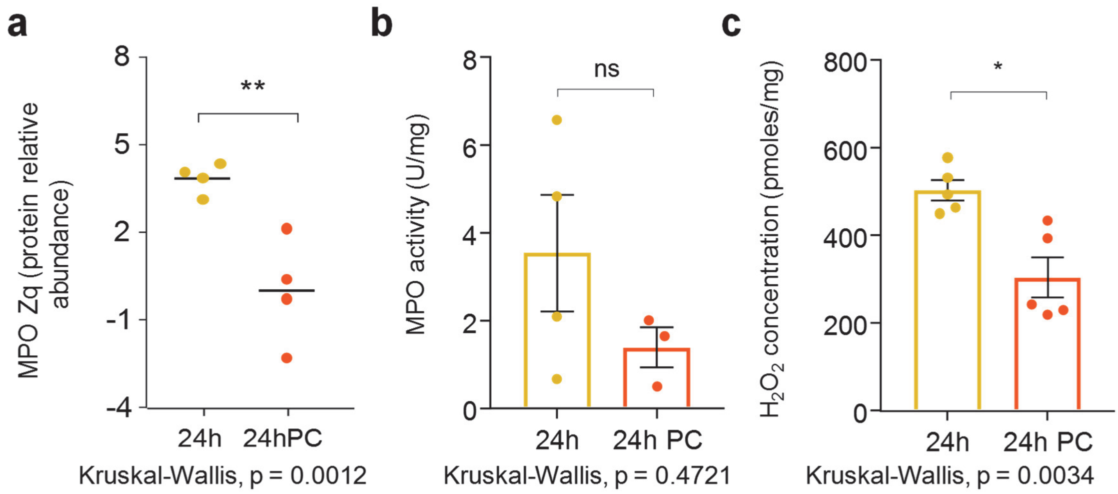

Figure 31 Effect of Preconditioning (PC) on MPO and H2O2. (a) Effect of Preconditioning (PC) on MPO protein expression. Zq relative abundance values are reported as the log2-fold changes of protein expression in each condition with respect to controls. (b) Effect of preconditioning (PC) on MPO activity. MPO activity was measured using Myeloperoxidase Colorimetric Activity Assay Kit. Activity is expressed as units of MPO per mg of tissue. P-values are calculated using Mann Whitney and Kruskal-Wallis test. (c) Effect of preconditioning (PC) on H2O2 levels in ischemic tissue. ns indicates p value > 0.05, * Indicates p value < 0.05, ** indicates p value <0.01. P-values are calculated using Kruskal-Wallis test.

Dynamic protein oxidative modifications and leukocyte migration-related processes in mouse model increase after I/R

With the anticipation of further validation interventions, we studied whether the results obtained in the pig model could be reproduced in a different animal model: a mouse model of I/R (n=3) at short time points (from 10 min to 48h) after I/R (Figure 32). In this model, whole hearts were analysed without separating ischemic and remote tissue.

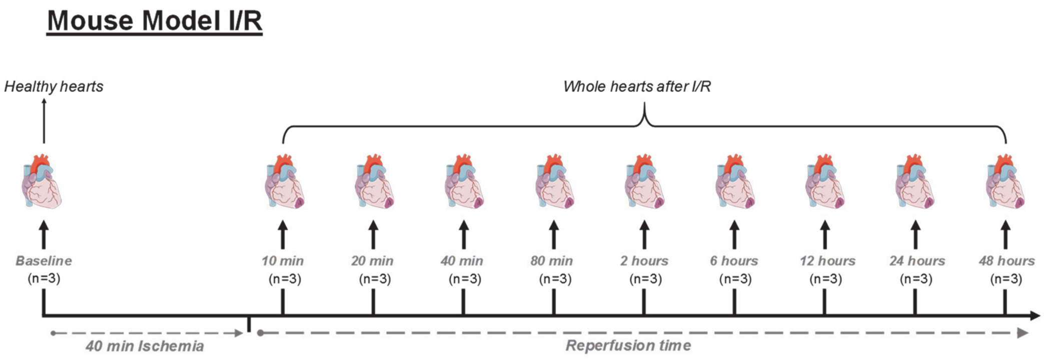

Figure 32 Study design. Mouse model of ischemia reperfusion (I/R). The study population comprised 10 groups of mouse (n=3/group). Groups 1 to 10 were used for the analysis of redox, PTMs and protein expression changes. Mice were subjected to 40 min of ischemia and sacrificed at 10 min, 20min, 40min, 80min, 2h, 6h, 12h, 24h and 48h after reperfusion. Additional group (n=3) of healthy mice served as controls.

Unbiased PTMs analysis of this model revealed an initial increase in irreversible oxidations at the earliest time point (10 min) (Figure 33a, Supplementary Table S12). This short-term increase in oxidative modifications was mostly composed of mono-oxidations localized at Lys, Asn, Phe, Trp and Tyr, being the last two residues the most frequently modified (Figure 33d-e). These results were in excellent agreement with those previously observed in pig, demonstrating that this first oxidative event could be reproduced in mouse.

We also detected a second episode of increased oxidations, which involved irreversible modifications (with Cys residue oxidations found as the most prevalent, Figure 33b, Supplementary Table S13, Figure 33d-e) and Cys reversible oxidation (Figure 33c, Supplementary Table S14), within 2h-24h of reperfusion. Again these changes mirrored those observed in the pig model.

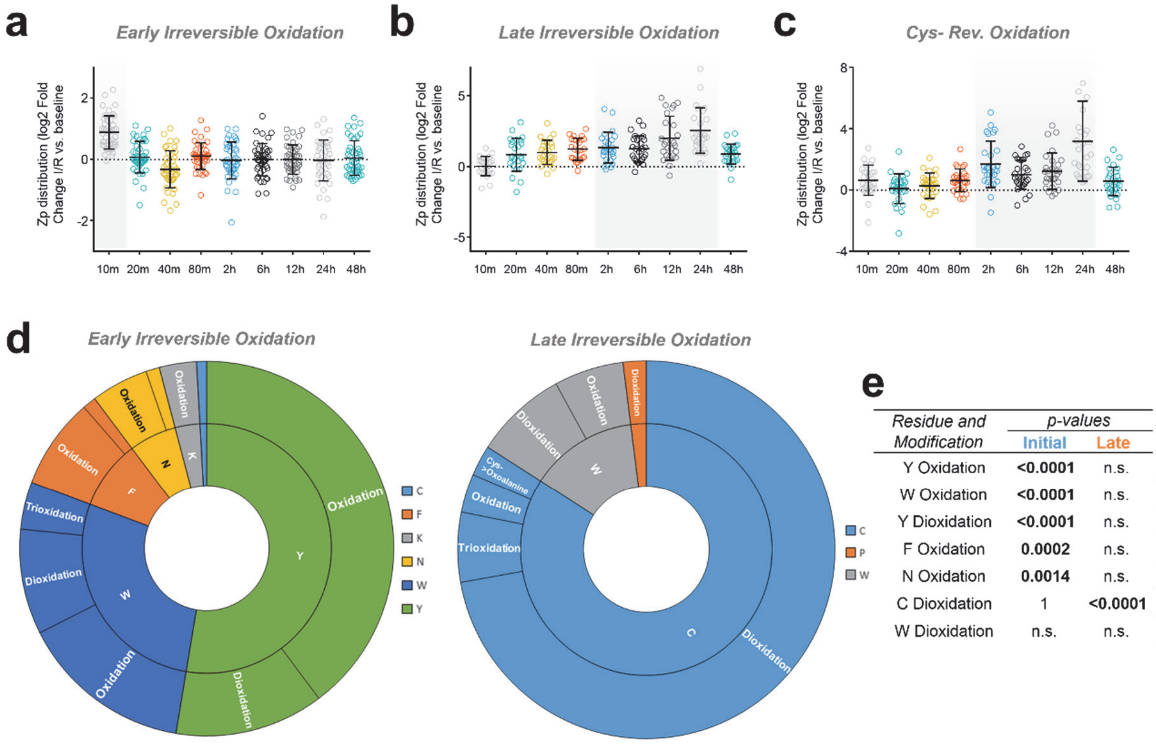

Figure 33 Oxidative events in mouse model of I/R (a) Irreversible oxidation after MI in mouse increases after 10 min of reperfusion. Oxidized peptides values log2-fold changes (Zp) are reported as the averages of 3 biological replicates in each condition with respect to controls. For full list of modified peptides see Supplementary Table S12. (b) Second episode of irreversible oxidation in mouse myocardial I/R model increased at 2h-24h. Full list of modified peptides from this scatter plot can be found in Supplementary Table S13. (c) Cysteine reversible oxidation in mouse MI model increased at 2h-24h. Only values with a total Zp average >0.5 are shown in the scatter plot. For full list of reversibly oxidized Cys-containing peptides, please refer to Supplementary Table S14. (d) Complete map of irreversible oxidation events after myocardial reperfusion in mice. Left panel shows the PTMs map for the initial irreversible oxidation at 10 min (Supplementary Table S12).Right panel shows the protein modification map for the secondary irreversible oxidation at 2h-24h (Supplementary Table S13). The circular inner bars and the outer bars show the modified amino acid residue and the modification type proportion (quantified in PSMs), respectively. (e) Hypergeometric p-values of each modification and amino acid site corresponding to each group of irreversible oxidations. P-values were calculated as the probability of having more occurrences (PSMs) in each cluster in comparison to the total population of PTMs and modified sites.

When comparing both animal models of I/R (mouse and pig), we were able to discern a list of homologous modified peptide sequences which were suffered similar abundance changes along the time after reperfusion corresponding to each of the three aforementioned subsets of oxidative modifications (early and late irreversible oxidation and Cys reversible oxidation, Figure 34). These results, affecting to the same residues of the same proteins in two animal models of I/R, confirmed the biological relevance of the different oxidative events after MI in the heart.

a

Modification	PIG Sequence	PIG Protein	MOUSE Sequence	MOUSE Protein
K Oxidation	AQIEFNQI[15.994843]K	MYH7	AQIEFNQI[15.994528]K	Myh7
F Oxidation	GADPEETIINAF[15.994843]K	MYL2	GADPEETIINAF[15.994528]K	Myl2
Y Oxidation	DY[15.994843]HIFYQIISNK	MYH7	NYHIFY[15.994528]QIISNK	Myh6
D Oxidation	I[15.994843]DEAEQIAIK	MYH6	I[15.994528]DEAEQIAIK	Myh7

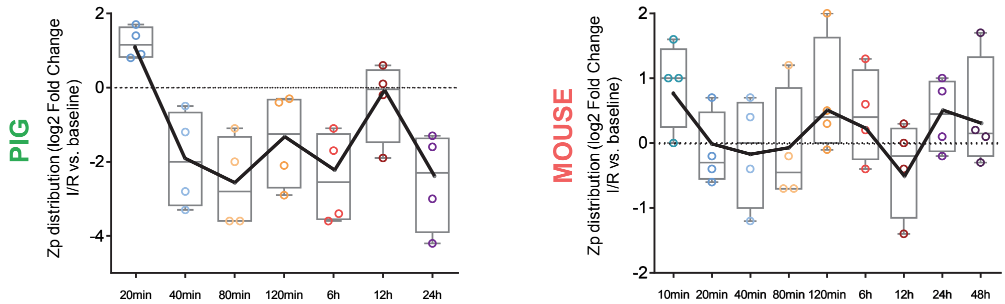

b

Modification	PIG Sequence	PIG Protein	MOUSE Sequence	MOUSE Protein
C Trioxidation	IMAGQEDSNGC[47.984762]INYEAFVK	MYL3	IMAGQEDSNGC[31.988854]INYEAFVK	Myl3
H Methyl	YPIEH[14.014847]GIVTNWDDMEK	ACTG1	YPIEH[14.014968]GIVTNWDDMEK	Actb
W Trp->Kynurenin	IEAPVEEDVW[3.993788]EIIR	MYBPC3	IEAPAEEDVW[3.994742]EIIR	Mybpc3
W Oxidation	IASEIIEW[15.994843]IR	ACTN2	IASEIIEW[15.994528]IR	Actn2
W Dioxidation	IEAPVEEDVW[31.988578]EIIR	MYBPC3	IEAPAEEDVW[31.988854]EIIR	Mybpc3

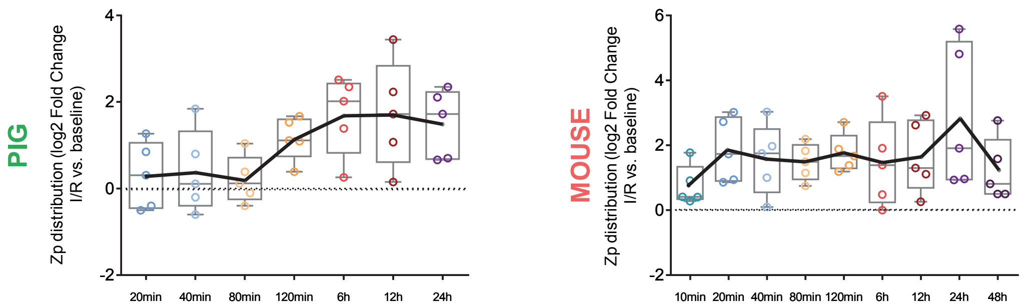

c

PIG Sequence	PIG Protein	MOUSE Sequence	MOUSE Protein
YQIDPDAC(ox)FSAK	VDAC1	YQVDPDAC(ox)FSAK	Vdac1
SLPSVETLGC(ox)TSVIC(ox)SDK	ATP2A2	SLPSVETLGC(ox)TSVIC(ox)SDK	Atp2a2
ILAC(ox)DDLDEAAK	SUCLA2	ILAC(ox)DDLDEAAK	Sucla2
LMAGQEDSNGC(ox)INYEAFVK	MYL3	LMAGQEDSNGC(ox)INYEAFVK	Myl3
GFVGSFEELC(ox)R	ACSL1	GLQGSFEELC(ox)R	Acsl1
VPTPNVSVVDLTC(ox)R	GAPDH	VPTPNVSVVDLTC(ox)R	Gapdh
EFTGLGNC(ox)LAK	SLC25A4	EFNGLGDC(ox)LTK	Slc25a4

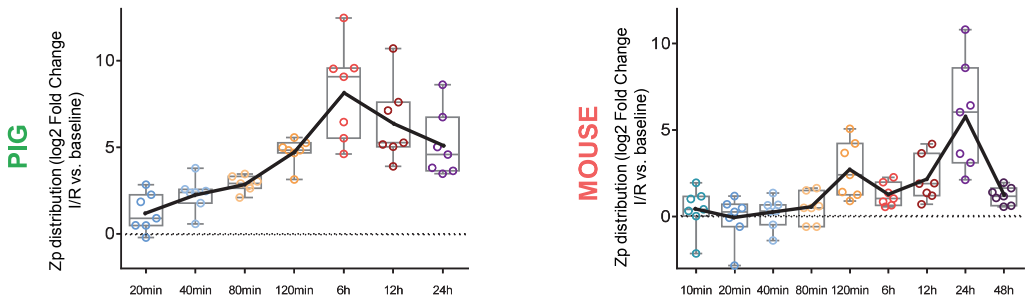

Figure 34 Similarity in abundance changes of homologous modified peptides between mouse and pig models of I/R. a) Homologous sequences from the first event of irreversible oxidation: cluster 1 in pig ischemic tissue (Figure 10) and mice (Figure 33a). b) Homologous sequences from the second event of irreversible oxidation: cluster 2 in pig ischemic tissue (Figure 10) and mice (Figure 33b). c) Homologous Cys reversibly oxidized sequences between pig oxidized cys (Figure 6) and mice (Figure 33c). Zp distribution of changes in pig (left panel) and in mouse (right panel) are reported as the log2-fold changes expressed in units of standard deviation around the averages with respect to controls. Black line delimitates the Zp means.

Additionally, we were able to corroborate that in mice these oxidative events affected the same biological processes as in pig. Enrichment of proteins affected by the different oxidative waves revealed that early oxidation affects ATP activity, contractile and stress response proteins in mice as well as in pig. Also, the second oxidative wave of cys-reversible and irreversible oxidation affected extracellular, membrane and metal ion proteins (Table 3).

Table 3 Functional enrichment of processes impacted by the oxidative events after MI in mouse model. P-values for enriched processes and homologous to pig (Table 1) are shown. Enrichment analysis was performed by calculating the hypergeometric P-value for the enrichment of functional categories from GO database, using total count of PSMs as frequency value. To account for the contribution of the background cardiac proteome, we used the identified non-modified proteome as reference population.

	Mouse Processes		Early Irrev. Oxidation	Later Irrev. Oxidation	Cys-Rev. Oxidation
ENRICHED IN EARLY IRREV. OXIDATION	*ATP activity*				
		ATP binding [GO:0005524]	**<0.0001**	n.s.	n.s.
		ATP metabolic process [GO:0046034]	**<0.0001**	n.s.	n.s.
		ATPase activity [GO:0016887]	**0.0018**	n.s.	n.s.
		Actin-dependent ATPase activity [GO:0030898]	**<0.0001**	n.s.	n.s.
		Mitochondrial ATP synthesis coupled proton transport [GO:0042776]	**<0.0001**	n.s.	n.s.
		Mitochondrial proton-transporting ATP synthase complex [GO:0005753]	**<0.0001**	n.s.	n.s.
		Regulation of ATPase activity [GO:0043462]	**<0.0001**	n.s.	n.s.
	Cardiac Contraction				
		Regulation of the force of heart contraction [GO:0002026]	**0.0066**	n.s.	n.s.
		Regulation of heart rate [GO:0002027]	**0.0036**	n.s.	n.s.
		Myosin filament [GO:0032982]	**0.0006**	n.s.	n.s.
		Microfilament motor activity [GO:0000146]	**<0.0001**	n.s.	n.s.
		Myosin complex [GO:0016459]	**<0.0001**	n.s.	n.s.
		Regulation of heart contraction [GO:0008016]	**<0.0001**	n.s.	n.s.
		Myofibril [GO:0030016]	**<0.0001**	n.s.	n.s.
	Stress and ROS response				
		Stress fiber [GO:0001725]	**0.0033**	n.s.	n.s.
ENRICHED IN LATER IRREV. AND REV. OXIDATION	*Extracellular and Membrane*				
		Cell adhesion [GO:0007155]	n.s.	**0.0449**	**0.0171**
		Extracellular matrix organization [GO:0030198]	n.s.	**<0.0001**	**<0.0001**
		Extracellular matrix [GO:0031012]	n.s.	**<0.0001**	**<0.0001**
		Extracellular matrix disassembly [GO:0022617]	n.s.	**<0.0001**	**<0.0001**
		Extracellular matrix structural constituent [GO:0005201]	n.s.	**<0.0001**	**<0.0001**
	Other				
		Response to hydrogen peroxide [GO:0042542]	n.s.	**<0.0001**	**0.0300**
		Anion transport [GO:0006820]	n.s.	**0.0090**	**0.0365**
		Copper ion binding [GO:0005507]	n.s.	**<0.0001**	**<0.0001**

Furthermore, we were also able to spot very specific systems biology changes several hours after the onset of reperfusion in the mouse model. Protein categories including cell movement of leukocytes, acute phase response signalling, immune response, phagocytosis and glycoproteins were found significantly increased and continued to increase until 24h/48h (Supplementary Figure S6), suggesting that neutrophil recruitment-related processes were also taking place in small animal model.

Table 4 Zp changes of modified peptides from enriched proteins in different oxidative events in mice: early irreversible oxidation at 10 min and irreversible and reversible oxidation at 2h-24h. Enrichment analysis was performed by calculating the hypergeometric P-value for the enrichment of functional categories from GO database, using total count of PSMs as frequency value and to account for the contribution of the background cardiac proteome, we used the identified non-modified proteome as reference population. P-values for enrichment can be found in Table 3. Zp values are reported as the log2-fold changes expressed in units of standard deviation around the averages with respect to controls.

		Enriched Categories	Gene	Sequence	Modification
Early Irreversible Oxidation	*ATP Activity, Cardiac Contraction, Stress and ROS response*	ATP binding [GO0005524] ATP metabolic process [GO0046034] actin-dependent ATPase activity [GO0030898]	**Ckm**	SFIVW[15.994528]VNEEDHIR	W Oxidation
			Atp5o	YATAIY[31.988854]SAASK	Y Dioxidation
			Atp5b	AHGGY[31.988854]SVFAGVGER	Y Dioxidation
				AHGGY[15.994528]SVFAGVGER	Y Oxidation
		response to reactive oxygen species [GO0000302]	**Ndufa8**	AAAHHYGAQC[31.988854]DK	C Dioxidation
			Pdha1	AAASTDYY[15.994528]K	Y Oxidation
			Pdlim5	IIEDTEDW[31.988854]RPR	W Dioxidation
			Cox5b	GIDPYN[31.988854]MIPPK	N Dioxidation
		actin-dependent ATPase activity [GO0030898] ATP binding [GO0005524] ATP metabolic process [GO0046034] ATPase activity [GO0016887] microfilament motor activity [GO0000146] muscle contraction [GO0006936] myosin complex [GO0016459] myosin filament [GO0032982] regulation of the force of heart contraction [GO0002026] response to reactive oxygen species [GO0000302]	**Myh**	DAIIVIQW[15.994528]NIR	W Oxidation
				DAIIVIQW[31.988854]NIR	W Dioxidation
				ITGAIMHY[15.994528]GNMK	Y Oxidation
				ITGAIMHYGN[15.994528]MK	N Oxidation
				TIEDQANEY[15.994528]R	Y Oxidation
				TIEDQANEY[31.988854]R	Y Dioxidation
				AQIEF[15.994528]NQIK	F Oxidation
				AQIEFN[15.994528]QIK	N Oxidation
				IY[15.994528]DNHIGK	Y Oxidation
Later Irreversible and Reversible Oxidation	*Extracellular, membrane, cell adhesion proteins*	extracellular exosome [GO0070062] extracellular region [GO0005576] extracellular space [GO0005615]	**Fgb**	YC[31.988854]GIPGEYWIGNDK	C Dioxidation
			Gapdh	VPTPNVSVVDLTC@R	Cys Reversible Ox
				VPTPNVSVVDITC[31.988854]R	C Dioxidation
			Ldha	SADTIW[15.994528]GIQK	W Oxidation
			Plg	WEYC[31.988854]DIPR	C Dioxidation
			Sod1	LAC@GVIGIAQ	Cys Reversible Ox
			Tpi1	DIGATW[31.988854]VVIGHSER	W Dioxidation
			Acta2	LC@YVALDFENEMATAASSSSLEK)	Cys Reversible Ox
			Actb	C@DVDIR	Cys Reversible Ox
				LC@YVALDFEQEMATAASSSSLEK)	Cys Reversible Ox
			Fbn1	GFMTNGADIDEC@K)	Cys Reversible Ox
				YDDEEC@TLPIAGR	Cys Reversible Ox
			Tf	LLEAC@TFHK)	Cys Reversible Ox
		extracellular exosome [GO0070062] extracellular region [GO0005576] extracellular space [GO0005615] cell adhesion [GO0007155]	**Lamc1**	SQEC@YFDPELYR	Cys Reversible Ox
				TIPTGC[31.988854]FNTPSIEKP	C Dioxidation
			Col6a3	GDSVDQC@ALIQSIR	Cys Reversible Ox
			Dpt	MTDYDC@EFENV	Cys Reversible Ox

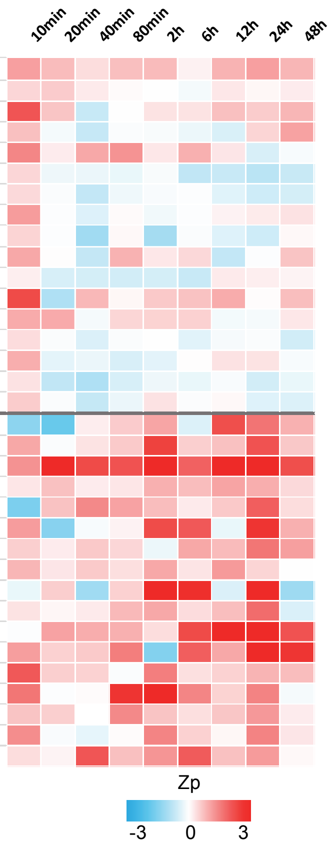

Moreover, biological categories alterations correlated with MPO protein expression changes (Zq) that showed maximal increase in mouse samples at 24h after I/R (Figure 35) and coincided with the increase in protein reversible and irreversible modifications (Figure 33b-c).

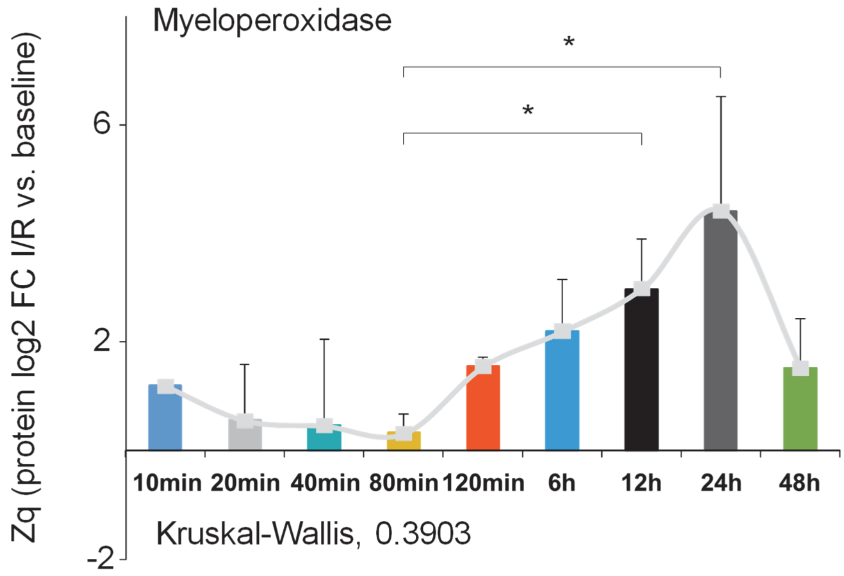

Figure 35 MPO expression changes along time course in mouse I/R model. Zq relative abundance values are reported as the log2-fold changes of protein expression values expressed in units of standard deviation around the averages with respect to controls. * Indicates p value < 0.05. P-values are calculated using Kruskal-Wallis test

These consistent results demonstrated the different nature (chemical and biological) of modifications and biological processes affected by the two oxidative waves along the time after reperfusion, strongly suggesting that they reflect a different pathophysiological mechanism (Table 4).

Neutrophil contribution to the increased protein oxidative levels after myocardial I/R

To elucidate the role of neutrophils in the oxidative events presented before, we performed an experiment of I/R in neutrophil depleted mice. Neutrophil depletion was performed by anti-Ly6G injection and IgG was used as vehicle (Figure 36).

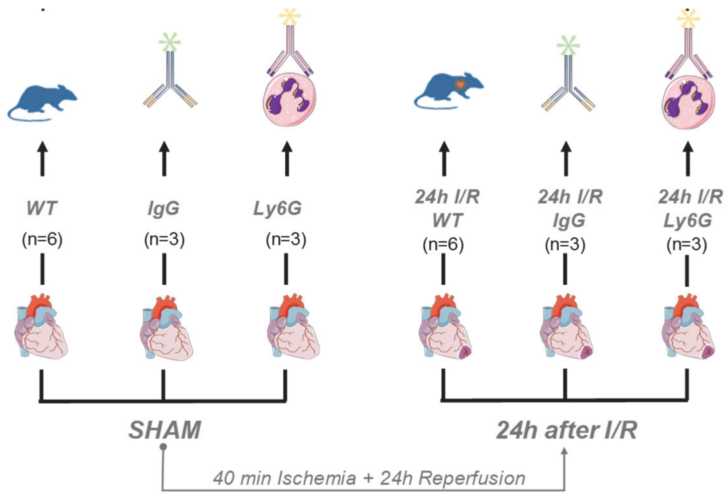

Figure 36 Study design. Sham and infarcted mice were injected with neutrophil depleting antibody anti-Ly6G. Negative controls were injected with IgG as a vehicle.

Depletion with anti-Lys6G resulted in significant reduction of circulating neutrophil counts (Figure 37) (n=3 mice per group), whereas blood monocytes were unaffected, when measured at 24h post-MI and repeated injections, which are in agreement with the previously reported study by Horckmans et al. [102].

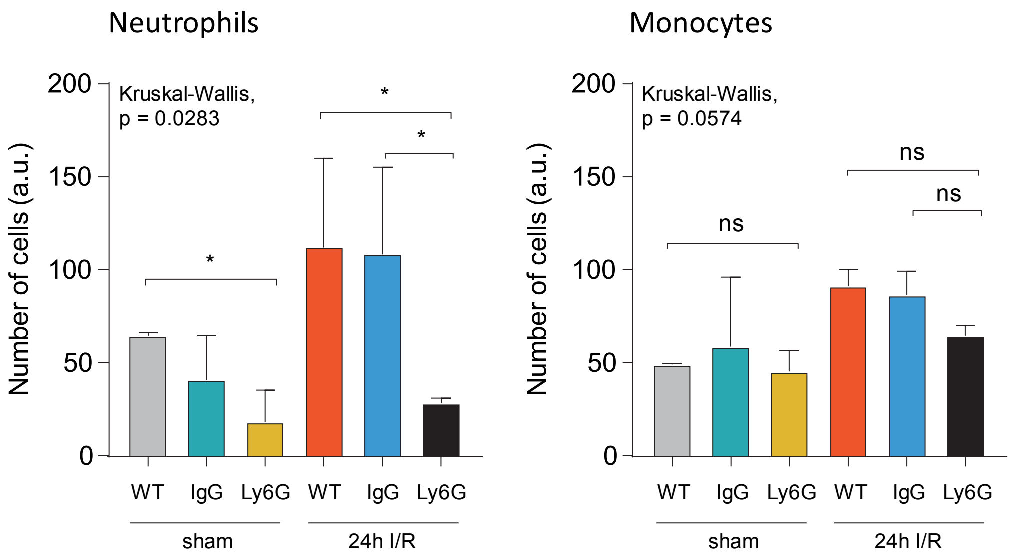

Figure 37 Cell count of circulating neutrophils and Monocytes in mice peripheral blood. Analysis performed by Borja Ibañez's lab in CNIC. ns indicates pvalue > 0.05, * Indicates p value <0.05. P-values are calculated using Kruskal-Wallis test

Moreover, the protein extracts from depleted mice showed significantly lower values for the functional categories related to immune response including proteins involved in complement response, blood clotting, transmembrane proteins interactions and ventricular hypertrophy (Figure 38).

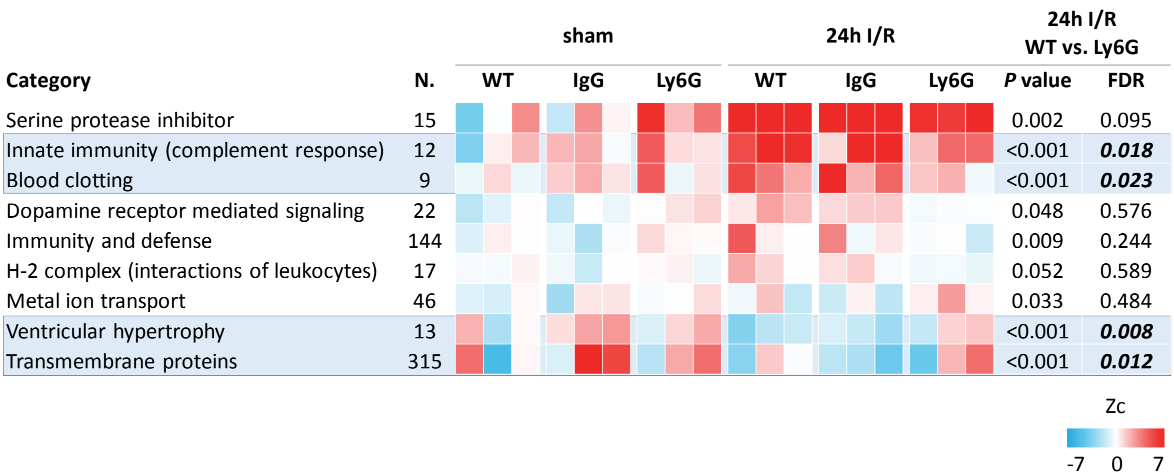

Figure 38 Categories affected by neutrophil depletion in the mouse I/R model. Functional categories values (Zc) significantly (P-values are calculated using Student's t-test, post hoc FDR Benjamini Hockberg) changing after 24h infarction in WT and neutrophil depleted animals. Full list of protein's Zq changes for each category can be found in Supplementary Table S15.

Similar results were observed for selected proteins from neutrophil granules subsets: azurophilic granules (primary), specific granules (secondary) and gelatinase granules (tertiary), which showed significantly lower abundance values (Zq) in depleted animals (Figure 39). These results confirm overall lower inflammatory response in cardiac tissue related to the reduced infiltration levels of neutrophils.

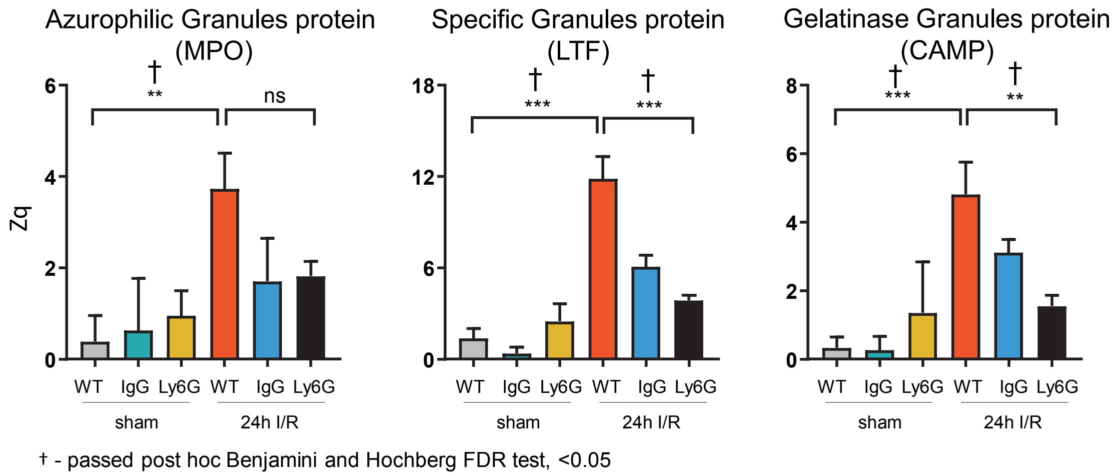

Figure 39 Proteins affected by neutrophil depletion in the mouse I/R model. Primary (myeloperoxidase, MPO), secondary (lactotransferrin, LTF) and tertiary (cathelicidin anitimicrobial peptide, CAMP) granules proteins significant changes in neutrophil depleted animals infarcted hearts. Zq relative abundance values are reported as the log2-fold changes of protein expression values expressed in units of standard deviation around the averages with respect to WT sham control pool. ns indicates p value > 0.05, ** Indicates p value < 0.01, *** indicates p value <0.001. P-values were calculated using Student's t-test, post hoc FDR Benjamini Hockberg.

24h after infarction, proteomics analysis revealed that neutrophil depletion led to lower reversible Cys oxidation levels which can be appreciated in the complete population (347 sequences) of oxidized Cys-containing peptides (Figure 40, left, Supplementary Table S16). The average abundance values of the whole oxidized Cys-containing peptide population in biological replicates (n=3) showed a significant reduction in reversible oxidation levels in the depleted mice with only a slight decrease in the animals injected with the vehicle (IgG) (Figure 40, right).

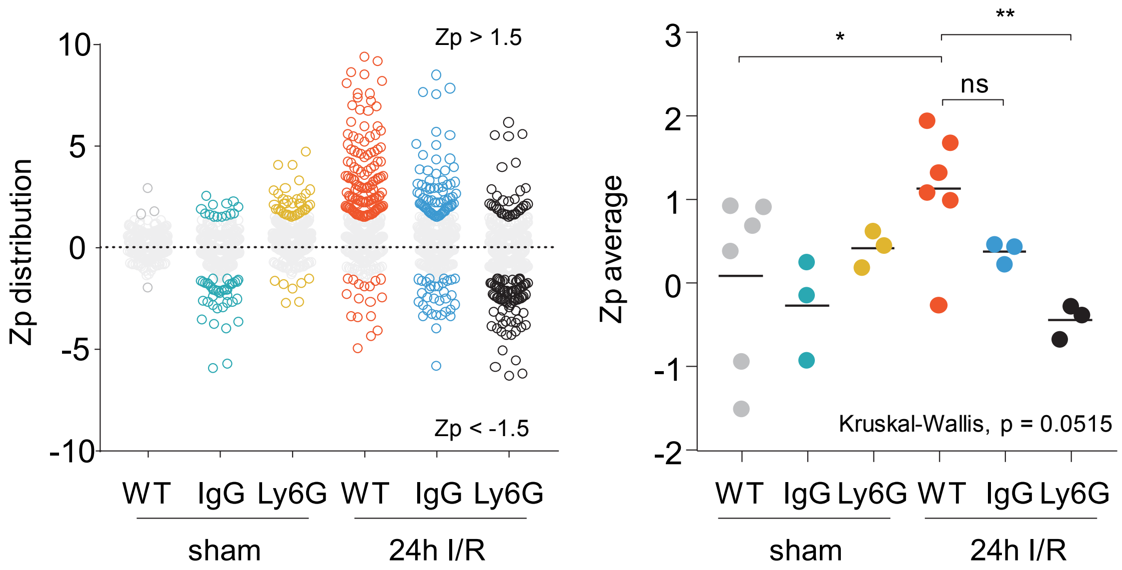

Figure 40 Total population of reversibly oxidized Cys-peptides changes in infarcted (24h I/R) and sham-operated mice. Wild-type (WT), vehicle (IgG) and neutrophil depletion (Ly6G) Zp oxidized peptide values are reported as the log2-fold changes in each condition with respect to pool (n=6) of sham-operated WT controls (left panel). Right panel shows averages of total Zp oxidized Cys-containing peptide population for each individual (n=3, n=6). ns indicates pvalue > 0.05, * Indicates p value < 0.05, ** indicates p-values < 0.01. P-values are calculated using Kruskal-Wallis test. Full list of reversible Cys-oxidized peptides can be found in Supplementary Table S16.

Additionally, global PTM analysis of irreversibly oxidized peptide population presented similar reduction in oxidation levels in depleted mice (Figure 41, left panel) containing mainly Cys and Trp irreversible oxidations (Supplementary Table S17). We also identified a peptide subpopulation that was previously detected in pig and mice longitudinal experiments as part of the second irreversible oxidative event of cluster 2 in pig ischemic tissue (Figure 41, right panel, Supplementary Table S17, marked in red, pig data showed on Figure 7).

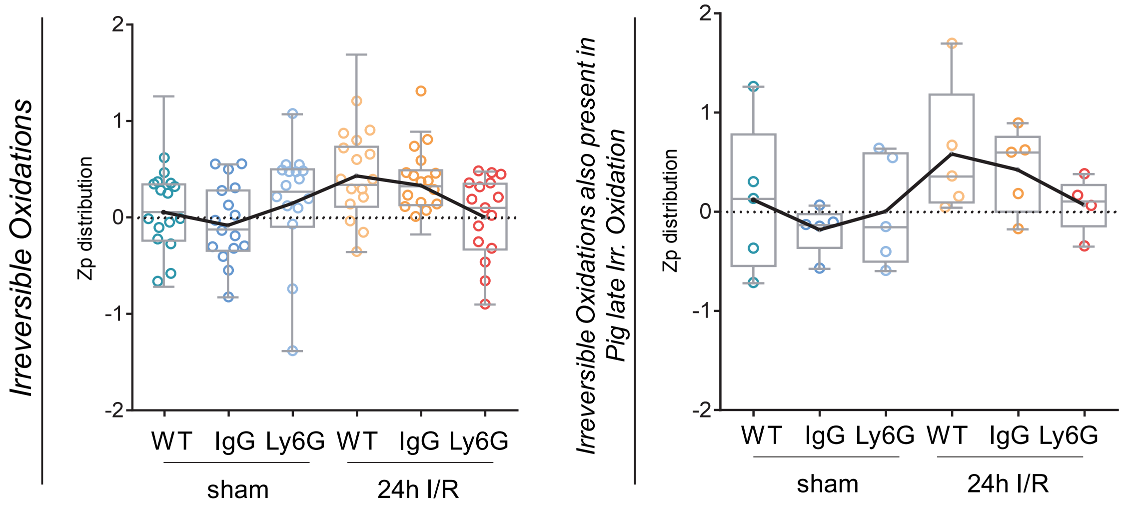

Figure 41 Changes of Irreversibly oxidized peptides in infarcted (24h I/R) and sham-operated mice. Zp irreversibly oxidized peptide values in wild-type (WT), vehicle (IgG) and neutrophil depletion (Ly6G) experimental groups are reported as the log2-fold changes in each condition with respect to pool (n=6) of sham-operated WT controls Right panel shows the Zp distributions of a subpopulation of irreversible oxidized peptides that were also present in cluster 2 of irreversible oxidation in pig I/R model. Full list of modified peptides from this scatter plot is reported in Supplementary Table S17. Black lines delimitates the peptides Zp means

Increased Cys reversible oxidations at 24h after reperfusion most affected by depletion of neutrophils (Ly6G), but not by the injection if IgG, are summarized in Table 5. Neutrophil-depleted mice 24h after I/R showed substantially lower reversible oxidation levels impacting on membrane and extracellular proteins, which were identified as characteristic oxidized proteins by the late wave (2h – 24h) of cys-reversible and irreversible modifications in pig (Table 1 and Table 2) and mouse (Table 3) models of I/R. Affected amino acid residues included proteins involved in ECM integrity and cell-cell junctions: fibrillin (FBN), laminin (LAM), alpha-sarcoglycan (SGCA), basement membrane-specific heparan sulfate proteoglycan core protein (HSPG2), glypican (GPC).

In conclusion, depletion of neutrophils at 24 h after reperfusion resulted in a decrease of granule components in the tissue as well as a decrease in reversible and irreversible oxidation, indicating the participation of neutrophils in the second event of oxidation between 2 and 24 hours after reperfusion. Moreover, neutrophils presence specifically affects the ECM integrity and cell-cell junction processes.

Table 5 Reversible Cys-oxidations affected by neutrophils in the infarcted hearts. Zp oxidized peptide values are reported as the log2-fold changes in each condition with respect to pool (n=6) of sham-operated WT controls. Cys-reversible oxidation is shown as "@" in the peptide sequence. Full list of reversible Cys-oxidized peptides can be found in Supplementary Table S16.

	Protein	Gene	Peptide
Extracellular	Kininogen-1	Kng1	ENEFFIVTQTC@K
	Complement C3	C3	AC@EPGVDYVYK
			DSC@IGTLVVK
	Laminin subunit gamma-1	Lamc1	HNTYGVDC@EK
			SQEC@YFDPELYR
	Laminin subunit beta-1	Lamb1	C@VC@NYLGTVK
	Fibronectin	Fn1	TFYSC@TTEGR
	Plasminogen	Plg	WEYC@DIPR
		Plg	SGVAC@QK
	Murinoglobulin-1	Mug1	ALSC@LESSWK
	Thrombospondin-1	Thbs1	DNC@QYVYNVDQR
	Serum paraoxonase/arylesterase 1	Pon1	EVTPVELPNC@NLVK
	Actin, aortic smooth muscle	Acta2	C@DIDIR
	Laminin subunit alpha-2	Lama2	IGPVTYSLDGC@VR
	Prosaposin	Psap	SLPC@DIC@K
			GC@SFLPDPYQK
			LGPGVSDIC@K
			GLSNAC@ALLPDPAR
	Laminin subunit beta-2	Lamb2	GSC@YPATGDLLVGR
	Fibrillin-1	Fbn1	C@PTGYYLNEDTR
			GWGPHC@EIC@PFEGTVAYK
	Collagen, type VI, alpha 3	Col6a3	ISC@SGNQLPTVR
	Fibrinogen	Fgb	TPC@TVSC@NIPVVSGK
			YC@GLPGEYWLGNDK
			VYC@DMK
	Cathepsin D, isoform CRA_a	Ctsd	AIGAVPLIQGEYM_IPC@EK
Membrane	Sarcoplasmic/endoplasmic reticulum calcium ATPase 2	Atp2a2	GTAVAIC@R
	Sodium/potassium-transporting ATPase subunit beta-1	Atp1b1	YNPNVLPVQC@TGK
	Alpha-sarcoglycan	Sgca	VGSATPFSTC@LK
	Basement membrane-specific heparan sulfate proteoglycan core protein	Hspg2	QC@SSSSWSR
			AGLSSGFVGC@VR
			VPSGLYLGTC@ER
	Sarcalumenin	Srl	NPGAPNC@DK
			TGC@GETPK
	Serotransferrin	Tf	NQQEGVC@PEGSIDNSPVK
	Glypican-1	Gpc1	QLHPQLLPDDYLDC@LGK
	CD36 antigen, isoform CRA_a	Cd36	FFSSDIC@R
	Enolase 1, alpha non-neuron	EG433182	VNQIGSVTESLQAC@K

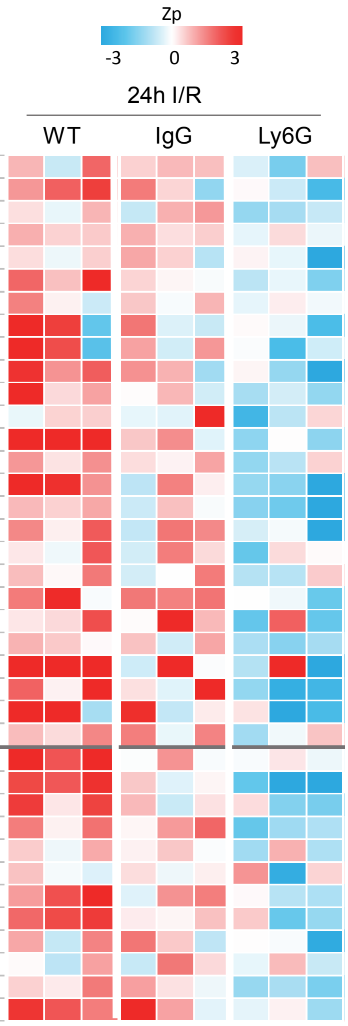

Discussion

AMI leads to three different oxidative events

AMI leads to large necrotic area generation, which in turn induces an inflammatory process for cellular debris clearance. In acute inflammatory response leukocytes are recruited to the lesion site and contribute to the tissue injury (by engaging in the respiratory burst) but also have been proven essential for the post-MI inflammation resolution and cardiac healing [102, 103]. Oxidative stress studies in the context of heart infarction mainly focused on biochemical measurements of free radicals at selected time points after reperfusion [93, 96, 104, 105]. In contrast, our study aimed at understanding the exact timeline of proteme-wide modifications and to decipher the pattern of PTMs that were affected during the first week after I/R. The proteome-wide analysis of modifications in AMI revealed the appearance of three clearly separated forms of oxidation as well as the scope of cardioprotection in the reperfusion-induced cardiac protein and PTM alterations.

Our unbiased approach identified two systematic behaviors in PTMs changes in the ischemic myocardium (at 20 min and 2h-24h) within the first 24h after I/R, which consisted in temporarily coordinated changes of irreversibly oxidized peptides. Moreover, the dynamics of the thiol redox proteome revealed that Cys reversible oxidation timely overlapped with one of the irreversible oxidation events (2h-24h) and that both affect similar proteins. The results presented suggest that there are at least two oxidative events of different nature reversibly and irreversibly affecting cardiac proteins during the first 24 hours after reperfusion in the infarcted myocardium; which are accompanied by a subsequent emergence of increased hydroxyprolination and lipid peroxidation towards the end of the week after I/R. In this study we hypothesized that these three timely separated events might be generated by diverse however inevitably complementary pathophysiological processes.

Reperfusion generates an initial wave of oxidative damage

On the start of reperfusion, with the return of oxygen, a large burst of ROS has been consistently shown to occur [92-97, 106], which agrees with the fast and early protein irreversible oxidation presented in our study. Furthermore, in the ischemic area, reperfusion was associated with an immediate formation of edema detected by sharp increase in T2 relaxation time above baseline values, reaching a peak at 40 minutes after reperfusion. This initial increase in ROS has been proposed to be the result of succinate accumulation under ischemia that, upon reperfusion, gets hastily oxidized resulting in a burst of ROS, probably mediated by reverse electron transport from complex II to complex I [106]. The initial ROS together with an I/R-induced calcium influx into mitochondria opens the MPTP, further increasing ROS formation, decreasing ETC activity, and finally causing cell death [107].

This locally-generated ROS might be prone to affect intracellular proteins and those more sensitive to ROS due to its energy-related functions. In this line, our study of initially oxidized proteins revealed that this wave of oxidation affected to intracellular proteins fundamental to cardiac contraction and energy production and transfer. This generalized oxidation produced by blood flow restoration and MPTP assembly suggests the origin of cardiac contractile and energetic machinery dysfunction observed by our group [20]. In agreement with our line of reasoning, these early stages (20min) of reperfusion are characterized by a decrease in mitochondrial matrix metabolism proteins and an increase in sarcoplasmic Ca^{2+} concentration regulators and myosin filament components.

Neutrophil infiltration contributes to the later event of oxidative damage

Recruitment of leukocytes such as neutrophils to the extravascular space in the necrotic lesion site is a critical step of the inflammation process and plays a major role in several cardiovascular diseases (CVDs); especially MI [103, 108]. Neutrophil-mediated oxidative burst is a critical mechanism of inflammation that involves the rapid generation and release of reactive oxygen species (ROS) [109]. A fundamental mechanism of I/R is the disruption of redox balance, whereby ROS–induced modifications might alter sarcomeric function or trigger pro- or anti-apoptosis signaling pathways [110, 111]. A reversible redox-dependent coupling of an NO or OH moiety to a reactive Cys thiol can rapidly regulate protein activity or subcellular localization [112] and interaction with other proteins, which is an important mechanism of redox-mediated signal transduction [113].

The increase in Cys reversible oxidation between 2h-24h coincided with the second irreversible oxidation episode and affected the same functional processes. Irreversible oxidation targeted mostly Cys residues, but also other amino acids sensitive to oxidation such as Trp. These two events temporally coincide with the reported maximum in neutrophil infiltration density in the ischemic tissue [18] and correlated with an increase in MPO abundance and activity as well as other proteins related to neutrophil recruitment. MPO is a peroxidase most abundantly expressed in neutrophils, stored in azurophilic granules and it is known to produce an increase in protein oxidation via generation of oxidative species such as hypochlorous (HOCl), hypobromous (HOBr), and hypothiocyanous (HOSCN) acids from H_2O_2 [114, 115]. *In vitro* experiments of MPO and its oxidative by-products proposed their specificity to rapidly oxidize protein thiols demonstrated by Cys fluorescent dye [114] and spectrophotometry [116] measurements. Fluorescence analyses have also shown Trp residues as specific target of MPO oxidation [117]. Moreover, our study demonstrated irreversible and reversible Cys oxidation of metal ion binding proteins, which suggests these might be specifically susceptible to MPO oxidation. This result stays in the agreement with spectroscopic and analytical measurements of MPO *in vitro* interaction with iron ions producing oxygenation of protein sulfide groups [116, 118, 119]. This property of MPO in neutrophil-induced oxidation should be taken into special consideration as majority of the enzymatic proteins contain metal ion clusters in their active centers.

Additionally, the study of a simpler model of I/R (mouse), allowed for the simultaneous validation of previous findings and the adaptation of the experimental set up to the further interventions aimed to reveal the role of neutrophils in protein oxidation. We were able to provide evidence that neutrophils contributed to the oxidative episode detected during 2h-24h of reperfusion. Interestingly, neutrophil depletion greatly decreased the oxidation levels of two enzymes whose proper activity is paramount for the destruction of free superoxide radicals in the cell, contributing to the increased oxidation. Extracellular and membrane proteins were also present within the group of the oxidatively impacted proteins during 2h-24h. Not only might they be more prone to direct exposure to neutrophils infiltrating the myocardial interstitium, but also ECM proteins such as perlecan bind MPO via its sulfate side chains, which can enhance the oxidative damage [120]. Neutrophil depletion also affected the oxidation levels of extracellular and membrane proteins which confirmed our previous observations in large animal model of I/R. Furthermore, our results also revealed that the presence of neutrophils oxidizes proteins involved in ECM integrity and cell-cell junctions, probably contributing to the cell-cell and ECM disassembly and disaggregation during the acute inflammation face, which contributes to the initiation of the resolution and repair fase [8, 103], as well as the second wave of edema at 7 days [18].

The second oxidative event accompanies general oxidative stress

As H_2O_2 represents a universal indicator of oxidative stress and, its overall concentration levels might represent the accumulation of oxidative phenomena corresponding to various sources. Our results show a maximum H_2O_2 concentration in the ischemic tissue after 24h of reperfusion as it might be generated by different biological events such as the reperfusion-induced oxidative stress and inflammation, stabilization of the neutrophils infiltration, their activity in the damaged area, and the opening of the MPTP, the hallmark of reperfusion-induced cardiomyocyte death. Nonetheless, H_2O_2 is essential for the oxidative activity of MPO [114, 115] which also showed an increased enzymatic activity during this period of reperfusion. Based on our findings, neutrophils recruited to the ischemic lesion site release MPO, which probably in the presence of high H_2O_2 levels from the necrotic tissue contribute to oxidative burst. Our data suggests that this inflammation-driven phenomenon particularly affects protein Cys and Trp residues by reversible and irreversible oxidation during the period of 2h-24h after reperfusion.

Reperfusion generates the early and later oxidative events and Preconditioning reduces the impact of the oxidative burst.

The study of the animals subjected to the prolonged episode of ischemia (2h) showed that reperfusion is the principal contributor to both the reversible and irreversible protein oxidation oxidative events. Levels of ROS generated during ischemia are generally low and the pathological significance of them is uncertain, as many studies have consistently demonstrated an increase in ROS on the start of reperfusion [92-97].

The analysis of the preconditioning intervention allowed us to identify the protein targets responsive to cardioprotection. Preconditioning experiment has shown that the probable components of MPTP structure (along with the muscle filament sliding regulators and sarcoplasmic Ca^{2+} transporter) are some of the most vulnerable proteins during the first 24h of reperfusion. Since MPTP releases free radicals during the extent of reperfusion, these provide abundant substrate supply for the MPO released from recruiting neutrophils, and might suggest that their presence intensifies the rupture of the already critically impaired mitochondrial and sarcomere integrity.

Oxidative events echoes in the remote myocardium

While reperfusion induces broad oxidation changes the ischemic tissue, remote myocardium tissue seemingly did not display any characteristics of acute oxidative events, as we did not detect any significant changes in the reversible thiol oxidation status. Conversely, irreversible oxidation in Cys residues of plasmatic proteins and a generalized slight increase in irreversible oxidation were observed 2h post-I/R, which suggests that plasma proteins impacted during the oxidative burst in the ischemic lesion site were collaterally delivered to the remote area. Moreover, we observed an increase (after 2h I/R) in the antioxidant enzymes abundance co-occurring with the increase in protein irreversible oxidation, which might reflect remote myocardium compensation mechanisms and an endeavor to reduce the excessive oxidative impact. Temporary oxidative imbalance detected in the remote tissue was followed by the dynamic alteration in the contractile and energetic machinery (2h-6h after I/R onset), which could be related to the irreversible protein oxidation appearance as well as to the transient dysfunctional contractility reported in the remote myocardium at the early stages of reperfusion [20].

Deferred oxidative event and lipid peroxidation

By the end of the first week after reperfusion, ischemic tissue undergoes a process of healing and repair that accompanies a second deferred edema wave [18, 19]. This process was previously described as a phenotypic change in the infarcted myocardial tissue caused by the removal of necrotic myocytes rich in mitochondria and with high metabolic activity; and the deposition of collagen, extracellular matrix proteins, and fibroblasts with lower mitochondrial content and metabolic activity [20]. Notably, we identified an increase in Proline hydroxylation in collagens in the ischemic myocardium that increases towards day 7, as well as an increase in prolyl-hydoxylases. It is well established that these hydroxylations are essential for fibrillar collagen structural stability, through the hydrogen bonding of the hydroxyprolines part of the triple helix [121-124]. Thus, we hypothesize that this late oxidative event might be triggered by the previous inflammatory processes, where immune cells infiltration generates an increase in ROS and the consecutive degradation of the ECM, contributing, together with the increase in prolyl-hydroxylases, to the fibrotic structure and scar formation in the ischemic tissue.

The progressive increase in Pro hydroxylation of collagen fibres co-occurs with lipid peroxidation. Oxidative stress signals are also widely known to generate numerous peroxidised lipid species, whose chemical stability can lead to their accumulation over time [125]. Increased lipid oxidation has especially been observed in heart failure patients [126, 127] where the heart switches from fat to glucose metabolism causing a defective mitochondrial FA oxidation [128, 129]. Gradual accumulation of peroxidised lipids might generate toxic end-products as MDA and 4-HNE [130], which are bioactive secondary messengers and eventually lead to cell death [131]. The results from pig infarcted myocardium show a steady accumulation of peroxidised lipids in the infarcted tissue reaching maximal values towards the end of the week. Moreover, by the end of the first week of reperfusion the secondary edema formation was observed in the ischemic myocardium [17, 19], and could be potentially related to lipid peroxidation products accumulation in the scarring myocardial tissue. Lipid peroxidation alters the physiological functions of cell membrane lipid bilayer as oxidized lipid tails become polar and can be shorter in length, due to the presence of aldehyde or hydroperoxide groups [132]. Changes in chemical properties of lipids in response to MI injury might therefore lead to their physical attraction to the collagen-enriched fibrous connective tissue formed during the reparative processes that are accompanied by pathophysiological edema. Hence, not only the extent of scarred tissue, but also the amount of peroxidised lipid species and collagen hydroxy-proline detected after MI might play an important role in the panel of disease prognostic factors.

Final considerations

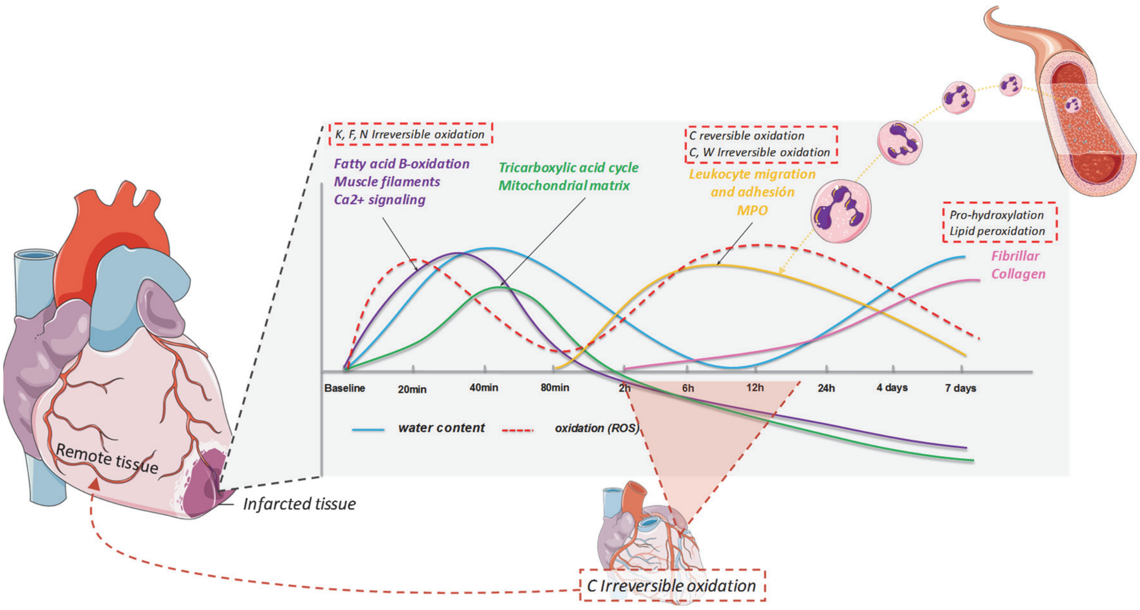

Figure 42 Schematic diagram of the three oxidative waves in the infarcted area the first week after I/R and its effect in the remote tissue: A transient and early (minutes after I/R) increase of irreversible oxidations in Lys, Phe and Asn residues, the second irreversible oxidation of Cys and Trp residues peaking at 24 h post-reperfusion related to neutrophil infiltration and the Pro-hydroxylation in a late phase of repair through collagen structure stabilization. Second wave of irreversible oxidation in the infarcted tissue might generate the extravasation of Cys irreversible oxidized proteins to the remote tissue. Protein oxidation levels after the onset of I/R during the first week are schematized in red discontinued line. Changes in water content are represented in blue. Some graphical elements from this figure were adapted from Servier Medical Art Powerpoint image bank. Servier Medical Art by Servier (http://www.servier.com/Powerpoint-image-bank).

This PhD Thesis presents the application of global PTMs analysis combined with the mapping of redox-active thiols in myocardial tissue proteins to study the oxidative stress in pig and mouse models of I/R. Our study aimed at gaining systematic understanding of the timeline of different oxidative processes, how their molecular targets are affected during the first week after I/R, the effect of these proceses in the remote tissue and what is the scope cardioprotection in the oxidation-induced cardiac protein alterations, which may be critical for heart outcome.

We were able to identify numerous oxidative events, caused by reperfusion and taking place during the first week after I/R in a very translational animal model. A short-term episode of irreversible oxidation is detected within first 20 min of reperfusion and might be closely related to reperfusion-driven oxidation and mitochondrial ROS release into cardiomyocytes. The recruitment of neutrophils to the lesion site at 2h-24 h contributes to the appearance of a second oxidative event (reversible and irreversible protein oxidations), which is secondary to reperfusion and can be ameliorated by cardioprotective intervention. As an outcome of multiphasic oxidative events, we detected a gradual accumulation of peroxidized lipids and fibrotic collagen. This comprehensive oxidative stress analysis highlights new clues in the molecular mechanisms of cardiac injury and repair following I/R.

Conclusions

1. There are three different oxidative events taking place in the ischemic myocardium after I/R detectable in different animal models. These oxidative events were produced by differentiated molecular mechanisms: they have a different origin, coincide with different changes in the proteome and affect different proteins and residues.

2. Blood flow restoration causes a disruption of the mitochondrial ETC, increasing ROS in the cardiomyocytes of the infarcted. This increase in ROS is detectable 20 min after reperfusion in pig and 10 min after reperfusion in mice, and irreversibly and generally monooxidizes Lys, Phe and Asn residues of CM's intracellular proteins that are closer to the source of oxidation and related to energy and cardiac contraction.

3. 2h after reperfusion, reperfusion damage in the infarcted tissue starts to recruit immune cells to the zone to start the physiological inflammation and repair of the area, whose higher presence peaks at 24h after reperfusion. Recruited neutrophils release the content of their granules, including MPO, which contributes to a second episode of Cys-reversible and Cys and Trp-irreversible oxidation in the infarcted area, affecting extracellular and membrane proteins more accessible to MPO in specific sensitive residues. This effect can be ameliorated by cardioprotective mechanisms.

4. Towards the end of the first week, the cardiac tissue undergoes a phase of fibrosis with an increase in fibrillar collagen formation through Pro-hydroxylation as well as an accumulation of peroxidized lipids that are deposited in the tissue, all together contributing to the scar formation.

5. The remote myocardium senses ischemic alterations as the oxidative events in the ischemic tissue produce oxidations in the remote myocardium through the deposit of Cys-irreversibly oxidized plasmatic proteins coming from the infarcted area, favored by the first wave of edema.

Conclusiones

1. Se dan tres eventos oxidativos diferentes en la zona infartada después de la reperfusión. Estos eventos son detectables en distintos modelos animales y están producidos por mecanismos moleculares diferenciados: tienen un origen diferente, coinciden con distintos cambios en el proteoma y afectan diferentes proteínas y residuos.

2. La restauración del flujo sanguíneo provoca una alteración de la ETC mitocondrial, aumentando ROS en los cardiomiocitos del área infartada. Este aumento en ROS es detectable 20 min después de la reperfusión en cerdos y tras 10 min en ratón, y provoca la monooxidación irreversible y general de residuos de Lys, Phe y Asn de proteínas de cardiomiocitos relacionadas con la energía y la contracción cardíaca por su situación más próxima a la fuente de oxidación.

3. 2 h después de la reperfusión comienza el reclutamiento de células inmunitarias a la zona infartada para iniciar la fase de inflamación y de reparación fisiológica, cuya presencia alcanza su punto máximo a las 24 h después de la reperfusión. Los neutrófilos liberan el contenido de sus gránulos, incluida la MPO, contribuyendo a un segundo episodio de oxidación reversible en Cys e irreversible en Cys y Trp, que afecta principalmente a proteínas extracelulares y de membrana más accesibles a la MPO. Este efecto puede ser minorado por tratamientos cardioprotectores.

4. Hacia el final de la primera semana, el tejido infartado experimenta una fase de fibrosis con un aumento en la formación de colágeno fibrilar a través de la hidroxilación en prolinas, así como una acumulación de lípidos peroxidados que se depositan en el tejido, todo ello contribuyendo a la formación de la cicatriz.

5. El tejido remoto percibe las alteraciones del tejido infartado debido al depósito de proteínas plasmáticas oxidadas irreversiblemente en Cys provenientes del área infartada, cuyo transporte está favorecido por la primera onda de edema.

References

1. Thygesen, K., et al., *Third universal definition of myocardial infarction*. J Am Coll Cardiol, 2012. **60**(16): p. 1581-98.

2. Boateng, S. and T. Sanborn, *Acute myocardial infarction*. Disease-a-Month, 2013. **59**(3): p. 83-96.

3. Anderson, J.L. and D.A. Morrow, *Acute Myocardial Infarction*. N Engl J Med, 2017. **376**(21): p. 2053-2064.

4. Robert O. Bonow, D.M., Douglas Zipes, Peter Libby, *Braunwald's heart disease: A textbook of cardiovascular medicine*. Tenth edition ed, ed. B. Eugene. 2015, Philadelphia, PA: Elsevier/Saunders.

5. Leal, J., et al., *Economic burden of cardiovascular diseases in the enlarged European Union*. Eur Heart J, 2006. **27**(13): p. 1610-9.

6. Badawi, R., *Hurst's the Heart Manual of Cardiology, 12th Edition, McGraw-Hill Companies*. Congenital Heart Disease, 2010. **5**(2): p. 195-195.

7. Reimer, K.A., et al., *The wavefront phenomenon of ischemic cell death. 1. Myocardial infarct size vs duration of coronary occlusion in dogs*. Circulation, 1977. **56**(5): p. 786-94.

8. Frangogiannis, N.G., *The inflammatory response in myocardial injury, repair, and remodelling*. Nature reviews. Cardiology, 2014. **11**(5): p. 255-65.

9. Larose, E., et al., *Predicting Late Myocardial Recovery and Outcomes in the Early Hours of ST-Segment Elevation Myocardial Infarction: Traditional Measures Compared With Microvascular Obstruction, Salvaged Myocardium, and Necrosis Characteristics by Cardiovascular Magnetic Resonance*. Journal of the American College of Cardiology, 2010. **55**(22): p. 2459-2469.

10. Hausenloy, D.J. and D.M. Yellon, *Time to Take Myocardial Reperfusion Injury Seriously*. New England Journal of Medicine, 2008. **359**(5): p. 518-520.

11. Kloner, R.A., *Current state of clinical translation of cardioprotective agents for acute myocardial infarction*. Circ Res, 2013. **113**(4): p. 451-63.

12. Ibanez, B., et al., *Lethal myocardial reperfusion injury: a necessary evil?* Int J Cardiol, 2011. **151**(1): p. 3-11.

13. Ibanez, B., et al., *Evolving therapies for myocardial ischemia/reperfusion injury*. J Am Coll Cardiol, 2015. **65**(14): p. 1454-71.

14. Tani, M. and J.R. Neely, *Role of intracellular Na+ in Ca2+ overload and depressed recovery of ventricular function of reperfused ischemic rat hearts. Possible involvement of H+-Na+ and Na+-Ca2+ exchange*. Circulation research, 1989. **65**(4): p. 1045-56.

15. Ladilov, Y.V., B. Siegmund, and H.M. Piper, *Protection of reoxygenated cardiomyocytes against hypercontracture by inhibition of Na+/H+ exchange*. The American journal of physiology, 1995. **268**(4 Pt 2): p. H1531-9.

16. Piper, H.M., Y. Abdallah, and C. Schafer, *The first minutes of reperfusion: a window of opportunity for cardioprotection*. Cardiovascular research, 2004. **61**(3): p. 365-71.

17. Fernandez-Jimenez, R., et al., *Myocardial edema after ischemia/reperfusion is not stable and follows a bimodal pattern: imaging and histological tissue characterization*. J Am Coll Cardiol, 2015. **65**(4): p. 315-323.

18. Fernandez-Jimenez, R., et al., *Pathophysiology Underlying the Bimodal Edema Phenomenon After Myocardial Ischemia/Reperfusion*. J Am Coll Cardiol, 2015. **66**(7): p. 816-828.

19. Fernandez-Jimenez, R., et al., *Dynamic Edematous Response of the Human Heart to Myocardial Infarction: Implications for Assessing Myocardial Area at Risk and Salvage*. Circulation, 2017. **136**(14): p. 1288-1300.

20. Binek, A., et al., *Proteomic footprint of myocardial ischemia/reperfusion injury: Longitudinal study of the at-risk and remote regions in the pig model*. Sci Rep, 2017. **7**(1): p. 12343.

21. Carrick, D., et al., *Pathophysiology of LV Remodeling in Survivors of STEMI: Inflammation, Remote Myocardium, and Prognosis*. JACC. Cardiovascular imaging, 2015. **8**(7): p. 779-89.

22. Carrick, D., et al., *Temporal Evolution of Myocardial Hemorrhage and Edema in Patients After Acute ST-Segment Elevation Myocardial Infarction: Pathophysiological Insights and Clinical Implications*. Journal of the American Heart Association, 2016. **5**(2).

23. Whalen, D.A., Jr., et al., *Effect of a transient period of ischemia on myocardial cells. I. Effects on cell volume regulation*. The American journal of pathology, 1974. **74**(3): p. 381-97.

24. Kloner, R.A., et al., *Effect of a transient period of ischemia on myocardial cells. II. Fine structure during the first few minutes of reflow*. The American journal of pathology, 1974. **74**(3): p. 399-422.

25. Friedrich, M.G., et al., *The salvaged area at risk in reperfused acute myocardial infarction as visualized by cardiovascular magnetic resonance*. Journal of the American College of Cardiology, 2008. **51**(16): p. 1581-7.

26. Bragadeesh, T., et al., *Post-ischaemic myocardial dysfunction (stunning) results from myofibrillar oedema*. Heart, 2008. **94**(2): p. 166-71.

27. Turschner, O., et al., *The sequential changes in myocardial thickness and thickening which occur during acute transmural infarction, infarct reperfusion and the resultant expression of reperfusion injury*. European heart journal, 2004. **25**(9): p. 794-803.

28. Carlsson, M., et al., *Myocardium at risk after acute infarction in humans on cardiac magnetic resonance: quantitative assessment during follow-up and validation with single-photon emission computed tomography*. JACC Cardiovasc Imaging, 2009. **2**(5): p. 569-76.

29. Dall'Armellina, E., et al., *Dynamic changes of edema and late gadolinium enhancement after acute myocardial infarction and their relationship to functional recovery and salvage index*. Circ Cardiovasc Imaging, 2011. **4**(3): p. 228-36.

30. Vogel, B., et al., *Acute DNase1 treatment improves left ventricular remodeling after myocardial infarction by disruption of free chromatin*. Basic research in cardiology, 2015. **110**(2): p. 15.

31. Ong, S.-B., et al., *The mitochondrial permeability transition pore and its role in myocardial ischemia reperfusion injury*. Journal of Molecular and Cellular Cardiology, 2015. **78**: p. 23-34.

32. Lindsey, M.L., et al., *Guidelines for experimental models of myocardial ischemia and infarction*. American Journal of Physiology-Heart and Circulatory Physiology, 2018. **314**(4): p. H812-H838.

33. Vunjak Novakovic, G., T. Eschenhagen, and C. Mummery, *Myocardial tissue engineering: in vitro models*. Cold Spring Harbor perspectives in medicine. **4**(3): p. a014076.

34. Chen, W., et al., *Endothelial Actions of ANP Enhance Myocardial Inflammatory Infiltration in the Early Phase After Acute Infarction*. Circulation research, 2016. **119**(2): p. 237-48.

35. Fesik, S.W. and Y. Shi, *Structural biology. Controlling the caspases*. Science, 2001. **294**(5546): p. 1477-8.

36. Cieniewski-Bernard, C., et al., *Proteomic analysis of left ventricular remodeling in an experimental model of heart failure*. Journal of proteome research, 2008. **7**(11): p. 5004-16.

37. Xiang, F., et al., *Proteomic analysis of myocardial tissue from the border zone during early stage post-infarct remodelling in rats*. European journal of heart failure, 2011. **13**(3): p. 254-63.

38. Peng, Y., et al., *Top-down proteomics reveals concerted reductions in myofilament and Z-disc protein phosphorylation after acute myocardial infarction*. Molecular & cellular proteomics : MCP, 2014. **13**(10): p. 2752-64.

39. Lunney, J.K., *Advances in swine biomedical model genomics*. Int J Biol Sci, 2007. **3**(3): p. 179-84.

40. Murry, C.E., R.B. Jennings, and K.A. Reimer, *Preconditioning with ischemia: a delay of lethal cell injury in ischemic myocardium*. Circulation, 1986. **74**(5): p. 1124-36.

41. Heusch, G., *Cardioprotection: chances and challenges of its translation to the clinic*. Lancet, 2013. **381**(9861): p. 166-75.

42. Rezende, P.C., et al., *Hypotheses, rationale, design, and methods for evaluation of ischemic preconditioning assessed by sequential exercise tests in diabetic and non-diabetic patients with stable coronary artery disease--a prospective study*. BMC cardiovascular disorders, 2013. **13**: p. 117.

43. Zhao, Z.Q., et al., *Inhibition of myocardial injury by ischemic postconditioning during reperfusion: comparison with ischemic preconditioning*. American journal of physiology. Heart and circulatory physiology, 2003. **285**(2): p. H579-88.

44. Staat, P., et al., *Postconditioning the human heart*. Circulation, 2005. **112**(14): p. 2143-8.

45. Przyklenk, K., et al., *Regional ischemic 'preconditioning' protects remote virgin myocardium from subsequent sustained coronary occlusion*. Circulation, 1993. **87**(3): p. 893-9.

46. Botker, H.E., et al., *Remote ischaemic conditioning before hospital admission, as a complement to angioplasty, and effect on myocardial salvage in patients with acute myocardial infarction: a randomised trial*. Lancet, 2010. **375**(9716): p. 727-34.

47. Zweier, J.L., J.T. Flaherty, and M.L. Weisfeldt, *Direct measurement of free radical generation following reperfusion of ischemic myocardium*. Proc Natl Acad Sci U S A, 1987. **84**(5): p. 1404-7.

48. Garlick, P.B., et al., *Direct detection of free radicals in the reperfused rat heart using electron spin resonance spectroscopy*. Circ Res, 1987. **61**(5): p. 757-60.

49. Kevin, L.G., et al., *Ischemic preconditioning alters real-time measure of O2 radicals in intact hearts with ischemia and reperfusion*. Am J Physiol Heart Circ Physiol, 2003. **284**(2): p. H566-74.

50. Zweier, J.L., *Measurement of superoxide-derived free radicals in the reperfused heart. Evidence for a free radical mechanism of reperfusion injury*. J Biol Chem, 1988. **263**(3): p. 1353-7.

51. Lesnefsky, E.J., et al., *Blockade of electron transport during ischemia protects cardiac mitochondria*. J Biol Chem, 2004. **279**(46): p. 47961-7.

52. Sack, M.N., *Mitochondrial depolarization and the role of uncoupling proteins in ischemia tolerance*. Cardiovasc Res, 2006. **72**(2): p. 210-9.

53. Chouchani, E.T., et al., *Ischaemic accumulation of succinate controls reperfusion injury through mitochondrial ROS*. Nature, 2014. **515**(7527): p. 431-435.

54. Ago, T., et al., *Upregulation of Nox4 by hypertrophic stimuli promotes apoptosis and mitochondrial dysfunction in cardiac myocytes*. Circ Res, 2010. **106**(7): p. 1253-64.

55. Kumar, V., et al., *Redox proteomics of thiol proteins in mouse heart during ischemia/reperfusion using ICAT reagents and mass spectrometry*. Free Radic Biol Med, 2013. **58**: p. 109-17.

56. Kohr, M.J., et al., *Simultaneous measurement of protein oxidation and S-nitrosylation during preconditioning and ischemia/reperfusion injury with resin-assisted capture*. Circ Res, 2011. **108**(4): p. 418-26.

57. Martinez-Acedo, P., et al., *A novel strategy for global analysis of the dynamic thiol redox proteome*. Mol Cell Proteomics, 2012. **11**(9): p. 800-13.

58. Ruiz-Meana, M., et al., *Ischemic preconditioning protects cardiomyocyte mitochondria through mechanisms independent of cytosol*. J Mol Cell Cardiol, 2014. **68**: p. 79-88.

59. Fuhrmann, D.C. and B. Brüne, *Mitochondrial composition and function under the control of hypoxia*. Redox biology, 2017. **12**: p. 208-215.

60. Burwell, L.S., S.M. Nadtochiy, and P.S. Brookes, *Cardioprotection by metabolic shut-down and gradual wake-up*. J Mol Cell Cardiol, 2009. **46**(6): p. 804-10.

61. Eltzschig, H.K. and T. Eckle, *Ischemia and reperfusion--from mechanism to translation*. Nat Med, 2011. **17**(11): p. 1391-401.

62. Matsushima, S., et al., *Broad suppression of NADPH oxidase activity exacerbates ischemia/reperfusion injury through inadvertent downregulation of hypoxia-inducible factor-1α and upregulation of*

peroxisome proliferator-activated receptor-α. Circulation research, 2013. **112**(8): p. 1135-1149.

63. Wu, B., et al., *Interleukin-37 ameliorates myocardial ischaemia/reperfusion injury in mice*. Clinical and experimental immunology, 2014. **176**(3): p. 438-451.

64. Prabhu, S.D. and N.G. Frangogiannis, *The Biological Basis for Cardiac Repair After Myocardial Infarction: From Inflammation to Fibrosis*. Circulation research, 2016. **119**(1): p. 91-112.

65. Raedschelders, K., D.M. Ansley, and D.D. Chen, *The cellular and molecular origin of reactive oxygen species generation during myocardial ischemia and reperfusion*. Pharmacol Ther, 2012. **133**(2): p. 230-55.

66. Binek, A., *Study of molecular mechanisms of myocardial infarction: analysis of deep proteome and redoxome in a pig model of ischema/reperfusion*. PhD Thesis. 2017, Universidad Autónoma de Madrid: Madrid.

67. Fu, Y. and X. Qian, *Transferred subgroup false discovery rate for rare post-translational modifications detected by mass spectrometry*. Mol Cell Proteomics, 2014. **13**(5): p. 1359-68.

68. Chick, J.M., et al., *An ultra-tolerant database search reveals that a myriad of modified peptides contributes to unassigned spectra in shotgun proteomics*. Nature biotechnology, 2015. **33**(7): p. 743-749.

69. Kong, A.T., et al., *MSFragger: ultrafast and comprehensive peptide identification in mass spectrometry-based proteomics*. Nat Methods, 2017. **14**(5): p. 513-520.

70. Cox, J. and M. Mann, *MaxQuant enables high peptide identification rates, individualized p.p.b.-range mass accuracies and proteome-wide protein quantification*. Nat Biotechnol, 2008. **26**(12): p. 1367-72.

71. Lu, P., et al., *Absolute protein expression profiling estimates the relative contributions of transcriptional and translational regulation*. Nat Biotechnol, 2007. **25**(1): p. 117-24.

72. Bagwan, N., et al., *Comprehensive Quantification of the Modified Proteome Reveals Oxidative Heart Damage in Mitochondrial Heteroplasmy*. Cell Rep, 2018. **23**(12): p. 3685-3697.e4.

73. Navarro, P., et al., *General statistical framework for quantitative proteomics by stable isotope labeling*. J Proteome Res, 2014. **13**(3): p. 1234-47.

74. Garcia-Marques, F., et al., *A Novel Systems-Biology Algorithm for the Analysis of Coordinated Protein Responses Using Quantitative Proteomics*. Mol Cell Proteomics, 2016. **15**(5): p. 1740-60.

75. Garcia-Prieto, J., et al., *beta3 adrenergic receptor selective stimulation during ischemia/reperfusion improves cardiac function in translational models through inhibition of mPTP opening in cardiomyocytes*. Basic Res Cardiol, 2014. **109**(4): p. 422.

76. García-Prieto, J., et al., *Neutrophil stunning by metoprolol reduces infarct size*. Nature Communications, 2017. **8**: p. 14780.

77. Martínez-Acedo, P., et al., *A Novel Strategy for Global Analysis of the Dynamic Thiol Redox Proteome*. Molecular & Cellular Proteomics : MCP, 2012. **11**(9): p. 800-813.

78. Martinez-Bartolome, S., et al., *Properties of average score distributions of SEQUEST: the probability ratio method*. Mol Cell Proteomics, 2008. 7(6): p. 1135-45.

79. Bonzon-Kulichenko, E., et al., *Revisiting peptide identification by high-accuracy mass spectrometry: problems associated with the use of narrow mass precursor windows*. Journal of proteome research, 2015. **14**(2): p. 700-10.

80. Navarro, P. and J. Vazquez, *A refined method to calculate false discovery rates for peptide identification using decoy databases*. Journal of proteome research, 2009. **8**(4): p. 1792-6.

81. Cox, J. and M. Mann, *MaxQuant enables high peptide identification rates, individualized p.p.b.-range mass accuracies and proteome-wide protein quantification*. Nature biotechnology, 2008. **26**(12): p. 1367-72.

82. Calvano, S.E., et al., *A network-based analysis of systemic inflammation in humans*. Nature, 2005. **437**(7061): p. 1032-7.

83. Ficenec, D., et al., *Computational knowledge integration in biopharmaceutical research*. Briefings in bioinformatics, 2003. **4**(3): p. 260-78.

84. Huang da, W., et al., *Extracting biological meaning from large gene lists with DAVID*. Current protocols in bioinformatics / editoral board, Andreas D. Baxevanis ... [et al.], 2009. **Chapter 13**: p. Unit 13 11.

85. Creasy David, M. and S. Cottrell John, *Unimod: Protein modifications for mass spectrometry*. PROTEOMICS, 2004. **4**(6): p. 1534-1536.

86. Cao, J. and S. Zhang, *A Bayesian extension of the hypergeometric test for functional enrichment analysis*. Biometrics, 2014. **70**(1): p. 84-94.

87. Camon, E., et al., *The Gene Ontology Annotation (GOA) Database: sharing knowledge in Uniprot with Gene Ontology*. Nucleic Acids Research, 2004. **32**(Database issue): p. D262-D266.

88. R Development Core Team, *R: A Language and Environment for Statistical Computing*. 2016, R Foundation for Statistical Computing: Vienna, Austria.

89. Wickham, H., *ggplot2: Elegant Graphics for Data Analysis*. 2016: Springer-Verlag New York.

90. Mundt, A.K.a.F., *factoextra: Extract and Visualize the Results of Multivariate Data Analyses*. 2017.

91. Simko, T.W.a.V., *R package "corrplot": Visualization of a Correlation Matrix*. 2017.

92. Tatarkova, Z., et al., *Effect of ischemia and reperfusion on protein oxidation in isolated rabbit hearts*. Physiological research, 2005. **54**(2): p. 185-91.

93. Chouchani, E.T., et al., *Ischaemic accumulation of succinate controls reperfusion injury through mitochondrial ROS*. Nature, 2014. **515**(7527): p. 431-435.

94. Chouchani, E.T., et al., *Cardioprotection by S-nitrosation of a cysteine switch on mitochondrial complex I*. Nature Medicine, 2013. **19**(6): p. 753-759.

95. Kevin, L.G., et al., *Ischemic preconditioning alters real-time measure of O2 radicals in intact hearts with ischemia and reperfusion*. American journal of physiology. Heart and circulatory physiology, 2003. **284**(2): p. H566-74.

96. Matsushima, S., et al., *Broad Suppression of NADPH Oxidase Activity Exacerbates Ischemia/Reperfusion Injury Through Inadvertent Downregulation of HIF-1α and Upregulation of PPARα*. Circ Res, 2013. **112**(8): p. 10.1161/CIRCRESAHA.111.300171.

97. Napankangas, J.P., et al., *Superoxide production during ischemia-reperfusion in the perfused rat heart: a comparison of two methods of measurement*. Journal of molecular and cellular cardiology, 2012. **53**(6): p. 906-15.

98. Wang, C., et al., *Apelin protects sarcoplasmic reticulum function and cardiac performance in ischaemia-reperfusion by attenuating oxidation of sarcoplasmic reticulum Ca2+-ATPase and ryanodine receptor*. Cardiovascular Research, 2013. **100**(1): p. 114-124.

99. Belevych, A.E., et al., *Redox modification of ryanodine receptors underlies calcium alternans in a canine model of sudden cardiac death*. Cardiovascular Research, 2009. **84**(3): p. 387-395.

100. Bovo, E., S.R. Mazurek, and A.V. Zima, *Oxidation of ryanodine receptor following ischemia/reperfusion increases propensity of Ca2+ waves*

during β-adrenergic receptor stimulation. American Journal of Physiology-Heart and Circulatory Physiology, 2018.

101. Shanmughapriya, S., et al., *SPG7 is an Essential and Conserved Component of the Mitochondrial Permeability Transition Pore*. Molecular cell, 2015. **60**(1): p. 47-62.

102. Horckmans, M., et al., *Neutrophils orchestrate post-myocardial infarction healing by polarizing macrophages towards a reparative phenotype*. European heart journal, 2017. **38**(3): p. 187-197.

103. Prabhu, S.D. and N.G. Frangogiannis, *The Biological Basis for Cardiac Repair After Myocardial Infarction: From Inflammation to Fibrosis*. Circ Res, 2016. **119**(1): p. 91-112.

104. Jong, W.M.C., et al., *Reduced acute myocardial ischemia–reperfusion injury in IL-6-deficient mice employing a closed-chest model*. Inflammation Research, 2016. **65**: p. 489-499.

105. Wu, B., et al., *Interleukin-37 ameliorates myocardial ischaemia/reperfusion injury in mice*. Clin Exp Immunol, 2014. **176**(3): p. 438-51.

106. Chouchani, E.T., et al., *Ischaemic accumulation of succinate controls reperfusion injury through mitochondrial ROS*. Nature, 2014. **515**(7527): p. 431-5.

107. Jang, S., et al., *Elucidating Mitochondrial Electron Transport Chain Supercomplexes in the Heart During Ischemia-Reperfusion*. Antioxid Redox Signal, 2017. **27**(1): p. 57-69.

108. Frangogiannis, N.G., *Regulation of the inflammatory response in cardiac repair*. Circ Res, 2012. **110**(1): p. 159-73.

109. Ma, Y., A. Yabluchanskiy, and M.L. Lindsey, *Neutrophil roles in left ventricular remodeling following myocardial infarction*. Fibrogenesis & tissue repair, 2013. **6**(1): p. 11.

110. Li, C., et al., *Cerebral ischemia-reperfusion induces GAPDH S-nitrosylation and nuclear translocation*. Biochemistry. Biokhimiia, 2012. **77**(6): p. 671-8.

111. Sun, N., et al., *GluR6-FasL-Trx2 mediates denitrosylation and activation of procaspase-3 in cerebral ischemia/reperfusion in rats*. Cell death & disease, 2013. **4**: p. e771.

112. Hess, D.T., et al., *Protein S-nitrosylation: purview and parameters*. Nature reviews. Molecular cell biology, 2005. **6**(2): p. 150-66.

113. Moris, D., et al., *The role of reactive oxygen species in myocardial redox signaling and regulation*. Annals of translational medicine, 2017. **5**(16): p. 324.

114. Cook, N.L., D.I. Pattison, and M.J. Davies, *Myeloperoxidase-derived oxidants rapidly oxidize and disrupt zinc-cysteine/histidine clusters in proteins*. Free Radic Biol Med, 2012. **53**(11): p. 2072-80.

115. Friedrichs, K., S. Baldus, and A. Klinke, *Fibrosis in Atrial Fibrillation – Role of Reactive Species and MPO*. Frontiers in Physiology, 2012. **3**: p. 214.

116. Garai, D., et al., *Mechanisms of myeloperoxidase catalyzed oxidation of H2S by H2O2 or O2 to produce potent protein Cys-polysulfide-inducing species*. Free Radic Biol Med, 2017. **113**: p. 551-563.

117. Ehrenshaft, M., L.J. Deterding, and R.P. Mason, *Tripping up Trp: Modification of protein tryptophan residues by reactive oxygen species, modes of detection, and biological consequences*. Free Radic Biol Med, 2015. **89**: p. 220-8.

118. Szuchman-Sapir, A.J., et al., *Site-specific hypochlorous acid-induced oxidation of recombinant human myoglobin affects specific amino acid residues and the rate of cytochrome b5-mediated heme reduction*. Free Radic Biol Med, 2010. **48**(1): p. 35-46.

119. Maitra, D., et al., *Mechanism of hypochlorous acid-mediated heme destruction and free iron release*. Free Radic Biol Med, 2011. **51**(2): p. 364-73.

120. Rees, M.D., et al., *Myeloperoxidase-derived oxidants selectively disrupt the protein core of the heparan sulfate proteoglycan perlecan*. Matrix Biol, 2010. **29**(1): p. 63-73.

121. Myllyharju, J. and K.I. Kivirikko, *Collagens, modifying enzymes and their mutations in humans, flies and worms*. Trends Genet, 2004. **20**(1): p. 33-43.

122. Eyre, D.R., M.A. Paz, and P.M. Gallop, *Cross-linking in collagen and elastin*. Annu Rev Biochem, 1984. **53**: p. 717-48.

123. Berg, R.A. and D.J. Prockop, *The thermal transition of a non-hydroxylated form of collagen. Evidence for a role for hydroxyproline in stabilizing the triple-helix of collagen*. Biochem Biophys Res Commun, 1973. **52**(1): p. 115-20.

124. Kotch, F.W., I.A. Guzei, and R.T. Raines, *Stabilization of the Collagen Triple Helix by O-Methylation of Hydroxyproline Residues*. Journal of the American Chemical Society, 2008. **130**(10): p. 2952-2953.

125. Muller, F.L., et al., *Trends in oxidative aging theories*. Free Radic Biol Med, 2007. **43**(4): p. 477-503.

126. Mallat, Z., et al., *Elevated levels of 8-iso-prostaglandin F2alpha in pericardial fluid of patients with heart failure: a potential role for in vivo*

oxidant stress in ventricular dilatation and progression to heart failure. Circulation, 1998. **97**(16): p. 1536-9.

127. Tang, H.Y., et al., *Lipidomics reveals accumulation of the oxidized cholesterol in erythrocytes of heart failure patients.* Redox biology, 2018. **14**: p. 499-508.

128. Sack, M.N., et al., *Fatty acid oxidation enzyme gene expression is downregulated in the failing heart.* Circulation, 1996. **94**(11): p. 2837-42.

129. Goldberg, I.J., C.M. Trent, and P.C. Schulze, *Lipid Metabolism and Toxicity in the Heart.* Cell Metabolism, 2012. **15**(6): p. 805-812.

130. Ayala, A., M.F. Munoz, and S. Arguelles, *Lipid peroxidation: production, metabolism, and signaling mechanisms of malondialdehyde and 4-hydroxy-2-nonenal.* Oxid Med Cell Longev, 2014. **2014**: p. 360438.

131. Gaschler, M.M. and B.R. Stockwell, *Lipid peroxidation in cell death.* Biochemical and biophysical research communications, 2017. **482**(3): p. 419-425.

132. Wong-ekkabut, J., et al., *Effect of Lipid Peroxidation on the Properties of Lipid Bilayers: A Molecular Dynamics Study.* Biophysical Journal, 2007. **93**(12): p. 4225-4236.

Appendices

SUPLEMENTARY FIGURES

Respiratory complex I

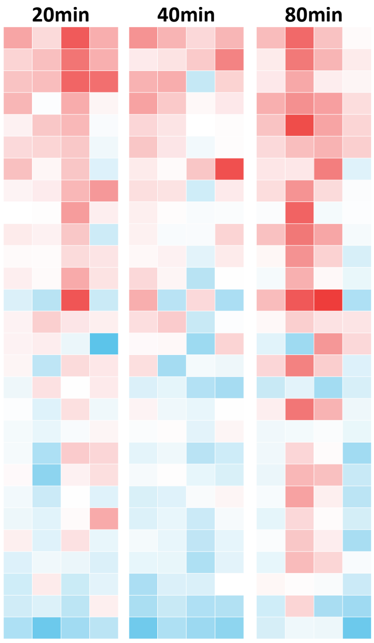

Uniprot	Protein	Gene	peptides N.
F1RNI5	Uncharacterized protein	NDUFA3	3
F1SI50	Uncharacterized protein	NDUFB3	3
Q9P0J0	NADH dehydrogenase [ubiquinone] 1 alpha subcomplex sub. 13	NDUFA13	7
Q16795	NADH dehydrogenase [ubiquinone] 1 alpha subcomplex sub. 9	NDUFA9	3
K7GSE5	NADH dehydrogenase [ubiquinone] 1 beta subcomplex sub. 10	NDUFB9	3
I3LGM4	Uncharacterized protein	NDUFA11	3
Q29259	NADH dehydrogenase [ubiquinone] 1 beta subcomplex sub. 6	NDUFB6	2
F1SGC6	Uncharacterized protein	NDUFB5	8
B8Y651	NADH dehydrogenase [ubiquinone] 1 beta subcomplex sub. 8	NDUFB8	8
O75306	NADH dehydrogenase [ubiquinone] iron-sulfur protein 2	NDUFS2	13
P28331	NADH-ubiquinone oxidoreductase 75 kDa sub.	NDUFS1	17
O75251	NADH dehydrogenase [ubiquinone] iron-sulfur protein 7	NDUFS7	4
I3LU33	Uncharacterized protein	NDUFS4	2
I3LPW0	NADH dehydrogenase [ubiquinone] 1 beta subcomplex sub. 3	NDUFB4	4
Q9UI09	NADH dehydrogenase [ubiquinone] 1 alpha subcomplex sub. 12	NDUFA12	2
F1SLY2	Uncharacterized protein	NDUFA5	4
A1XQS6	Uncharacterized protein	NDUFC1	2
F1SIF2	NADH dehydrogenase [ubiquinone] iron-sulfur protein 4	NDUFS3	10
F1SV23	Uncharacterized protein	NDUFS5	3
I3LDC3	Uncharacterized protein	NDUFB10	6
O00217	NADH dehydrogenase [ubiquinone] iron-sulfur protein 8	NDUFS8	4
O43678	NADH dehydrogenase [ubiquinone] 1 alpha subcomplex sub. 2	NDUFA2	2
F1STY1	NADH dehydrogenase [ubiquinone] 1 sub. C2	NDUFC2	6
P49821	NADH dehydrogenase [ubiquinone] flavoprotein 1	NDUFV1	6
P19404	NADH dehydrogenase [ubiquinone] flavoprotein 2	NDUFV2	9
A1XQS3	Mitochondrial NDUFA4	NDUFA4	5
O95182	NADH dehydrogenase [ubiquinone] 1 alpha subcomplex sub. 7	NDUFA7	4
O14561	Acyl carrier protein	NDUFAB1	2

Respiratory complex II

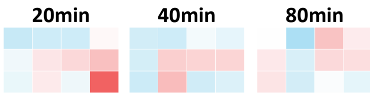

Uniprot	Protein	Gene	N.
Q007T0	Succinate dehydrogenase [ubiquinone] iron-sulfur subunit	SDHB	10
Q0QF01	Succinate dehydrogenase [ubiquinone] flavoprotein subunit	SDHA	14
D0VWV4	Succinate dehydrogenase cytochrome b560 subunit	SDHC	1

Respiratory complex III

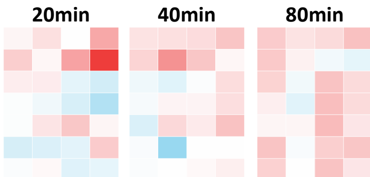

Uniprot	Protein	Gene	N.
I3LFK0	Mitochondrial chaperone BCS1	BCS1L	3
Q2EN79	Ubiquinol-cytochrome c reductase complex	UQCR10	2
F1RPD2	Cytochrome b-c1 complex subunit 1	UQCRC2	12
F1SKM0	Cytochrome b-c1 complex subunit 1	UQCRC1	14
O75439	Mitochondrial-processing peptidase subunit beta	PMPCB	3
P14927	Cytochrome b-c1 complex subunit 7	UQCRB	3
F1RNZ1	Cytochrome b-c1 complex subunit Rieske	UQCRFS1	17

Respiratory complex IV

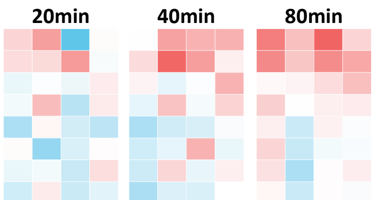

Uniprot	Protein	Gene	N.
P13073	Cytochrome c oxidase subunit 4 isoform 1	COX4I1	3
P50667	Cytochrome c oxidase subunit 2	MT-CO2	9
I3LTV6	Cytochrome c oxidase subunit 6A	COX6A2	2
Q95283	Cytochrome c oxidase subunit 4 isoform 1	COX4I1	8
F1SJ34	Cytochrome c oxidase subunit 5A	COX5A	9
F1RJI7	Cytochrome c oxidase subunit 6A	COX6A1	2
I3LER5	Cytochrome c oxidase subunit 4 isoform 1	COX4I1	4
A1XQS3	Mitochondrial NDUFA4	NDUFA4	5

Respiratory complex V

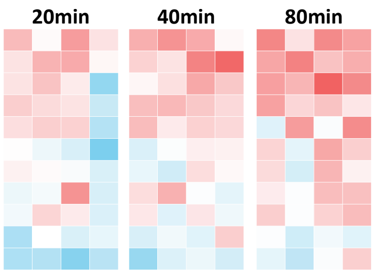

Uniprot	Protein	Gene	N.
Q95339	ATP synthase subunit f	ATP5J2	3
Q9MYT8	ATP synthase subunit e	ATP5I	4
F1SAK6	ATP synthase subunit g	ATP5L	3
P80021	ATP synthase subunit alpha	ATP5A1	7
P36542	ATP synthase subunit gamma	ATP5C1	3
Q2EN81	ATP synthase subunit O	ATP5O	13
F1SBN7	Uncharacterized protein	ATP5F1	7
F1SLA0	ATP synthase subunit beta	ATP5B	4
F1S6Q7	ATP synthase subunit delta	ATP5D	5
P13618	ATP synthase-coupling factor 6	ATP5J	8
O75947	ATP synthase subunit d	ATP5H	4

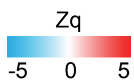

Supplementary Figure S1 Changes in expression of mitochondrial respiratory complexes proteins during the initial (20-80min) reperfusion. Zq values are reported as the log2-fold changes expressed in units of standard deviation with respect to baseline animals.

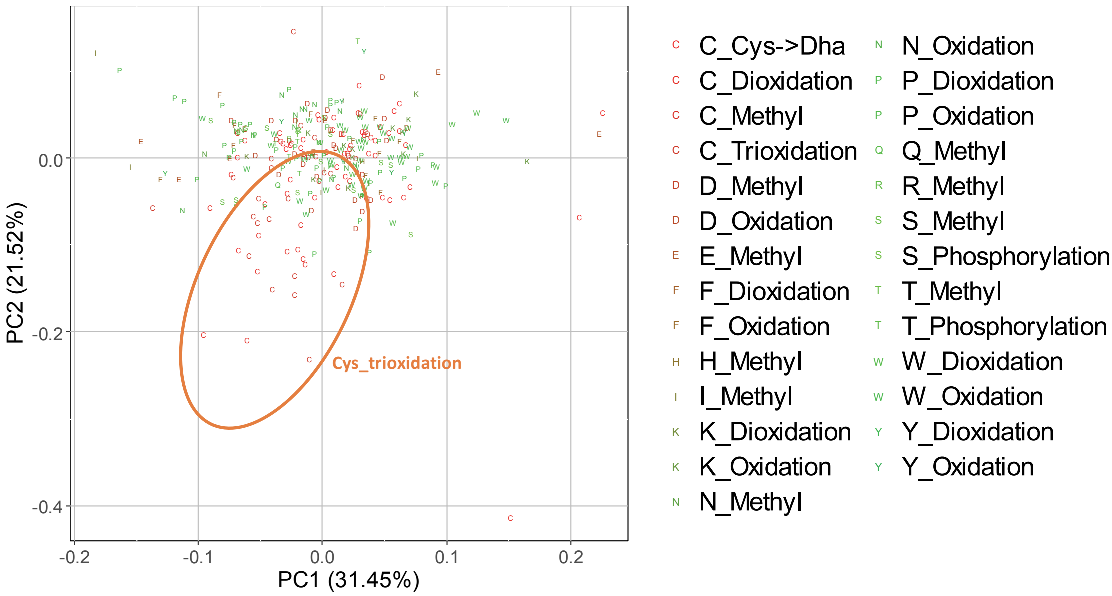

Supplementary Figure S2 Principal Components Analysis (PCA) of PTMs in the Remote tissue. 309 peptides present in all biological replicates (n=4) and corresponding to known biologically relevant PTMs in the accurate modified residue were subjected to PCA analysis. The circled area in orange shows a distinctive behaviour a group of trioxidations in Cys (C).

Uniprot Ac. No	Protein	Gene	N.
P04178	PIG Superoxide dismutase [Cu-Zn]	SOD1	6
Q99757	HUMAN Thioredoxin	TXN2	1
K7GPB0	PIG Superoxide dismutase	SOD2	5
P62895	PIG Cytochrome c	CYCS	12
D0G0C7	PIG Antioxidant protein 1 homolog	ATOX1	2
P04179	HUMAN Superoxide dismutase [Mn]	SOD2	5
P52552	PIG Peroxiredoxin-2	PRDX2	8
P18650	PIG Apolipoprotein E	APOE	3
P30048	HUMAN Thioredoxin-dependent peroxide reductase	PRDX3	8
Q9GLW8	PIG Peroxiredoxin 5	PRDX5	4
P08294	HUMAN Extracellular superoxide dismutase [Cu-Zn]	SOD3	1
Q9TSX9	PIG Peroxiredoxin-6	PRDX6	15
P80031	PIG Glutathione S-transferase P	GSTP1	6
P50584	PIG Bis(5'-nucleosyl)-tetraphosphatase	NUDT2	1
P62995	HUMAN Transformer-2 protein homolog beta	TRA2B	2
Q8MJ14	PIG Glutathione peroxidase 1	GPX1	3
Q06830	HUMAN Peroxiredoxin-1	PRDX1	8
O62839	PIG Catalase	CAT	14
Q9MYY8	PIG Thioredoxin reductase 1	TXNRD1	2
B6CVD7	PIG ERO1-like protein alpha	ERO1A	4
F1RHN4	PIG Uncharacterized protein	TXNRD2	7
P79293	PIG Myosin-7	MYH7	29
P12883	HUMAN Myosin-7	MYH7	55
P31151	HUMAN Protein S100-A7	S100A7	1
P22352	HUMAN Glutathione peroxidase 3	GPX3	1

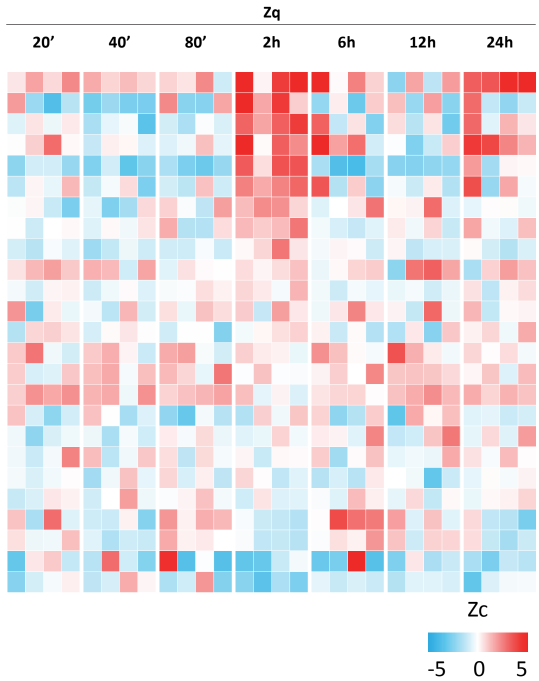

Supplementary Figure S3 Oxidative stress protein values temporarily increase at 2h after reperfusion in remote pig myocardium tissue. Zq values of ROS detoxifying enzymes are reported as the log2-fold changes expressed in units of standard deviation around the averages with respect to controls for each individual (n=4). N represent the number of peptides identified for each protein.

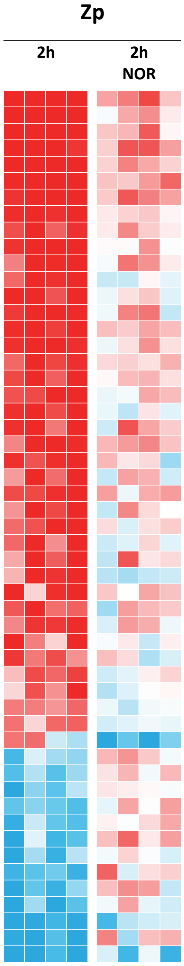

Uniprot Ac. No.	Protein	Gene	Sequence	Zp$_{av}$ 2h	Zp$_{av}$ 2h NOR	*P* value	FDR
Q14896	Myosin-binding protein C, cardiac-type	MYBPC3	LTIDDVTPADEADYSFVPEGFAC@NLSAK)	9.09	2.33	2.5E-13	4.2E-11
A0A024QZT0	Voltage-dependent anion channel 2, isoform CRA_c	VDAC2	WC@EYGLTFTEK)	8.80	1.03	1.0E-15	1.0E-15
F1SID7	Myosin-binding protein C, cardiac-type	MYBPC3	EGC@SEWVDALQGLTER	8.32	1.52	1.8E-13	4.2E-11
P32418	Sodium/calcium exchanger 1	SLC8A1	GGGEDFEDTC@GELEFQNDEIVK)	7.31	2.44	1.3E-07	3.9E-06
F1SID7	Myosin-binding protein C, cardiac-type	MYBPC3	VGAGGLDGYSLEYC@R	6.87	1.48	5.1E-09	3.1E-07
P68363	Tubulin alpha-1B chain	TUBA1B	SIQFVDWC@PTGFK)	6.72	1.81	9.7E-08	3.4E-06
Q02218	2-oxoglutarate dehydrogenase	OGDH	FGLEGC@EVLIPALK)	6.44	2.19	4.0E-06	7.5E-05
A0A024QZT0	Voltage-dependent anion channel 2, isoform CRA_c	VDAC2	WNTDNTLGTEIAIEDQIC@QGLK)	5.89	0.66	1.4E-08	6.7E-07
P41367	Medium-chain specific acyl-CoA dehydrogenase	ACADM	AVPQC@EPGSGFSFELTEQQK)	5.77	1.03	2.6E-07	7.1E-06
O75323	Protein NipSnap homolog 2	NIPSNAP2	IC@QEVLPK)	5.75	0.58	1.9E-08	8.6E-07
P13804	Electron transfer flavoprotein subunit alpha	ETFA	LGGEVSC@LVAGTK)	5.42	1.28	6.7E-06	1.2E-04
F1SED0	Short/branched chain specific acyl-CoA dehydrogenase	ACADSB	LATEQLGSFC@LSEPSAGSDSFSLK)	5.33	-0.62	1.1E-10	1.1E-08
Q02218	2-oxoglutarate dehydrogenase	OGDH	ELEQIFC@QFDSK)	5.29	0.18	3.0E-08	1.2E-06
Q6B339	Acyl coenzyme A synthetase long-chain 1	N/A	GFVGSFEELC@R	5.27	0.94	2.6E-06	5.6E-05
F1S4D5	Kynurenine aminotransferase 3	KYAT3	WC@SSDWTLDPQELASK)	5.22	1.31	2.2E-05	3.3E-04
P29804	Pyruvate dehydrogenase E1 component subunit alpha	PDHA1	NFYGGNGIVGAQVPLGAGIALAC@K)	5.05	0.75	3.0E-06	6.1E-05
P11607	Sarcoplasmic/endoplasmic reticulum calcium ATPase 2	ATP2A2	SLPSVETLGC@TSVIC@SDK)	4.99	0.94	1.1E-05	1.8E-04
P11607	Sarcoplasmic/endoplasmic reticulum calcium ATPase 2	ATP2A2	VGEATETALTC@LVEK)	4.88	0.88	1.4E-05	2.3E-04
A0A140VJX1	Testicular tissue protein Li 198	N/A	QAVLGAGLPISTPC@TTINK)	4.85	0.59	3.7E-06	7.3E-05
P00355	Glyceraldehyde-3-phosphate dehydrogenase	GAPDH	VPTPNVSVVDLTC@R	4.84	-0.43	1.1E-08	6.1E-07
P21796	Voltage-dependent anion-selective channel protein 1	VDAC1	YQIDPDAC@FSAK)	4.83	1.33	1.4E-04	1.9E-03
Q2HYU2	ATP-dependent 6-phosphofructokinase, muscle type	PFKM	LPLMEC@VQVTK)	4.79	1.71	8.2E-04	7.9E-03
P09571	Serotransferrin	TF	VTC@VAEELLK)	4.76	0.16	6.1E-07	1.5E-05
O97580	Succinate--CoA ligase [ADP-forming] subunit beta	SUCLA2	ILAC@DDLDEAAK)	4.68	0.32	2.3E-06	5.1E-05
P13639	Elongation factor 2	EEF2	YVEPIEDVPC@GNIVGLVGVDQFLVK)	4.53	1.26	3.7E-04	4.2E-03
A0A024R4K3	Malate dehydrogenase	MDH2	EGVVEC@SFVK)	4.51	0.47	1.2E-05	1.9E-04
Q14315	Filamin-C	FLNC	LYAQDADGC@PIDIK)	4.47	0.39	9.6E-06	1.7E-04
P00355	Glyceraldehyde-3-phosphate dehydrogenase	GAPDH	IVSNASC@TTNC@LAPLAK)	4.41	-0.34	2.6E-07	7.1E-06
A0A024R4K3	Malate dehydrogenase	MDH2	GYLGPEQLPDC@LK)	4.18	0.86	3.0E-04	3.5E-03
F1SED0	Short/branched chain specific acyl-CoA dehydrogenase	ACADSB	ASSTC@PVTLENAK)	4.18	-1.32	2.5E-09	1.8E-07
Q96I99	Succinate--CoA ligase [GDP-forming] subunit beta	SUCLG2	SC@NGPVLVGSPQGGVDIEEVAASNPELIFK)	4.14	1.00	6.5E-04	6.8E-03
A0A024QZT0	Voltage-dependent anion channel 2, isoform CRA_c	VDAC2	SC@SGVEFSTSGSSNTDTGK)	4.00	0.58	2.1E-04	2.6E-03
Q6B339	Acyl coenzyme A synthetase long-chain 1	N/A	NVVSDC@SAFVK)	3.97	0.62	2.7E-04	3.2E-03
Q14896	Myosin-binding protein C, cardiac-type	MYBPC3	ISNVGEDSC@TVQWEPPAYDGGQPILGYILER	3.51	-0.13	7.7E-05	1.1E-03
K7GQB8	Cerruloplasmin precursor	CP	SGAGIDDSPC@IPWVYYSTVDQVK)	3.21	-0.10	3.3E-04	3.7E-03
P68363	Tubulin alpha-1B chain	TUBA1B	AYHEQLSVAEITNAC@FEPANQMVK)	3.05	-0.08	6.8E-04	6.8E-03
F1S9I9	Mitochondrial amidoxime reducing component 2	MARC2	DC@GDEAAQWFTSFLK)	2.94	-0.48	2.0E-04	2.6E-03
P62831	60S ribosomal protein L23	RPL23	ISLGLPVGAVINC@ADNTGAK)	2.59	-0.55	6.6E-04	6.8E-03
P09571	Serotransferrin	TF	DQYELLC@R	2.47	-0.55	1.0E-03	9.6E-03
F1RRT2	Myosin light chain 4	MYL4	ITYGQC@GDVLR	0.78	-4.88	8.0E-10	6.5E-08
P01025	Complement C3	C3	QC@QDLANFSENMVVFGC@PN	-2.17	1.07	4.3E-04	4.7E-03
P50828	Hemopexin	HPX	SLQEEFPGVPSPLDAAVEC@HR	-2.64	0.76	2.3E-04	2.8E-03
P06867	Plasminogen	PLG	TAC@YITGWGETK)	-3.00	0.22	4.7E-04	5.0E-03
Q8WZ42	Titin	TTN	DC@GFPDEGEYIVTAGQDK)	-3.04	0.80	3.0E-05	4.5E-04
Q29545	Inhibitor of carbonic anhydrase	ICA	QC@FPSELLDAC@TFHGN	-3.09	0.68	4.2E-05	6.1E-04
P50828	Hemopexin	HPX	ELGSPHGISLDAVDATFVC@PGTSR	-3.40	1.64	4.7E-08	1.8E-06
P06867	Plasminogen	PLG	FPLAGLEENYC@R	-3.67	-0.07	9.1E-05	1.2E-03
F1STC5	Immunoglobulin kappa constant	IGKC	DSTYSLSSTLSLPTSQYLSHNLYSC@EVTHK)	-3.68	1.00	3.8E-07	9.8E-06
P06867	Plasminogen	PLG	VIPAC@LPTPNYVVADR	-3.85	1.05	1.1E-07	3.6E-06
P06867	Plasminogen	PLG	ATTVAGVPC@QEWAAQEPHR	-4.46	0.04	1.1E-06	2.5E-05
K7GQB8	Cerruloplasmin precursor	CP	DIASGLIGPLIHC@R	-4.85	-1.74	7.4E-04	7.3E-03
F1STC5	Immunoglobulin kappa constant	IGKC	EQLETQTVSVVC@LLNSFFPR	-5.15	0.85	7.7E-11	9.4E-09
Q03472	Apolipoprotein R	APOR	IITC@TEDGTWHPR	-5.39	-2.36	9.7E-04	9.2E-03

Zc

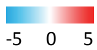

Supplementary Figure S4 Oxidized Cys-containing peptide sequences statistically different between nonreperfused animals (2hNOR) and the group subjected to regular I/R protocol (2h I/R). Zp values are reported as the log2-fold changes expressed in units of standard deviation around the averages with respect to controls. P-values are calculated using Student's t-test, post hoc FDR Benjamini Hockberg.

Uniprot Ac. No.	Protein	Gene	Sequence	Zp_{av} 24h	Zp_{av} 24h PC	*P* value	FDR
P42639	Tropomyosin alpha-1 chain	TPM1	C@AELEEELK)	9.14	2.73	4.0E-11	9.8E-09
F1RZQ6	ADP/ATP translocase 1	SLC25A4	EFTGLGNC@LAK)	8.62	1.69	9.4E-13	4.6E-10
P63317	Troponin C, slow skeletal and cardiac muscles	TNNC1	AAFDIFVLGAEDGC@ISTK)	8.23	4.73	3.1E-04	5.1E-03
P07951	Tropomyosin beta chain	TPM2	C@GDLEEELK)	8.14	2.67	1.7E-08	1.6E-06
Q02218	2-oxoglutarate dehydrogenase	OGDH	ELEQIFC@QFDSK)	6.83	1.67	1.1E-07	7.4E-06
P21796	Voltage-dependent anion-selective channel protein 1	VDAC1	YQIDPDAC@FSAK)	6.75	2.47	9.9E-06	4.4E-04
A0A024R4K3	Malate dehydrogenase	MDH2	EGVVEC@SFVK)	6.55	2.96	2.1E-04	3.9E-03
Q02218	2-oxoglutarate dehydrogenase	OGDH	FGLEGC@EVLIPALK)	6.39	2.79	2.0E-04	3.9E-03
Q9TV61	Myosin-1	MYH1	C@DQLIK)	6.36	0.83	1.2E-08	1.5E-06
P13533	Myosin-6	MYH6	C@SSLEK)	6.18	1.76	4.9E-06	2.4E-04
P33198	Isocitrate dehydrogenase [NADP]	IDH2	EPIIC@K)	5.55	2.18	5.1E-04	7.0E-03
O75323	Protein NipSnap homolog 2	NIPSNAP2	IC@QEVLPK)	5.44	0.48	3.0E-07	1.8E-05
P33198	Isocitrate dehydrogenase [NADP]	IDH2	DLAGC@IHGLSNVK)	5.42	1.47	4.3E-05	1.2E-03
Q8WNV7	Dehydrogenase/reductase SDR family member 4	DHRS4	VNC@LAPGLIK)	5.35	1.15	1.4E-05	5.3E-04
P32418	Sodium/calcium exchanger 1	SLC8A1	GGGEDFEDTC@GELEFQNDEIVK)	5.34	1.74	2.0E-04	3.9E-03
P33198	Isocitrate dehydrogenase [NADP]	IDH2	VC@VETVESGAMTK)	5.31	1.35	4.4E-05	1.2E-03
F1SID7	Myosin-binding protein C, cardiac-type	MYBPC3	EGC@SEWVDALQGLTER	5.25	0.51	9.7E-07	5.3E-05
P68363	Tubulin alpha-1B chain	TUBA1B	SIQFVDWC@PTGFK)	5.14	1.62	2.7E-04	4.7E-03
Q8HY46	Carnitine O-palmitoyltransferase 1, muscle isoform	CPT1B	LQWDIPEQC@QAVIESSYQVAK)	4.50	0.97	2.7E-04	4.7E-03
P11607	Sarcoplasmic/endoplasmic reticulum calcium ATPase 2	ATP2A2	VGEATETALTC@LVEK)	4.49	0.30	1.5E-05	5.4E-04
F1SIS9	NADH dehydrogenase [ubiquinone] 1 alpha subcomplex subunit 10	NDUFA10	VITVDGNIC@SGK)	4.31	0.16	1.8E-05	6.0E-04
F1SM61	Fibulin-1	FBLN1	DC@SLPYTSESK)	4.28	0.76	2.8E-04	4.8E-03
P09571	Serotransferrin	TF	VTC@VAEELLK)	4.09	0.64	3.7E-04	5.5E-03
P29804	Pyruvate dehydrogenase E1 component subunit alpha	PDHA1	NFYGGNGIVGAQVPLGAGIALAC@K)	3.86	0.57	6.6E-04	8.6E-03
P11607	Sarcoplasmic/endoplasmic reticulum calcium ATPase 2	ATP2A2	SLPSVETLGC@TSVIC@SDK)	3.82	-0.44	1.1E-05	4.4E-04
P00355	Glyceraldehyde-3-phosphate dehydrogenase	GAPDH	VPTPNVSVVDLTC@R	3.65	0.02	1.8E-04	3.9E-03
P02540	Desmin	DES	HQIQSYTC@EIDALK)	3.54	-0.30	7.4E-05	1.7E-03
F1RRT2	Myosin light chain 4	MYL4	ITYGQC@GDVLR	3.52	0.13	4.6E-04	6.5E-03
Q6B339	Acyl coenzyme A synthetase long-chain 1	N/A	GFVGSFEELC@R	3.48	-0.23	1.3E-04	2.8E-03
F1S4D5	Kynurenine aminotransferase 3	KYAT3	WC@SSDWTLDPQELASK)	3.22	-0.03	8.0E-04	9.9E-03
Q6B339	Acyl coenzyme A synthetase long-chain 1	N/A	NVVSDC@SAFVK)	3.07	-0.40	3.3E-04	5.2E-03
Q8WZ42	Titin	TTN	GQPLYLSC@ELNK)	2.65	-0.65	6.3E-04	8.4E-03
F8UQW4	Insulin-like growth factor 2 receptor	IGF2R	VGGAYLVDDSDPDASLFINVC@R	-0.01	3.44	3.6E-04	5.5E-03
T1RTP3	PDZ and LIM domain protein 1	PDLIM1	AAIANLC@IGDVITAIDGENTSNMTHLEAQNK)	-0.37	3.02	4.6E-04	6.5E-03
F1STC5	Immunoglobulin kappa constant	IGKC	EQLETQTVSVVC@LLNSFFPR	-1.89	2.22	2.2E-05	6.6E-04
P50828	Hemopexin	HPX	ELGSPHGISLDAVDATFVC@PGTSR	-1.97	1.97	4.6E-05	1.2E-03
Q63ZY3	KN motif and ankyrin repeat domain-containing protein 2	KANK2	SELC@LDLPDPPEDPVALETR	-2.66	1.21	6.4E-05	1.6E-03
Q8WZ42	Titin	TTN	DC@GFPDEGEYIVTAGQDK)	-2.89	2.29	9.0E-08	7.3E-06
K7GQB8	Cerruloplasmin precursor	CP	DIASGLIGPLIHC@R	-3.44	2.70	2.5E-10	4.0E-08
Q03472	Apolipoprotein R	APOR	IITC@TEDGTWHPR	-5.12	-1.87	7.7E-04	9.7E-03

Zc

-5 0 5

Supplementary Figure S5 Cys-containing peptide sequences significantly affected by preconditioning. Zp values are reported as the log2-fold changes expressed in units of standard deviation around the averages with respect to controls. P-values are calculated using Student's t-test, post hoc FDR Benjamini Hockberg.

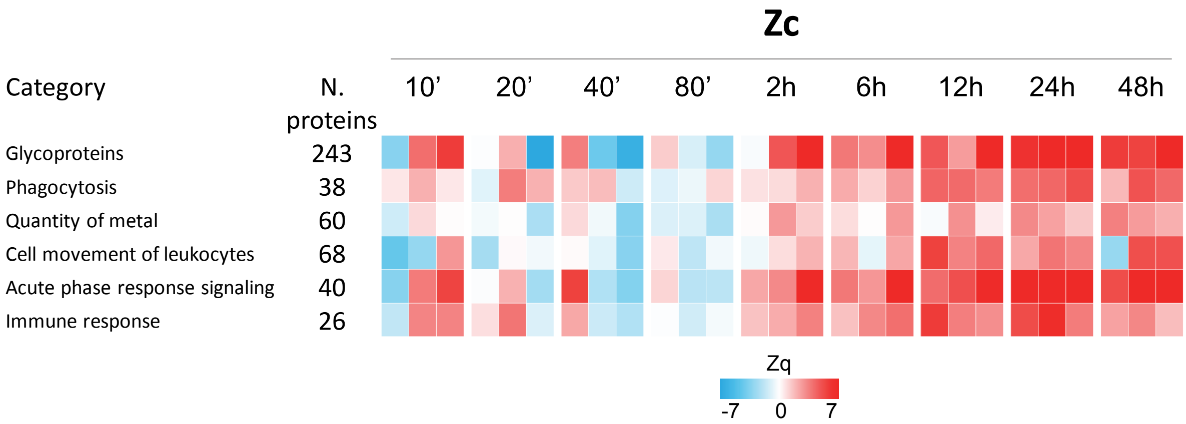

Supplementary Figure S6 Inflammatory and leukocyte migration related protein categories affected in the mouse I/R model and increasing at the same time (2h-48h) as reversible and irreversible oxidations detected in the same model. Functional categories values (Zc) are reported as log2 fold changes with respect to baseline, in units of standard deviation.

SUPLEMENTARY TABLES

Below you can find the headers of Supplementary Tables that provide additional material to this Doctoral Thesis. Due to their large size they can be found on the CD attached to this dissertation.

Sup. Table S1 List of oxidized-Cys-containing peptides detected in pig ischemic myocardium region. Zp values for each I/R time point are reported as the log2-fold changes expressed in units of standard deviation around the averages with respect to controls. Sequences selected from HCA are marked in bold red.

Sup. Table S2 Cluster 1 of irreversible oxidations in pig ischemic tissue increased immediately (20min) after reperfusion. Zp values for each I/R time point are reported as the log2-fold changes expressed in units of standard deviation around the averages with respect to controls.

Sup. Table S3 Cluster 2 of irreversible oxidations in pig ischemic tissue increased between 2-24h after reperfusion. Zp values for each I/R time point are reported as the log2-fold changes expressed in units of standard deviation around the averages with respect to controls.

Sup. Table S4 Complete list of Zp changes of modified peptides from enriched proteins in different clusters: Cluster 1 (early irreversible oxidation at 20 min), Cluster 2 (Irreversible oxidation at 2h-24h) and Cys reversible oxidation (2h-24h).

Sup. Table S5 List of proteins from each category analyzed by SBT in the infarcted tissue. Zq values for each I/R time point are reported as the log2-fold changes expressed in units of standard deviation around the averages with respect to controls.

Sup. Table S6 List of oxidized-Cys-containing peptides in remote region of pig myocardium. Zp values for each I/R time point are reported as the log2-

fold changes expressed in units of standard deviation around the averages with respect to controls.

Sup. Table S7 Cluster 1 of irreversible oxidations in pig remote tissue increased at 120m after reperfusion. Zp values for each I/R time point are reported as the log2-fold changes expressed in units of standard deviation around the averages with respect to controls.

Sup. Table S8 Cluster 2 of irreversible oxidations in pig remote tissue increased between 80min-12h after reperfusion. Zp values for each I/R time point are reported as the log2-fold changes expressed in units of standard deviation around the averages with respect to controls.

Sup. Table S9 List of proteins from each category analyzed by SBT in the remote tissue. Zq values for each I/R time point are reported as the log2-fold changes expressed in units of standard deviation around the averages with respect to controls.

Sup. Table S10 List of Hydroxilated-Prolines identified in collagens in a pig model of I/R. Zp values for each I/R time point are reported as the log2-fold changes expressed in units of standard deviation around the averages with respect to controls.

Sup. Table S11 List of proteins from each category analyzed by SBT affected by non-reperfusion and preconditioning. Zq values for each I/R time point are reported as the log2-fold changes expressed in units of standard deviation around the averages with respect to controls.

Sup. Table S12 List of initial irreversible oxidations in mouse model of I/R. Zp values for each I/R time point are reported as the log2-fold changes expressed in units of standard deviation around the averages with respect to controls.

Sup. Table S13 List of irreversible oxidations at 2-24h in mouse model of I/R. Zp values for each I/R time point are reported as the log2-fold changes expressed in units of standard deviation around the averages with respect to controls.

Sup. Table S14 List of Cys reversible oxidation in mouse model of I/R. Zp values for each I/R time point are reported as the log2-fold changes expressed in units of standard deviation around the averages with respect to controls.

Sup. Table S15 List of proteins from each category analyzed by SBT in depleted mice. Zq values for each I/R time point are reported as the log2-fold changes expressed in units of standard deviation around the averages with respect to controls.

Sup. Table S16 List of Cys reversible oxidations identified in neutrophil depletion mouse model. Zp values for each experimental condition are reported as the log2-fold changes expressed in units of standard deviation around the averages with respect to WT sham controls pool.

Sup. Table S17 List of irreversibly oxidized peptides identified in neutrophil depletion mouse model. Sequences common to irreversible oxidations at 2-24h in mouse or pig model of I/R are marked in bold red. Zp values for each I/R time point are reported as the log2-fold changes expressed in units of standard deviation around the averages with respect to controls.

OTHER STUDIES PUBLISHED DURING PHD

Ruiz-Meana M, Minguet M, Bou-Teen D, Miro-Casas E, **Castans C**, Castellano J, Bonzon-Kulichenko E, Igual A, Rodriguez-Lecoq R, Vazquez J and García-Dorado D. *Ryanodine Receptor Glycation Favors Mitochondrial Damage in the Senescent Heart*. Circulation, 20